HIGH TEMPERATURE MICROPOROUS COATINGS: THE EFFECTS OF WETTING AND WICKING ON NUCLEATE BOILING AND CHF

By

ROSS E. PIVOVAR

Presented to the Faculty of the Graduate School of

The University of Texas at Arlington in Partial Fulfillment

of the Requirements

for the Degree of

MASTER OF SCIENCE IN MECHANICAL ENGINEERING

THE UNIVERSITY OF TEXAS AT ARLINGTON

MAY 2009

ACKNOWLEDGEMENTS

Experimentation requires a great deal of experience. Dr. Gilbert Moreno has done a fantastic job of giving any type of wisdom he has gained over the years. He happily gave me the knowledge needed to properly create an experiment and get my hands dirty. Dr. Sang-muk Kwark was always there to look at the brighter side. Even when an experiment would go terribly wrong, he would always answer with “enjoy it.” Dr. Mauricio Salinas cannot be left out. This fellow provided many philosophically financial conversations much to my amusement. I definitely need to thank Dr. Liangshan Chen for taking the time out of his busy schedule to take many SEM pictures for me. Thanks, you guys will not be forgotten.

April 20, 2009

ABSTRACT

HIGH TEMPERATURE MICROPOROUS COATINGS: THE EFFECTS OF WETTING AND WICKING ON NUCLEATE BOILING AND CHF

Ross E. Pivovar, M.S.

The University of Texas at Arlington, 2009

Supervising Professor: Seung Mun You

Porous coatings have long been a method to enhance boiling heat transfer. Previous researchers have thoroughly explained most of the physics behind the enhancement, but some holes still exist. Correlations, setup to predict nucleate boiling, are often only accurate in specific scenarios. CHF correlations that take into account wettability do not consider microstructure changes that decrease contact angle, but do not enhance CHF. A solution to these problems is presented via the wicking and wetting of liquid on a porous surface. CHF is found to be enhanced with increases in wicking speeds and flow rate. Wetting, measured by apparent contact angle, is found to coincide with changes in nucleate boiling. Contact angle measurements may be able to indicate the level of hydraulic resistance where decreases in apparent contact angle led to decreases in nucleate boiling performance. Nucleate boiling predictions made by wetting measurements were not found to always correctly predict enhancement or degradation. The degree of wetting or wicking is manipulated via corrosion, oxidation, material change, and particle size. It is believed that the CHF of porous materials is determined by either the wicking limit (capillary limit) or the macrolayer dryout limit. The exact mechanism was found to depend on the coating thickness and wicking flow rate.

TABLE OF CONTENTS

LIST OF ILLUSTRATIONS

LIST OF TABLES

NOMENCLATURE

γ	Surface Tension [N/m]
π_{sl}	Adhesive tension [N/m]
θ	Static equilibrium contact angle (intrinsic contact angle) [deg]
θ_W	Wenzel apparent contact angle [deg]
θ_{CB}	Cassie-Baxter apparent contact angle [deg]
r(x)	Roughness factor
f	Area fraction
P	Pressure [Pa]
A	Area [m^2]
P_c	Capillary Pressure [Pa]
P_P	Perimeter [m]
r	Pore radius [m]
r*	Critical Pore radius [m]
d	Bubble diameter [m]
d_h	Hydraulic diameter [m]
l	Wicked height [m]
η	Viscosity [Pa-s]
t	Time [s]
u	Velocity [m/s]
K	Permeability [m^2]
υ	Kinematic Viscosity [m^2/s]

P_o Poisuille number

υ Specific Volume [m^3/kg]

O(n) Order of magnitude

V_m Molar Volume [m^3/mol]

R Gas constant [m^3Pa/Kmol]

h Enthalpy [J/kg]

T_{sat} Temperature at saturated conditions [℃]

k Thermal conductivity[W/mK]

ε Porosity

g Gravity [m/s^2]

ρ Density [kg/m^3]

Ω Heater orientation angle [deg]

q" Heat flux [W/m^2]

Subscripts

t Thickness [μm]

p Particle size [μm]

r Ratio

e Equivalent

s Solid

f Fluid

SV *Solid-vapor*

Sl *Solid-liquid*

lV *Liquid-vapor*

sat-P-l *Parameter at the saturation pressure of the liquid*

l *Liquid*

v *Vapor*

CHAPTER 1

BACKGROUND

1.1 Overview of Porous Coating History

Porous coatings are by no means a new subject. Research in two-phase heat transfer has been studied for decades and so has the enhancement via porous coatings, albeit to a lesser extent. Initially, Malyshenko [1], as well many other Russian researchers investigated the boiling stabilization effect of mesoporous coatings. These coatings were mostly non-conducting particles and often the thicknesses were on the order of several millimeters.

Many years later, the nucleate boiling enhancement of porous coatings was utilized to create commercial products to enhance the efficiency of industrial two-phase devices. Most notable was the Linde High Flux boiling surface. These coatings were conductive, irregular shaped particles, brazed to the surface. The cavity size of the coatings had been reduced to fractions of a micron and was subsequently called microporous. The performance of these coatings was tested by many researchers; see Bergles and Chyu [2] and You et al. [3]. Many other fancy fabrication techniques were developed to enhance nucleate boiling through the artificial creation of nucleation sites. Cieslinksi [4] used various methods of deposition including electrolytic treatment, plasma spraying, gas-flame spraying, and sandblasting. These methods required extensive preparation compared to the techniques utilized in this thesis, which are brazing and soldering. The parameters that significantly affected performance were the thickness, bonding, and porosity. If the particles failed to sufficiently bond to the surface, performance was severely degraded. Unfortunately, the majority of the techniques investigated created porosities less than 0.3. This pales in comparison to much newer techniques which create porosities greater than 0.5.

Chang and You [5] investigated the boiling effects of particle type and size. This included aluminum, copper, diamond particles, and silver flakes. Their results showed that the type of particle made no difference in the boiling curve. To optimize the coatings, the thickness should be minimized and the average cavity diameter must be optimized with the properties of the boiled fluid. Following this study, Rainey and You [6] showed that the orientation of coated heaters had virtually no effect on nucleate boiling performance. It was found that CHF steadily reduced as the angle of inclination increased. This is expected since a plain surface exhibits a similar decrease in performance.

Kim et al. [7] investigated various electroplating techniques as well as particle soldering. These soldered coatings had porosities between 0.5 and 0.6. Up to 2006, the nucleate boiling performance of these coatings has shown to be superior to any other technique.

1.2 Physics of Porous Coatings

The physics of porous coatings is well theorized and a review is given here. The natural convection region is a power law relationship between the heat flux and superheat. This region is completely single phase and advection is the dominant mode of heat transfer. Microporous coatings have no affect on the curve at this level of power input.

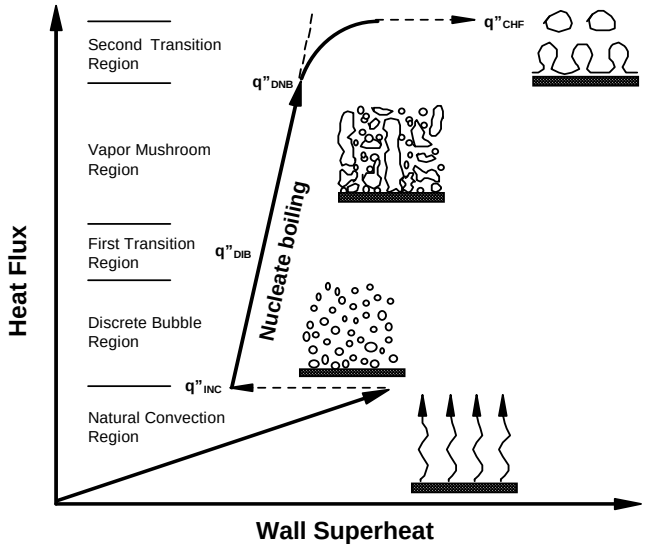

Figure 1.1 – Typical nucleate boiling curve. [3]

Once boiling incipience occurs, the effect of micro-pores is immediately apparent. A significantly smaller heat flux is required to induce boiling when compared to a plain surface. Bergles and Chyu [2] proved that the existence of reentrant cavities, depicted in Figure 1.2, causes an increase in heat transfer. The coating creates numerous cavities that are smaller than the working fluid can penetrate. In other words, an increase in nucleation sites causes an increased use of latent energy. Obviously, this greatly depends on the fluid's surface tension and vapor pressure. If the cavities are completely saturated with liquid, a coating can be rendered useless. Overall, it is thought that the increase in performance of porous coatings is caused by the increased use of latent energy and convection caused by bubble agitation within the coatings.

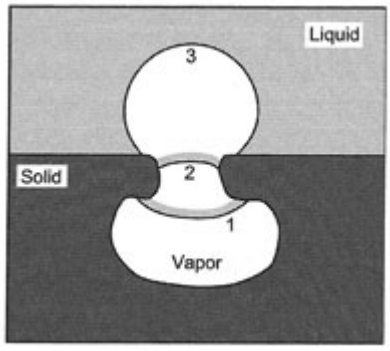

Figure 1.2 - Growth of reentrant bubble. [3]

Several factors other than nucleation site density also affect the boiling efficiency. Most importantly is the rewetting of the nucleation site once a bubble departs. Moss and Kelly [8] revealed that porous coatings effectively wicked fluid into the dry areas and allowed for a smooth escape of vapor thus showing that vapor stacks would not be a choking point in the coating.

However, not all nucleation points are activated during incipience. Application of low heat flux gives way to “patch boiling”. As described by Bergles and Chyu [2], random distributions of active nucleation sites remained isolated from other inactivated distributions. The vapor did not spread until higher heat flux was applied.

In the nucleate boiling region, bubble sizes are observed to be smaller and more frequent than plain surface boiling. You et al. [3] showed increasing heat transfer comes from the increased micro-convection brought on by more violent boiling.

The exact mechanism of the cause of CHF on plain surfaces with or without microporous structures is still not fully understood. Katto [9] thoroughly describes the advantages and disadvantages to most CHF theories. The two main theories are the hydrodynamic instability [10] and the macrolayer dryout [9] model.

The basic idea behind the hydrodynamic instability model is that the vapor leaving the surface is traveling at a much higher velocity than the liquid traveling back to the surface. The interface between the liquid and vapor eventually becomes unstable. This is known as the Helmholtz instability. Once the interface becomes unstable and grows exponentially, the vapor columns coalesce into a blanket vapor layer over the entire surface. Boiling efficiency subsequently drops tremendously and temperature explodes upward. The only hole in this theory is that the instability criterion can only happen at one velocity difference (u_v-u_l) for a specified system. This value has been shown to be unreasonably high.

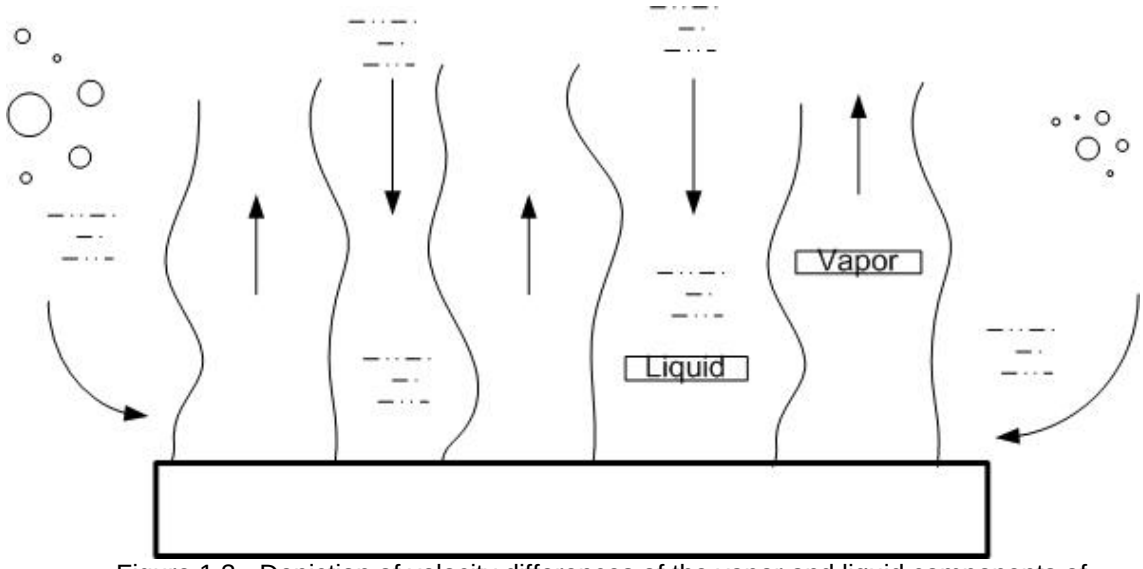

Figure 1.3 - Depiction of velocity differences of the vapor and liquid components of nucleate boiling.

The macrolayer dryout model states that a vapor clot is formed above a macrolayer[1] of fluid. As the vapor clot grows with increasing heat flux, the inflow of bulk liquid into the macrolayer is blocked. This eventually leads to the entire surface drying out and once again boiling efficiency decreases and temperature drastically increases. A third model is the wicking or capillary limit. The wicking limit states that CHF occurs when there is more fluid being vaporized than is pulled inward. Fluid is pulled towards the surface dry spots via capillary

[1] The macrolayer is the layer of fluid below the hovering bubble. It includes the liquid sublayer and vapor stems, see Figure 1.4.

pressure. As heat flux increases the vapor removal rate increases, but fluid motion stays relatively constant. Thus, a hydrodynamic limit is reached causing vapor channel coalescence [11]. The wicking limit also encompasses two other mechanisms that *delay* CHF. Both stem from the additional nucleation sites. Additional sites cause more micro-convection[2] to be used and less latent energy [12]. In addition, the coating/wick forces the bubble departure diameter to resemble the pore size. This prevents larger bubbles from forming and subsequently coalescing into even larger vapor clots [5].

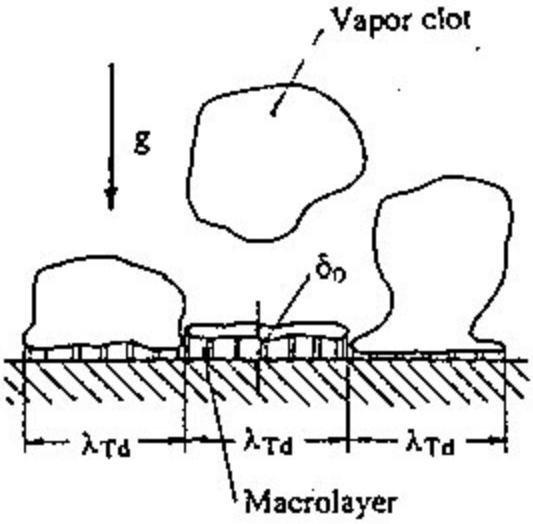

Figure 1.4 - Behavior of the vapor clot and the macrolayer in the macrolayer dryout model. **[9]**

Newer concepts have been developed in order to explain CHF based off parameters that affect CHF. Bar-Cohen and Mcneil [13] observed heater effusivity[3], heater width, system pressure, and liquid subcooling. The CHF values were observed to decrease with decreases in heater thickness and effusivity. Kumada et al. [14] developed a modified macrolayer model stating that the macrolayer thickness was related to “secondary” bubbles. The time to complete dryout was assumed to be the inverse of the departure frequency of “tertiary” bubbles. This model still neither confirmed nor invalidated either CHF models. Dhir [15] experimentally

[2] Micro-convection is the removal of thermal energy via bubble departure. When a bubble departs from the surface it both pushes hot fluid away from the surface and allows cooler fluid to flow towards the surface. As heat flux increases the rate of departure increases which leads to increased micro-convection due to increased bubble agitation.
[3] Effusivity is the measure of a materials ability to exchange thermal energy with the surrounding environment.

determined that partially wetted surfaces depend on the vapor production rate whereas well wetted surfaces depend on the vapor removal rate (hydrodynamic limit). His conclusion was that surface properties dictate which CHF mechanism occurs. Furthermore, the specific CHF mechanism determines the CHF values, which may or may not be the same for both mechanism theories.

Unal et al. [16] theorized that dry spots occurred when the surface temperature reached a point where liquid could no longer contact the surface. Via analytical methods, it was suggested that the cause of CHF was the dry spots after reaching a critical temperature. This result is similar to the inability of the fluid to properly quench the surface at a certain heat flux.

It has also been suggested by several researchers [17,18] that when the heater is thin, surface material properties such as conductance and capacitance play a role in CHF. Heaters used in our experimentation are thick enough to allow us to disregard such phenomena.

None of these models can fully explain the surface effects on CHF. Further experimentation and possibly new models are needed to fully predict how and when CHF will occur.

As for the effect of porous coatings on CHF, several mechanisms have been shown active. Rainey and You [6] displayed the numerous vapor columns disrupting the formation of a vapor clot. Tehver [19] stated that capillary pressure would cause the replenishment of liquid in the macrolayer and further delaying CHF. Liter and Kaviany [11] solidified this idea with highly wicking conical structures sintered to the surface. Li and Peterson [20] concluded that fin effects of the coating would also enhance CHF. The tests done by Li and Peterson included samples that were thicker than a millimeter. Rainey and You [21] provide evidence that sub-millimeter thickness most likely would provide no fin effects. Moss and Kelly [8] showed that if the coating is open on the sides, CHF is enhanced, otherwise CHF was found to be lower than plain surface.

Malyshenko [1] theorized, and Li and Peterson [22] proved, that for thick coatings, a vapor layer forms within the coating and slowly grows. Eventually CHF occurs once the vapor layer exceeds the coating thickness. Hence, a capillary flow and hydraulic limit controls the CHF.

1.3 Overview of Relevant Contact Angle Theory

A relatively new perspective to two-phase heat transfer is the effect of surface energy. While surface energy science has been around since the late 19th century and the controlling factors are well theorized, the application of this of theory is very difficult due to the myriad of variables. A brief review of wetting theory is needed before application to nucleate boiling. Once a fluid encounters a surface, the fluid will continue to wet the surface until the surface energies are balanced. The Young equation, Eqn.1.1, demonstrates the change in contact angle as the surface energy balances. The driving force is the difference between the solid-liquid surface tensions and the solid-vapor surface tension $(\gamma_{SV}-\gamma_{sl})$. The horizontal force $\gamma_{lV}\cos\theta$ must balance the equation in order to reach equilibrium. Figure 1.5 depicts several different wetting regimes on both a plain surface and in a tube.

$$\gamma_{SV} = \gamma_{lV}\cos\theta + \gamma_{Sl} \qquad \textbf{Eqn. (1.1)}$$

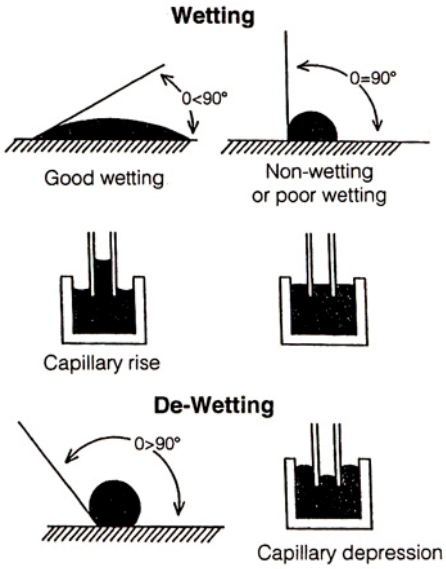

Figure 1.5 – Depiction of different wetting surfaces. **[67]**

The contact angle measured on a perfectly smooth surface is the equilibrium contact angle. The contact angle just before the three-phase contact angle begins to move is called the static receding or advancing contact angle. The dynamic receding or advancing contact angle is the angle created once the three-phase line begins to move. Typically, these angles are measured via a sessile drop test shown in Figure 1.6.

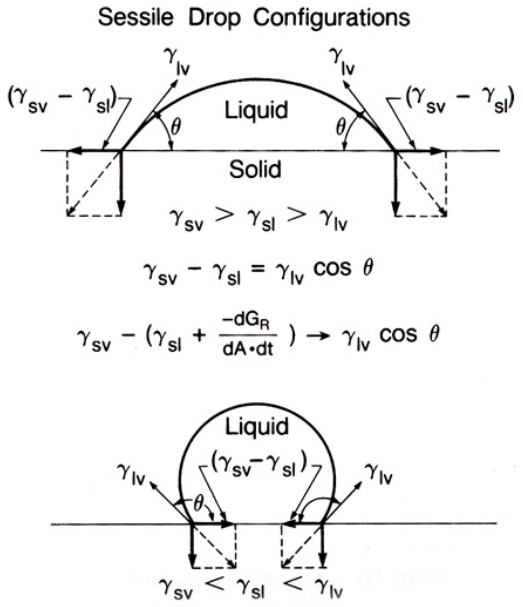

Figure 1.6 – Sessile drop and the application of Young's theorem. **[67]**

Any change in surface energy will alter the contact angle. Hence, oxidation, corrosion, surfactants, roughening, etc. will either increase or decrease the contact angle. In general, experimentation is needed to determine how a system will react due to a lack of material property data. The effects of cohesion and adhesion also come into play depending on the liquid. Several different equations have been developed to properly handle different situations, see [23,24] for more info.

As the contact angle asymptotically approaches zero, a variation of the Young's equation is now applicable. This is called the Antonoff equation, Eqn. 1.2. If the Antonoff equation is applicable then the fluid film is called a duplex.

$$\gamma_{SV} = \gamma_{lV} + \gamma_{Sl} \qquad \textbf{Eqn. (1.2)}$$

Adhesion and cohesion are two important concepts. Cohesion is the molecular attraction between similar molecules. Due to hydrogen bonding, water exhibits a high cohesive force. On the contrary, ethanol exhibits a low cohesive attraction, which is observable in the

surface tension. Adhesion is the molecular attraction between dissimilar molecules. This force is what causes two different substances to cling to each other. The contact angle can be viewed as the ratio of the adhesive forces to the cohesive forces as seen in Eqn. 1.3. In general, if the contact angle is larger than zero, the adhesive forces are small enough to be ignored.

$$cos\,\theta = \frac{\pi_{sl}}{\gamma_{lv}} \qquad \textbf{Eqn. (1.3)}$$

Roughening a surface has been shown to affect the contact angle by increasing the area needed to be balanced in Eqn. 1.1. The effects of roughening are characterized by the Wenzel equation, Eqn. 1.4.

$$\cos\theta^{W} = r(x)\cos\theta \qquad \textbf{Eqn. (1.4)}$$

Here, θ is the static equilibrium contact angle, or intrinsic contact angle, of the un-roughened surface. θ^{W} is the apparent contact angle caused by the surface roughening. If the intrinsic contact angle is less than 90°, then the Wenzel equation is applicable with the result of roughness decreasing the contact angle. The Wenzel equation is no longer applicable if the intrinsic contact angle is greater than 90°. Instead, the Cassie-Baxter equation is used, Eqn. 1.5.

$$\cos\theta^{CB} = f_1\cos\theta_1 + f_2\cos\theta_2 \qquad \textbf{Eqn. (1.5)}$$

This equation was originally derived for a surface consisting of two or more different materials. If θ_2 is set to 180°, this will simulate a roughened hydrophobic material. The end result, in contrast to Wenzel, is that roughening of the surface will result in a greater contact angle than the intrinsic contact angle.

Adsorption is a problem that must be considered in all wettability measurements. Adsorption is caused by the affinity of surrounding vapor for the solid surface. Adsorption, to a lesser extent, can also affect the vapor-liquid interface as well. Atoms or ions are weakly retained on the surface and can affect the wettability. While all surfaces can be affected by

adsorption, metals and glass are particularly vulnerable to drastic changes in contact angle. Once adsorption has occurred, Young's equation is no longer valid. Wettability based engineering systems must take care to thoroughly minimize adsorption.

Wicking is a phenomena related to the wettability of a surface and the pore size of the material. Within a tube, a fluid will rise or fall in order to satisfy the Young-Laplace equation. The Young-Laplace equation in combination with the hydrostatic pressure is shown (Eqn. 1.6). Here it is assumed an open to atmosphere scenario.

$$\Delta P_c = \frac{2\gamma \cos\theta}{r} \qquad \textbf{Eqn. (1.6)}$$

This equation determines the pressure created inside a capillary tube. As the pore size decreases or the surface tension increases, the capillary pressure increases. Washburn [25] performed extensive research on this subject and developed the Washburn equation, Eqn. 1.7.

$$l^2 = \left(\frac{\gamma}{\eta}\frac{\cos\theta}{2}\right) rt \qquad \textbf{Eqn. (1.7)}$$

The r-value is an empirical constant that does not change no matter the liquid properties. It is a representation of the pore size, tortuosity, and any other unknowns associated with the porous geometry. From this equation, Washburn took the derivative and showed that the pore rate of wicking fluid was given by Eqn. 1.8.

$$\frac{dl}{dt} = \frac{r}{\eta}\frac{\gamma}{4l}\cos\theta \qquad \textbf{Eqn. (1.8)}$$

Van Oss [26] describes several different ways these equations can be utilized to experimentally determine properties of the porous material. This includes determining the contact angle of porous materials in conjunction with polar fluids. This entails using hexane or octane to create a contact angle of zero and backtracking the r-value.

1.4 Corrosion Theory Review

Virtually all engineering systems must keep corrosion in mind. Porous coatings deal with two or more dissimilar metals in contact with each other that are then exposed to elevated

temperatures and an electrolyte. Hence, corrosion can be a major issue for engineering purposes.

When corrosion occurs on a metal, electrons of the metallic atoms are given up to other atoms in the system. The term for this loss of electrons is oxidation. The other material, usually the electrolyte is "reduced" and gains electrons, termed redox. An example of this would be

$$Fe \rightarrow Fe^{2+} + 2e^{-} \text{ and } 2H^{+} + 2e^{-} \rightarrow H_2$$

The free iron ions, Fe^{2+} may or may not form a new compound. Typically, the iron ion forms $Fe(OH)_2$ (rust). The more commonly cited oxidation is actually only one type of oxidation. This is the scaling oxide that occurs in an oxygenated environment. Many pure materials immediately react with O_2 to create a passivation layer on the surface of the metal, such as CuO. This scaling oxide is what most people refer to and is often visible to the naked eye.

In porous coatings, the use of two different metals gives way to galvanic corrosion. While technically all corrosion is galvanic corrosion, in general corrosion refers to a redox scenario. Galvanic corrosion refers to the exchange of electrons between two metals in any type of electrolyte.

The galvanic series (shown in Appendix A) can be used as a guide to predict corrosion. The series is found by measuring the nobility of a material in a specific electrolyte. The more reactive the material, the lower it is on the list. The farther apart two materials are the more the anode (lower material) will corrode. The series has limited use as it is for idealized scenarios. A more useful guide is the Anodic Index (shown in Appendix A). Unfortunately, the index can only be used to compare two metals. If three or more metals are used then experimentation is a required, although, the index can still be used as an excellent guide.

There are only a small number of options to prevent corrosion. These options are:

- Lower the system temperature (retards corrosion, does not stop it).
- Choose metals that are close together in the galvanic series.

- Avoid unfavorable anode-cathode surface area ratios. In general, use an anode area as large as possible.
- Stop dissimilar metals from making electrical contact with each other.
- Cathode protection: Electrically connect a third anodic metal to the other two. This causes the corrosion of the third metal instead of the original anodic metal i.e. galvanized steel.
- Apply a voltage that has the opposite polarity of the potential created by the couple.
- Use additives to alter the properties of the electrolyte.

1.5 Effects of Contact Angle on Nucleate Boiling and CHF

The effect of surface tension of the working fluid has been investigated by Bar-Cohen [27]. A change in surface tensions has a huge impact on the performance of microporous coatings. If the fluid surface tension drops significantly, then the fluid can more easily penetrate the pores. This results in less nucleation sites thus poor boiling performance. The coating developed by Kim et al. [7] had to contain optimized particle sizes in order to maintain maximum enhancement in three different fluids: water, R-123, and FC-72.

From the opposite perspective, the surface energy can be altered in order to increase or decrease wetting. Jansen et al. [28] altered the surface energy of a copper block without altering the number of nucleation points. This was done by coating the surface with PTFE (Telfon) and then re-sanding the surface. The contact angle was decreased from approximately 85º to 55º. It is questioned whether the change in contact angle is due to surface roughening in addition to the PTFE. Either way, negligible changes in the heat transfer coefficient were observed. Thus, unless the nucleation site density is decreased, wettability (in regards to contact angles between 10º-150º) has shown little or no effect on boiling efficiency.

Surfaces exhibiting contact angles approaching 0° or 180° exhibit much different results. With Eqn. 1.3 in mind, as the contact angle approaches zero the physics of the system changes. No longer can the adhesive forces be ignored. A zero contact angle system is

analogous to liquids spreading on liquids. The adhesive force acts as a capillary force and pulls the liquid along the surface. Takata et al. [29] used TiO_2 to create a true super-hydrophilic surface. Two thicknesses were tested, 250nm and 4μm. The 250nm samples produced approximately a 5º nucleate boiling enhancement. As for the 4μm thickness, the very low thermal conductivity of TiO_2 was assumed to cause the nucleate boiling to perform worse than plain surface. Both thicknesses showed CHF enhancement with an average of 57% enhancement.

Takata et al. [30] later went on to create a super-hydrophobic surface. This was done by electrolytic nickel plating with the suspension of PTFE fine particles (10μm thickness). The contact angle was measured to be greater than 150º. Referring again to Eqn. 1.3, the cohesive force is so great relative to the adhesive forces that the baseline of a sessile drop is virtually non-existent. This resulted in enhanced incipience, but nucleate boiling appeared to be nonexistent leading immediately into a semi-film boiling. CHF occurred approximately 73% lower than plain surface.

Several researches have tried to tie a material's contact angle to the CHF. Dhir [15] concluded that CHF was enhanced with decreasing contact angle. His analysis was done by manipulating the contact angle through oxidation. Different degrees of oxidation lead to different contact angles that corresponded with varying CHF values. Based off of SEM photos and data collected by Lee et al. [31], we can easily say that oxidation causes a substantial whisker microstructure to grow on the plain surface. While Dhir observed from experimental data that a decreasing contact angle corresponded with increasing CHF, this may not always be the case. The microstructure (more info in chapter 5) indicates that a capillary force will be created which affects the CHF. Clearly the extremes of contact angle measurements do not coincide with medium-ranged contact angle measurements.

1.6 Previous lab coatings, pros and cons of ABM and TCMC

Coatings previously developed in this lab are the ABM (Aluminum - devcom Brushable ceramic epoxy - Methyl ethyl ketone) by Chang and You [5] and the MTSP (Multi-Temperature Soldering Process) by Kim et al. [7]. TCMC (Thermally Conductive Microporous Coating) was also developed by Kim et al. [7] at a later time, but the only difference is that MTSP used nickel particles and TCMC uses copper particles.

ABM had two major disadvantages. It had a low thermal conductivity and the max temperature was around 170ºC. Two substantial advantages ABM has over all other types of coatings are that it can be fabricated at room temperature and it can be sprayed on to the sample. This means ABM has a multitude of applications even if the boiling performance is not as good as other porous coatings. Even though aluminum is very anodic, the epoxy effectively separates the metals and prevents corrosion. The main components of these coatings are shown in Table 1.1.

Table 1.1 - Composition of microporous coatings analyzed. Alloy composition shown in Appendix B.

	Particles	**Binder**	**Substrate**	**Thinner**
ABM	Aluminum	Brushable Ceramic Epoxy	Copper	MEK (Methyl Ethyl Ketone)
MTSP	Nickel	96/4 Solder	Copper	Denatured Alcohol
TCMC	Copper	96/4 Solder	Copper	Denatured Alcohol
HTMC-Ag	Copper	Ag 50-5 Brazing Paste	Copper	Isopar M ™ (Isoparaffin)
HTMC-Cu	Copper	Cu 0-7 Brazing Paste	Copper	Isopar M ™ (Isoparaffin)

MTSP both increased the thermal conductivity and the max temperature (220ºC). The disadvantages of MTSP are that nickel is somewhat difficult to solder and nickel still leaves room for improvement as far as conductivity is concerned. Using copper particles in TCMC allowed for a much easier fabrication process. Up to the date of the TCMC creation, TCMC outperformed all other porous coatings, commercial and academic.

Table 1.2 – Common potential differences between metallic systems

Anodic Differences	
Cu-Sn(solder)	.3V
Cu-Ag	.2V
Cu-Zn	.9V
Cu-Ni	.05V
Cu-Al	.6V
Al-Ni	.65V
Al-Sn(solder)	.3V
Al-Zn	.3V

Since TCMC and MTSP contain dissimilar metals electrically connected, corrosion issues needed to be considered. Currently no short term effects of corrosion have arisen in which the electrolyte is degassed distilled water. Long-term corrosion analysis is currently in process. Referring to Table 1.2, the galvanic potential of the copper-tin combination gives reason for concern. Boiling in an aqueous environment can be considered corrosively harsh. Thus, it can be reasoned that the coating will be heavily corroded in a couple years time.

While TCMC is fine for electronic cooling applications, a broader range of applications was desired. The nuclear power industry seeks CHF enhancement not only for safety, but looser design constraints. This meant increasing the max temperature since the TCMC coating is destroyed if CHF is achieved.

1.7 Mixed Wetting/CHF Conclusions in Available Literature

As already described in section 1.5, previous researchers have tried to relate the wettability of the surface to CHF enhancement. Much of the work done showing enhancement of CHF with decreasing contact angle was done on structures that also create capillary forces. Thus, the CHF enhancement was most likely caused by the capillary action and not the wettability alone. This section does not deal with any new experimental results and is simply an

overview of the contradictions in the available literature. The subjects that contradict themselves are surface energy manipulation and surface roughening resulting in CHF enhancement, which in turn is caused by increased wetting. Some contemporary researchers are beginning to dispute the use of contact angle and wetting as a CHF predictor [32]. The general base line idea of this thesis is that wicking is a much better indicator of CHF rather than contact angle measurements.

It is argued that increased wetting does not necessarily mean enhanced CHF. Kandlikar [33] has created a new model for plain surface CHF including both contact angle and surface orientation, Eqn. 1.9.

$$q"_{max} = \rho_v h_{lv} \frac{1+\cos\theta}{16}\left[\frac{2}{\pi} + \frac{\pi}{4}(1+\cos\theta)\cos\Omega\right]^{1/2}\left[\frac{\gamma(\rho_l-\rho_v)g}{\rho_v^2}\right]^{1/4} \quad \textbf{Eqn. (1.9)}$$

This equation is very promising, but needs modification and the effects of wettability require further investigation. Kandlikar cited Ramilison and Lienenhard [34] as a main source of contact angle measurements in development of this model. Ramilison and Lienenhard's data do not show a consistent trend of lower contact angle leading to enhanced CHF. Their experiments consisted of a Teflon coated, mirror, and roughened copper surface. The receding and advancing contact angles were measured for each surface. The Teflon coated surface consistently exhibited the lowest dynamic contact angles and the roughened surface had the largest contact angles. Teflon consistently resulted in the highest CHF, but the roughened surface consistently had a higher CHF than the mirror surface but lower than that of the Teflon surface. It is unknown why the roughened copper surface resulted in a higher contact angle than the mirror surface. The point is that CHF enhancement did not follow the trend of decreasing contact angle leading to higher CHF values. Although, many researchers, [35,36,37], have shown much evidence of wettability having some effect on CHF. It is conceded that wetting could have a large effect on vertical heaters such that the effects of departure frequency, gravity, and buoyancy become major factors in coalescence along the heater wall, which is the subject of the often cited Liaw and Dhir [36] research.

Berenson [38] showed that roughening a surface would significantly increase nucleation site density, but only slightly increase CHF. Berenson's working fluid was n-pentane and the heater was a copper block. Bonilla et al. [39] roughness tests do not result in CHF enhancement. These tests consist of parallel scores on a stainless steel surface that are 760µm wide and 100µm deep. Each test consisted of different channel spacing. The working fluid is liquid metal mercury mixed with a small amount of sodium that acts as a wetting agent. Haramura [40] uses a copper surface with R113 as the working fluid to show that roughness has a significant effect on CHF. Each of these studies resulted in different roughness conclusions and different degrees of CHF enhancement. The working fluid and heater surface is different for each test, which greatly affects the Wenzel equation, Eqn. 1.4. For a given roughness, the better the fluid wets the surface, the lower the apparent contact angle. Hay and Dragila [41] describe how a roughened surface enhances "half-pipe flow" by way of capillarity. Therefore, the reason roughening enhances CHF is much more likely caused by wicking flows rather than any decrease in contact angle.

Berenson [38] went on to test whether the intrinsic contact angle made a difference on CHF. These tests consisted of lapping each surface to achieve equal roughness. The materials tested were copper, nickel, and inconel. Each of these surfaces exhibits a completely different surface energy. If the contact angle has a significant effect on CHF then its effects will arise in this type of experiment. While the nucleate boiling for each material was quite different from each other, CHF was found to be the same for each material. This supports the argument that contact angle is not a good CHF indicator.

Joudi and James [42] corroded surfaces that result in a large degradation of nucleate boiling, but no change in CHF. Corrosion is known to completely change the surface energy of a given material. This phenomenon is further discussed in chapter 8. This article is mentioned here as it is another example of how the surface energy was changed yet the CHF did not

change. This cannot be explained by any contact angle theory and a capillary measurement most likely would reveal the reason for no CHF change.

Urquiola and Fujita [43] use surfactants to alter the surface tension as well as aging and chemicals to alter the surface energy. Several different resultant fluid surface tensions are used to show the effect on nucleate boiling. As they increased the surface tension, the nucleate boiling improved, but CHF appeared to be unaffected. Furthermore, they chemically decreased the surface contact angle, which resulted in increasingly poorer boiling performance with still no change in CHF.

The study done by Diesselhorst et al [44] is one of the most cited works connecting contact angle to CHF. Although, almost all citations fail to note that the tests were done on wire and cylindrical heaters. As already stated, the wettability enhancement should greatly affect the vapor buoyancy effects when traveling along a wall. Diesselhorst states that while the diameter effects on the CHF are small in comparison to the change in wettability, the diameter effect was unable to be eliminated from the data. Diesselhorst's argument was that as the contact angle increased, the bubble departure diameter increases and frequency slows. Since the bubbles are attached to the surface for a longer period of time, they have more of a chance of coalescing on the surface. This should not be the case; as the surface temperatures increases, the *dynamic* contact angle will decrease due to the fluid surface tension decreasing. The difference between the well wetting and poor wetting surfaces should approach each other as higher temperatures are reached. Diesselhorst even comments that his theory is only observable at low heat fluxes. In the end, their "dry patch" model of CHF, which is supposed to justify the use of contact angle, is actually quite similar to the macrolayer dryout model, section 1.2. The "dry patch" model states that hot spots will occur throughout the surface in which fluid is unable to rewet and is instantly vaporized. CHF occurs when these dry spots coalesce due to the surface failing to rewet or choked off as stated in the macrolayer dryout model. The dry spots are theorized to be larger for poor wetting surfaces.

As stated in section 1.5, super-hydrophobic and super-hydrophilic surfaces rely on a different type of physics. The chemistry of the surface resembles that of fluids spreading on fluids, which creates a strong capillary force and is therefore not considered here.

Other researchers, such as Carey [24], agree that the hydrodynamic limitation theory has too many holes and Eqn. 1.9 holds large potential but needs further study before active use. Nagai and Carey [32] went on to fully investigate the different parameters of wetting. Their first major point is that static contact angle measurements are not a useful CHF index as they virtually never appear in a boiling scenario. Dynamic measurements are a much more meaningful type of measurement, which is the required parameter of Eqn.1.9. Another major point is that during boiling, thermocapillary forces are involved which don't exist at room temperature. The paper concluded that wettability cannot be satisfactorily quantified by simply using the contact angle. The contact angle, solid surface energy, potential energy scale between liquid and solid molecules, and thermodynamically derived measures each provide a different perspective of the wetting phenomenon. None have been proven to be completely infallible when applied to boiling applications.

The data given in Chapters 8 and 9 demonstrate that contact angle measurements of porous coatings do not always agree with changes in CHF. Hence, it is believed that in porous coatings as well as plain surfaces, measurements of capillary force will lead to a good index of CHF. Obviously, plain surfaces would need to use a measure other than wicking, like a tensiometer or the Wilhelmy method, to determine the capillary force.

1.8 Thesis Objective

The main reason for starting this research was to alleviate the temperature restraints imposed by TCMC so the customer can design for higher working temperatures without coating degradation. This meant the new coating must be re-optimized via thickness, particle size, and composition ratio analysis. Furthermore, it became apparent that mechanisms, other than the reported wettability, were affecting the value of CHF.

It was hypothesized that wetting does not affect CHF. Wetting is a static characteristic and the exact physics as to why wetting would enhance a dynamic characteristic like CHF was unknown. Wicking was theorized to play a much bigger role. This, in addition to an improvement of previous lab coatings, was to be investigated.

CHAPTER 2

EXPERIMENTAL APPARATUS AND TEST PROCEDURES

2.1 Pool Boiling Testing Apparatus and Heater Design

2.1.1 Pool boiling test apparatus

Safety was the number one concern when building a pressure vessel that could not only withstand a vacuum, but pressures up to 5atm as well. While no tests above 1atm were performed for this thesis, future students will have the ability to easily go above 1atm. The initial design process started with the consulting of several design textbooks, [45,46,47]. Using Excel, the overall design was laid out with a safety factor of 3. From here the pressure vessel was modeled in Pro/e and an FEM analysis was done in ANSYS workbench.

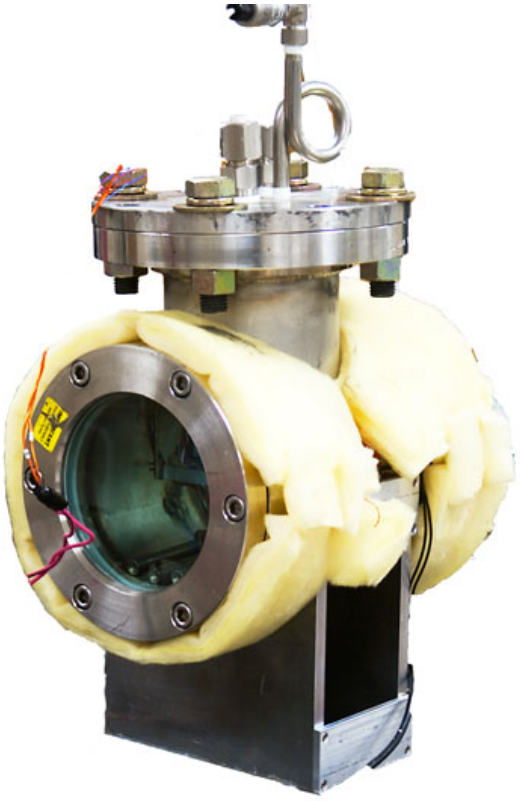

Figure 2.1 – Fully constructed pressure vessel.

Table 2.1 – Dimensions of pressure vessel.

Cylinder Volume	Diam (in)	(cm)	Length (in)	(cm)	Volume (cm^3)
	6.07	15.41	8.00	20.32	3787.4
Other Dimensions	Thickness (cm)	Outer Diam (cm)	(in)		
	0.71	16.83	6.63		
Face Plate Dimensions		Thickness (cm)	Diam (cm)		
		0.83	15.41		
Entry Plate Dimension		Thickness (cm)	Diam (cm)	Pipe Thickness (cm)	OD (cm)
		1.32	12.82	0.66	14.13
Flange Thickness		2.39			

Standard Grade 8 SAE bolts and nuts were used for the lid. The entire bulk material is stainless steel type 304. The viewport seals are Teflon, rated from vacuum to 100psi and a service temperature of 232ºC.

The weld points would be the weakest area of the pressure vessel. ANSYS predicted a safety factor of 9. The welds were done by a trained professional with more than 30 years experience and so the weak point of the welds was of no concern.

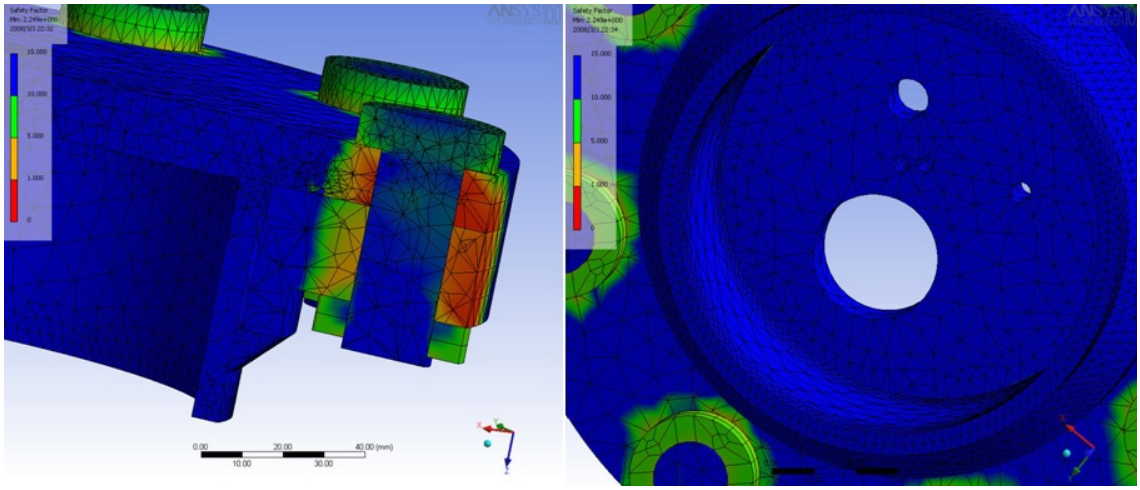

Figure 2.2 – ANSYS lid analysis.

The flange was ASME rated at 150psi and used 8 bolts at 7/8inch diameter. FEM was used to ensure a seal groove cut in the lid did not create any stress concentration. As seen in Figure 2.2, none of the holes cut in the lid created any kind of dangerous stresses.

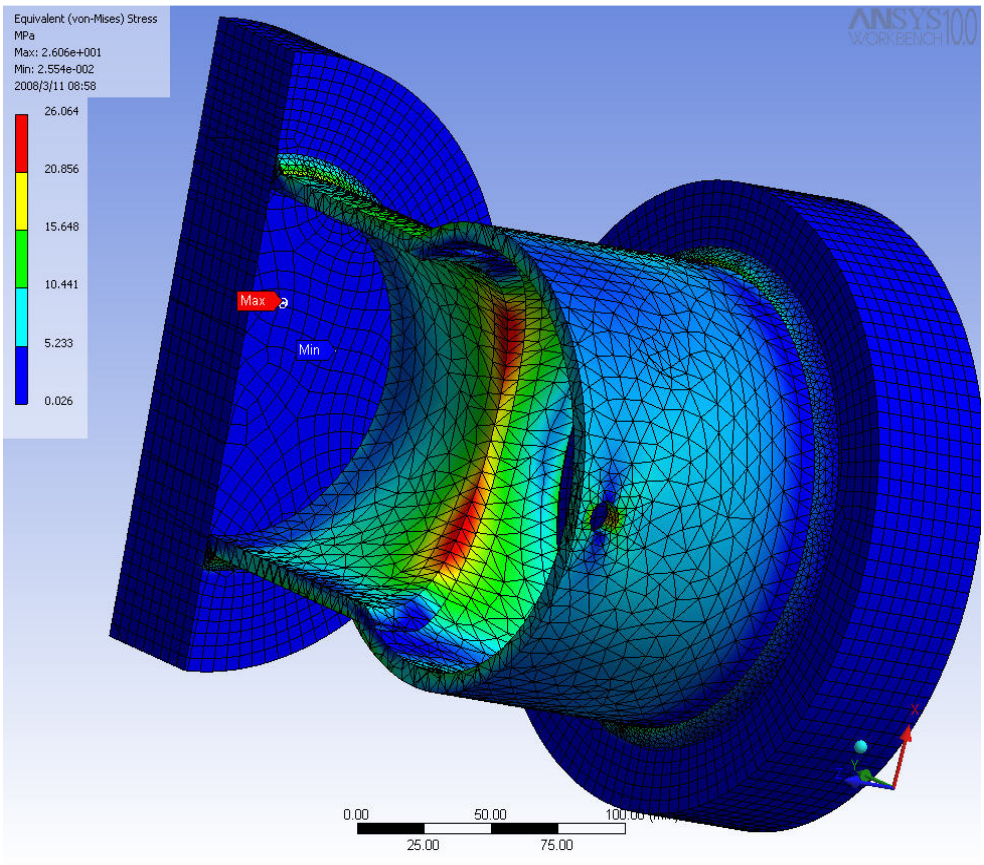

Figure 2.3 – ANSYS analysis of weld weak points.

2.1.2 Test Heaters

The heaters used for all experimentation are a 1x1cm 20-ohm resistor, provided by Component General Company. The heater was then soldered to a 1x1cm copper block (3mm thick) with epoxy surrounding the heater to ensure good insulation. 3M DP420 and DP460 epoxies were used for this experimentation. Type T thermocouples were embedded in the copper blocks at 1.5mm from the surface of the copper block. Wall temperature was calculated through the assumption of 1D conduction.

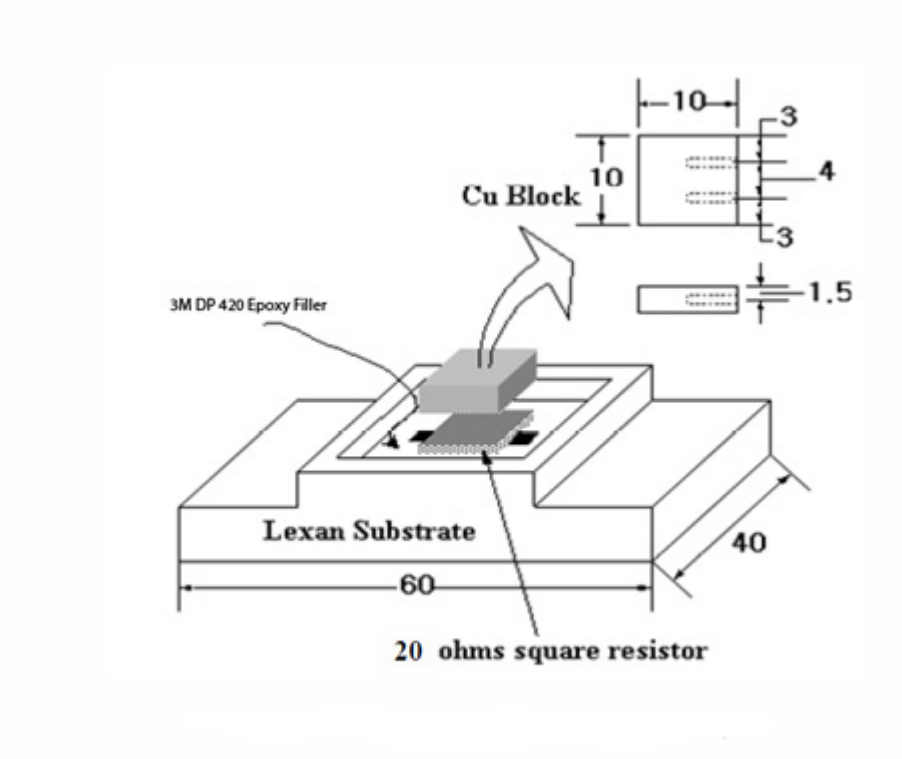

Figure 2.4 – Pool boiling heater assembly.

2.2 Wicking Test Procedure

Wicking tests were performed by coating a 1x4inch copper substrate. Under the recommendation of Van Oss [26], Hexane was chosen as it should have a contact angle of zero with metals. In fact, most of the alkane hydrocarbons should have a zero contact angle with metals. The sample was plunged into the fluid and the time taken to reach a predefined height was recorded. These measurements were then inserted into the Washburn equations, Eqn. 1.5, where the r-value is solved.

Obviously, the most meaningful data would be wicking tests with distilled water, but this proved impractical with the current equipment. Over 70% of the coatings did not seem to wick water at room temperature. Further examination under a microscope revealed the coatings were indeed flooded. Hence the coatings wicked, but the amount of fluid was not large enough to change the optical properties of the surface that would have allowed us to observe the fluid

movement. The coatings that were visually observed to wick did so in a random non-level advancement.

Using the limited amount of data with water, the r-value in the Washburn equation (Eqn. 1.7) is used to find the internal contact angle. To reiterate chapter 1, the r-value is a property of the material and does not change with changes in fluid properties. Wicking height and time as well as the hexane viscosity and surface tension are inserted into equation 1.7 resulting in the r-value. The water properties, wicking height, and time are inserted into equation 1.7 which results in the internal contact angle; this was found to be approximately 81º. With an estimate of the internal contact angle, we can use the Washburn equation to make projections of wicking heights at other temperatures.

After viewing the effect of temperature on contact angle results of Rajayi et al. [48] as well as some unpublished data, it was apparent that the contact angle of water only decreased by 7º-10° with a change in temperature from 20ºC to 90℃. This information and the previously determined data were used to make an estimation of the wicking height at 100℃. As shown in Figure 2.5, Hexane at room temperature simulates the behavior of water at 100ºC.

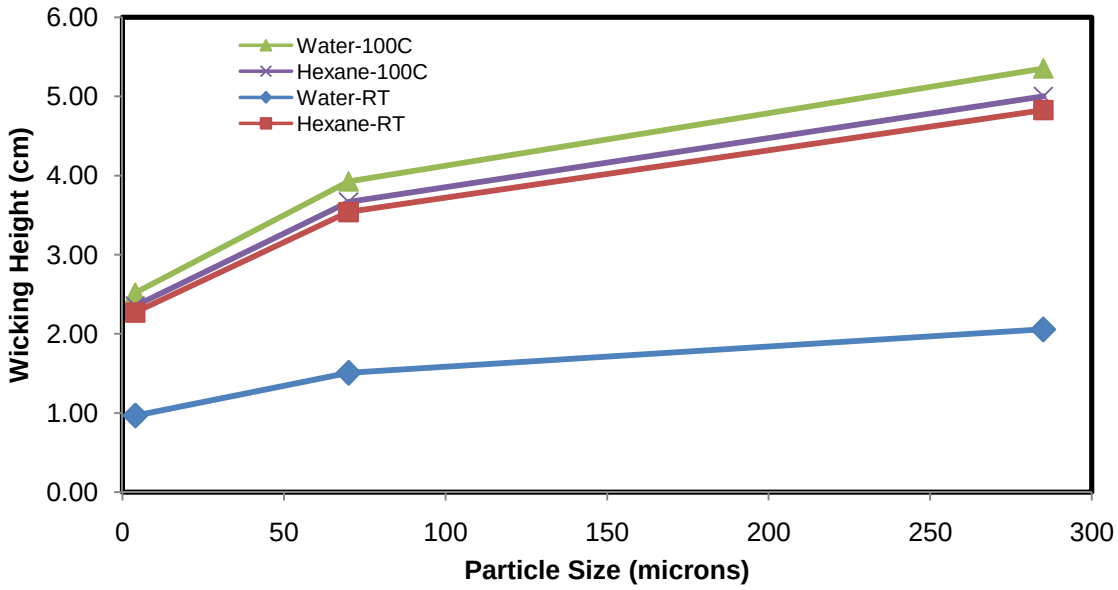

Figure 2.5 – Wicking Height projections based of the Washburn equation. RT: Room Temperature, 100C: T-sat:100℃

Hexane not only simplified many wetting/wicking equations, but it was highly visible as a wicking agent. Most importantly, it wicked in a level fashion which allowed the accurate measurement of the liquid advancement. While the wicking of water, the working fluid in all boiling tests, would be interesting data to collect, it simply was not visible to the naked eye.

The predefined distance (20mm) divided by the time gave the bulk velocity of the wick. Coating thickness multiplied by the substrate width multiplied by the bulk velocity gave the flow rate.

In order to solidify the validity of using Hexane, wicking tests were attempted at elevated temperatures. This was done by heating distilled water to 95ºC±1.5ºC. The coated surface was then heated just past 100ºC. The coated substrate was then slowly submerged into the water at which point small amounts of boiling occurred on the submerged portion of the substrate. The water quickly wicked up the exposed portion of the substrate. No precision measurements were taken due to the difficulty as well as uncertainty of this experiment. The observations made it clear that Hexane is a viable alternative. The 4µm particle coatings wicked the water very slowly (around 2mm/s) with only a light color change. The 285µm particle coatings exploded with wicking (around 10mm/s) with a very dark color change. Color change signifies the optical change where the darker the color, the more mass carried.

Wu [49] experimentally showed that the contact angle of water, and all other liquids tested on a polymer surface, increase or decrease on an average of .05deg/℃. However, as temperatures approach the boiling point the dynamic contact angles rapidly approached zero. He showed that since the adhesive forces can be ignored, this phenomenon is independent of the surface and is the result of the change in surface tension. This information sheds more light on how a coating either will not wick at room temperature or weakly wicks, yet wicks quite well at higher temperatures.

2.3 Contact Angle Measurements

Contact angle measurements were done through the use of a goniometer. 1x4inch samples were cleaned via 5% acetic acid in an ultrasound bath for 10-20min followed by 10min ultrasound in distilled water. A hotplate was used to slightly raise the temperature to evaporate all the water; a large cold plate was immediately used to cool the sample back down to room temperature. This process was repeated three times for each sample to ensure repeatability of measurements. If the measurement was not repeatable, the sample was considered dirty and re-cleaned. The sample was continuously re-cleaned until the contact angle stopped increasing compared to the measurement taken prior to the current cleaning.

Every sample was first cleaned before a contact angle measurement. This minimized the effects of adsorption. Acetic acid is considered the best cleaning agent for the coatings. Chavez and Hess [50] effectively showed that acetic acid not only removes oils and other contaminants, it removes all oxides. It was also shown that acetic acid will not etch the copper surface.

Xia et al. [51] proved conclusively that distilled water alone will not harm the copper surface. Once the samples were pulled from the acetic acid bath and immersed in distilled water, the passivation layer was recreated.

Previous lab researchers used acetone to clean the TCMC coatings. Kagwade et al. [52] demonstrated that acetone with copper, in the presence of ambient light, will grow copper acetate crystals. This will falsely indicate a much lower contact angle for the porous coatings. Copper acetate is thermally unstable and has no affect on the boiling curve.

In most cases it is impossible to measure a perfectly static contact angle on a porous surface. Very small amounts of wicking continuously occur which leads to the very slow decrease in contact angle. Thus, all goniometer measurements hence forth will be referred to as apparent contact angle. The apparent contact angle will be defined as the measure of the initial apparent contact angle and the subsequent transient angles.

2.4 Coating Fabrication

The new coating utilized brazing as the active binding process. The coating was named HTMC (High Temperature Microporous Coating). Most other porous coatings are destroyed at higher temperatures. This metallic powder binding process is thus dubbed high temperature as it can perform up to 677ºC. In addition to this current variant, simple changes can be made to push the max temperature above 1000ºC.

2.4.1 Brazing Process

Brazing was chosen as the active binding procedure in order to improve upon the soldering process previously developed. The difference between brazing and soldering is as follows:

- Brazing - is a group of joining processes that produce coalescence of materials by heating them to the brazing temperature that contain a filler metal having a liquidus above 840℉ (450℃) and below the solidus of the base metals.
    - Almost any material can be bonded together. Metal is easily bonded to all types of ceramics.
    - Often requires a controlled environment.
    - Given the correct environment, no flux is used.
    - Very strong bond, used for structural applications.
- Soldering – the same definition as brazing except that the filler metal has a liquidus below 840℉ (450℃) and below the solidus of the base metals.
    - Limited materials can be bonded to each other.
    - Flux must be used.
    - Often weak bond, no structural applications.

A reduced oxygen environment was required when brazing with the particular compositions used in this thesis. Using a Sentrotech oven (max temperature 1200ºC), nitrogen was pumped into the chamber and maintained for the entire duration of the brazing process. The oven chamber dimensions were 6x7x8inches. Even this small chamber required a large quantity of gas. Liquid nitrogen tanks were required to produce sufficient gas required throughout the entire brazing process. A typical brazing process is as follows:

1. 8 minute ramp up from room temperature to 65ºC.
2. Hold for 21 minutes at 65ºC.
3. 60 minute ramp up to 727ºC.
4. Hold for 5 minutes at 727ºC.
5. Nitrogen cool.

2.4.2 Mixture Ratios

These ratios were found to work best for each type of coating. The strength of bonding was determined via 60 minutes in an ultrasound bath. If less than an approximate 5% of particles detached from the surface, the coating was considered satisfactory. Also, coating uniformity was examined under a microscope to determine performance of each coating.

Table 2.2 – Composition ratios used for all porous coatings.

	Cu to paste	Oil to total mass	Average Particle Size (µm)
HTMC-Ag505	2	.172	70
HTMC-Cu07	2	.233	4
HTMC-Cu07	2	.167	70
HTMC-Cu07	1.8	.225	285
TCMC	2	NA	70

2.5 Particle Size Distributions

While the metal powder distributor stated an average particle size, this was based on the probability from a mesh. SEM photos were taken to obtain our own particle size stats. Image processing software was used to measure the diameter of many particles and then statistical analysis was used to obtain a histogram.

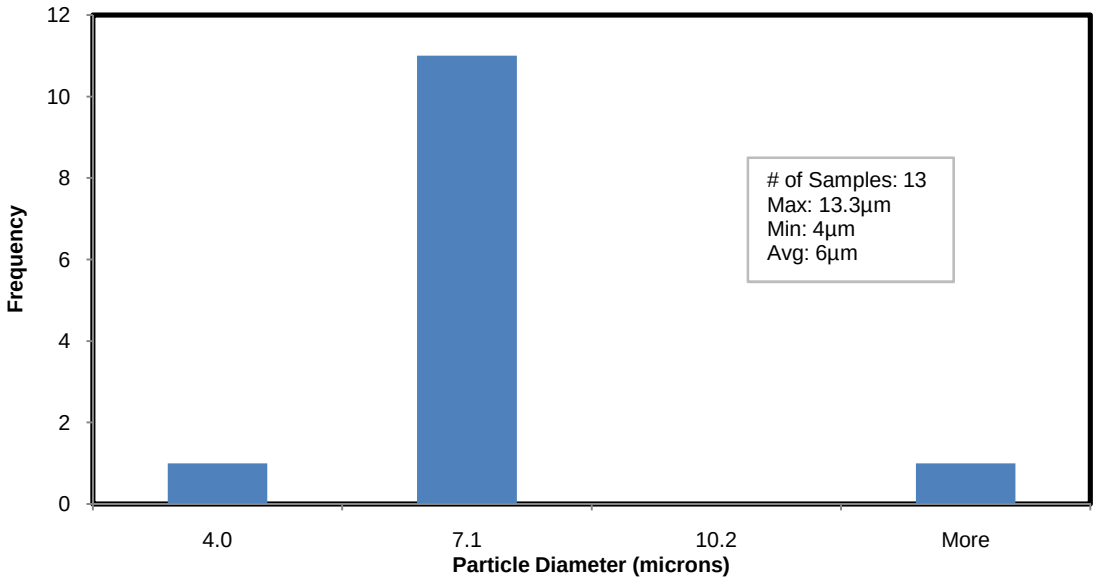

Figure 2.6 – Particle size distribution of rated 4µm particle.

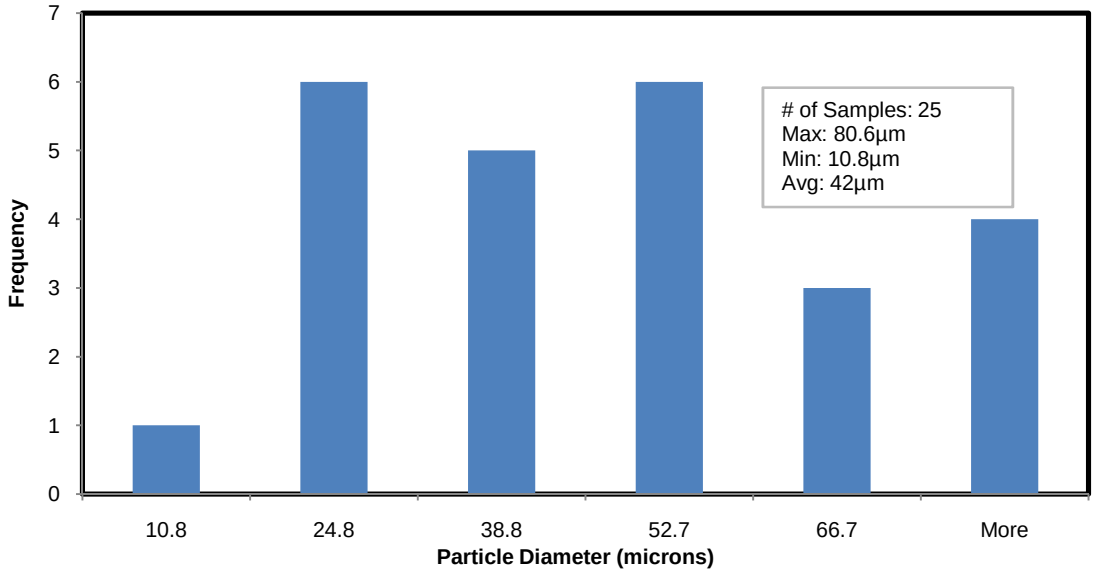

Figure 2.7 - Particle size distribution of rated 70µm particle.

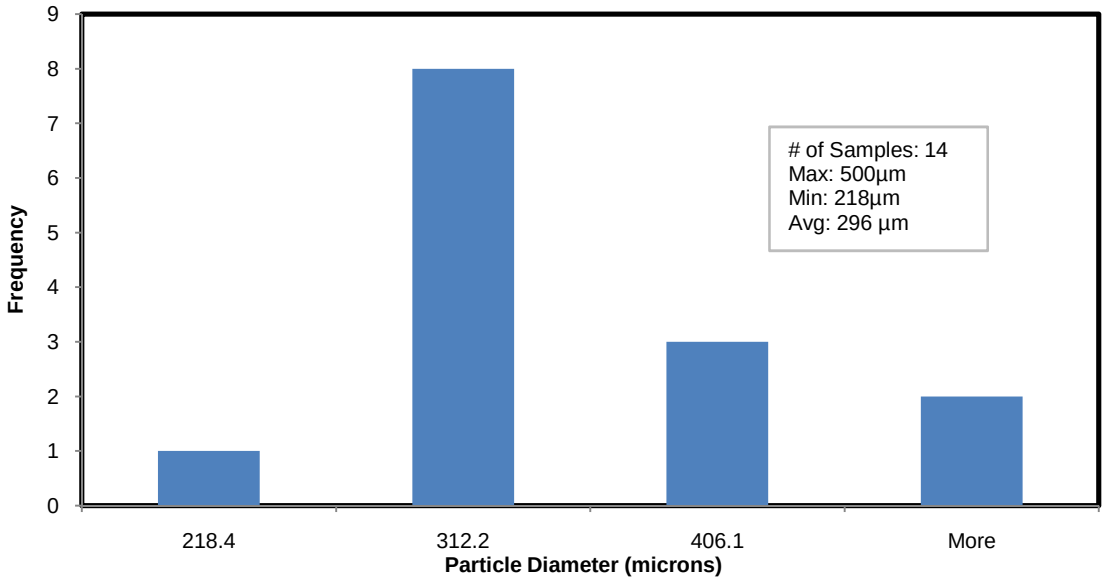

Figure 2.8 - Particle size distribution of rated 285µm particle.

2.6 Uncertainty Analysis

The pool boiling heater setup was identical to that used by Kim et al. [7] and O'Connor et al. [53]. Thus, the heat flux uncertainty was estimated at ±.08W/cm^2 for values around .5W/cm^2 and ±6% for values ranging from 16-120W/cm^2. The uncertainty of the temperature measurements was ±.5ºC.

As for the wicking and wetting measurements, tests were run on at least three separate samples of each coating configuration. A minimum of five measurements of each sample were taken for both wicking and contact angle tests. A t-distribution was assumed and the confidence interval was calculated from these values. As stated before, all samples were cleaned with 5% acetic acid in an ultrasound bath for 10-20 minutes followed by 10 minute ultrasound, distilled water bath. Thicker coatings (>400µm) often required 40 minutes in the ultrasound to fully clean. This process was repeated before each measurement to ensure no corrosion, oxidation, and/or adsorption interfered with the measurements. The largest bulk speed uncertainty was ±1.6mm/s for the 285µm particle size. An uncertainty of ±1.3 mm/s and

±1.2 mm/s for the 70μm and 4μm particle sizes was evident. This proved satisfactory for our experimentation. Most of this error stemmed from the randomness of a coating. Using the rules of propagating error, the uncertainty of the volume metric flow was ±11 mm^3/s. Coating thicknesses were determined through the use of a micro-meter. This left us with an uncertainty of ±15μm. All steady-state (static) apparent contact angle measurements had an uncertainty of ±7º. This error stems mostly from the random nature of porous coatings. The thickness uncertainty is thought to have minimal effect on the contact angle uncertainty.

CHAPTER 3

WETTING VS. WICKING

Contact angle measurements are generally, static measurements. Since boiling is a highly dynamic physical phenomenon, it seems illogical to assume that a static measurement can predict a dynamic activity. There is a somewhat new area called dynamic contact angles. This is the contact angle a fluid exhibits when forced to move at some velocity. This is not considered in this work and is left for future researchers.

Wicking is a dynamic measurement which seems much more applicable to boiling predictions. Both the wicking and apparent contact angles are measured as to quantitatively determine whether either is useful in boiling.

3.1 Apparent Contact Angle

The apparent contact angles for each particles size are shown in Figures 3.1, 3.2, 3.3, and 3.4. Each plot shows both the apparent contact angle as well as the base area of the sessile drop.

If the coating is sufficiently thin, the wicking capacity will be minimized. An indication of this is through the base area. If the base area quickly increases, the sessile drop is spreading over the top of the porous coating [54]. If the base area stays relatively constant, then the coating structure now has a large enough capacity to quickly wick the fluid away. It is again noted that the contact angle is never truly static since wicking cannot be completely removed from the porous structure.

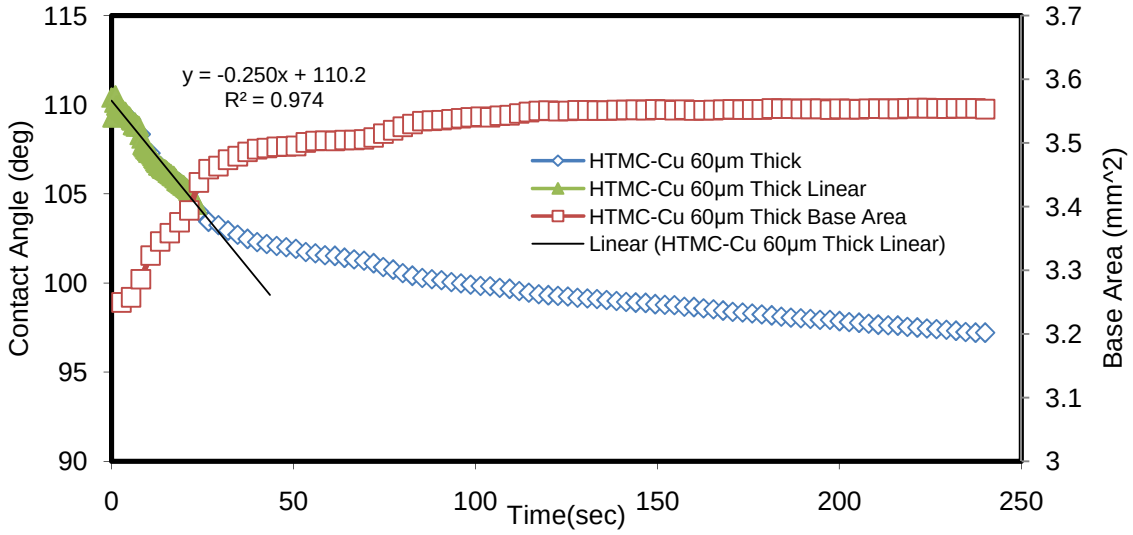

Figure 3.1 – Apparent contact angle of the 4µm particle size.

The dynamic characteristic associated with the first 30 seconds of each measurement theoretically may hold more meaningful information than the remaining measured time. Boiling is a very fast exchange of vapor and liquid, measurements taken after 2 or 3 minutes might be meaningless. In an effort to characterize in detail the difference between each apparent contact angle, a line regression was applied to the linear part of each particles size. The slope of these line regressions are tabulated in Table 3.1. Comparing Table 3.1 to Figure 3.4, the same trend was observed for both the fast and slow parts of the apparent contact angle measurement.

Table 3.1 – Slope of apparent contact angle line regressions applied to each particle size.

	4µm	70µm	285µm
Slope(negative deg/s)	.25	.3	.83

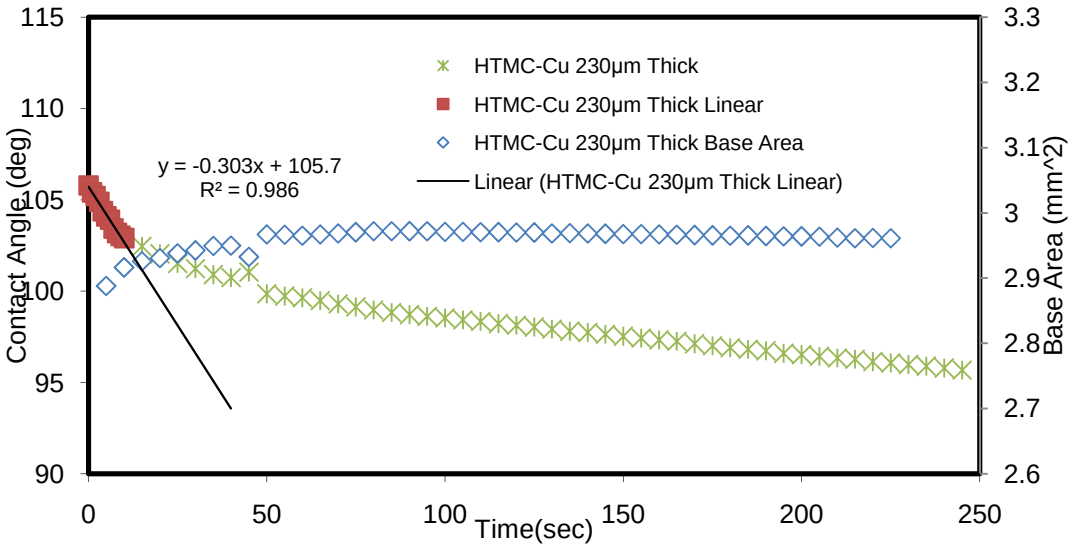

Figure 3.2 - Apparent contact angle of the 70µm particle size.

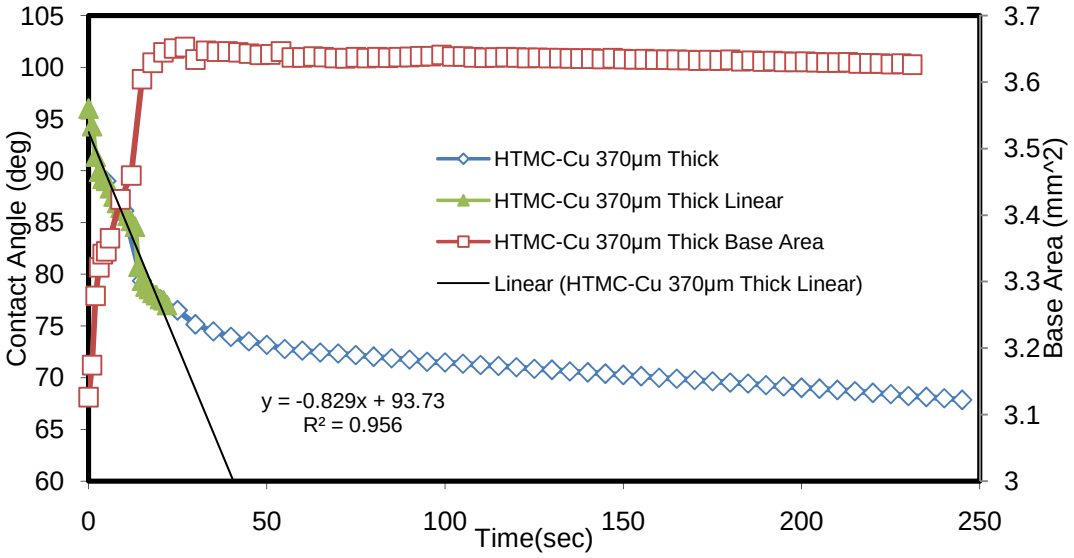

Figure 3.3 - Apparent contact angle of the 285µm particle size.

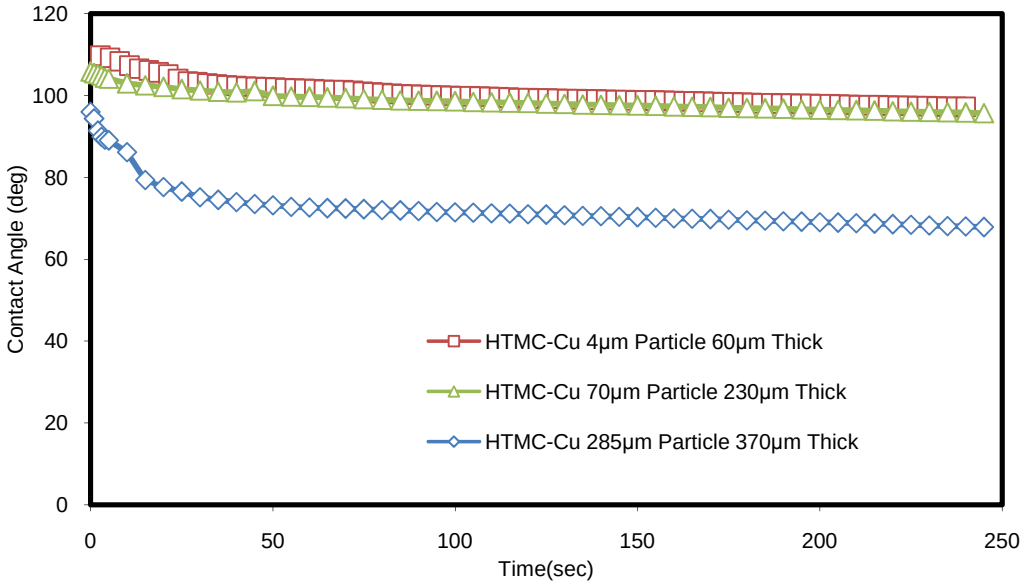

Figure 3.4 - Apparent contact angle of all particle sizes.

The 285µm coating exhibited a lower apparent contact angle due to the large pore size. The pores created by the 285µm particles allowed the fluid to easily reach the substrate. Thus according to Wenzel, Eqn. 1.4, increased surface area will lead to a decrease in contact angle. Even though smaller particles will offer a larger surface area, the fluid cannot effectively penetrate the pores compared to larger particles. Hence, the substrate has a greater effect on the sessile drop for larger pores.

Figure 3.5 illustrates two different wetting regimes. In Figure 3.5a, the sessile drop fluid rim spreads over the surface of a porous coating according to Fick's law of diffusion in Poiseuille flow. The central drop spreads according to a power law relationship [55]. The fluid may also spread (wick) internally as shown in Figure 3.5b under Fick's law in Poiseuille flow. The 285µm coating spreads the fluid, regime A, quicker than the other particles sizes. This indicates the fluid is in contact with a greater surface area that needs to be balanced according to the Young equation, Eqn. 1.1. For a given particle size, theoretically, increasing the thickness of a coating will lead to regime B. Due to the low density of pores, thin coatings spread in regime A since the sessile drop will meet the substrate surface and thus become

balanced in the y-direction. Thick coatings should increase the number of pores and overall surface area requiring additional balancing in the y-direction since the sessile drop will now meet many more particles instead of the substrate. Hence, there are many more paths for wicking to take place. As long as the intrinsic contact angle is hydrophilic, either regime A or B is possible. If the intrinsic contact angles switches to hydrophobic, the fluid will never penetrate the coating.

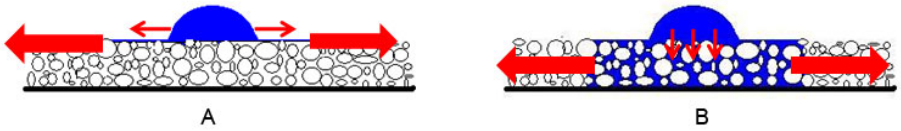

Figure 3.5 – A) Fluid Spreading over top of the porous coating B) Fluid spreading thorough the interior of the porous coating. Images provided by Amaya **[56]**.

Wang and Dhir [57] found that a reduction in plain surface contact angle, by oxidation, reduced the nucleation site density. A nucleation site density change due to wetting may not apply for porous surfaces. A more likely cause for boiling degradation in porous media is the change in hydraulic resistance. Poisuille flow determines the hydraulic resistance defined as the resistance a fluid must overcome in a pore. Where the flow velocity is defined as [41]:

$$U = -\left(\frac{d_h^2}{2P_0\eta}\right)\frac{\Delta \mathrm{P}}{\Delta \mathrm{R}}$$

P_o is the Poisuille number, d_h is the hydraulic diameter of the pores, and R is the radius of spreading. If we insert capillary pressure into this equation, assuming circular pores, we obtain:

$$U = -\left(\frac{d_h}{2P_0\eta}\right)\frac{\gamma \cos\theta}{\Delta \mathrm{R}}$$

It is apparent that for a given intrinsic contact angle, the particle size will determine the pore size which dictates the rate of spreading. This equation is equivalent to Eqn. 1.8 derived by Washburn.

Many features affect the overall hydraulic resistance. The overall resistance is a combination of path bends, contractions, expansions, thermocapillary flows, et cetera. The quantity of these parameters will increase with increasing coating thickness and cause greater impedance to exit vapor flow. The reader is forwarded to Bear [58] who extensively analyzes resistances in porous media.

Wetting experts will question how a roughened surface, with hydrophilic intrinsic contact angles, can result in an apparent contact angle higher than 90º. This violates both the Wenzel, Eqn.1.4, and Cassie-Baxter, Eqn. 1.5, equations. This is made possible due to a huge contact hysteresis. Unfortunately, our software could not measure the dynamic angles. The reason for the huge hysteresis is far beyond the scope of this thesis.

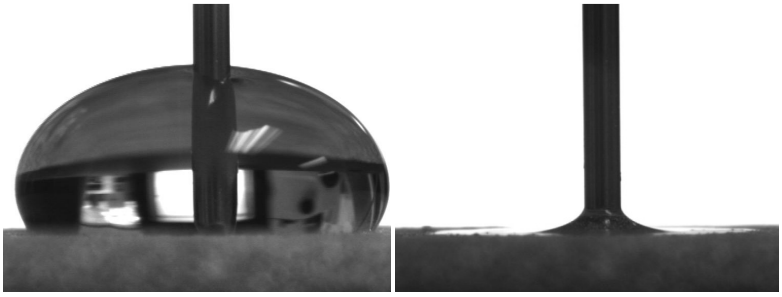

Figure 3.6 - The large and extremely small advancing and receding contact angles measured for the microporous coatings.

3.2 Wicking Results (Hexane)

As stated in chapter 2, the vertical bulk wicking speed was calculated by measuring the time required to travel 20mm. Figure 3.7 displays the wicking speeds of all coating configurations. While each particle exists in its own speed band, coating thickness had no affect on the speed. No matter how thick or thin the coating was made, the speed of wicking showed no significant change. This is of course what the Poisuille flow predicts. If the overall cross sectional area is increasing with a constant speed, then the volumetric flow must be increasing, as shown in Figure 3.8. Flow rate is found by multiplying the bulk velocity by coating cross sectional area. Observing the flow rate data in Figure 3.8 brings up a reasonable question: what affect did the particle size have on the wicking? Figure 3.7 implies that the

wicking speed depends on the particle size. Yet, Figure 3.8 indicates that the flow rate may depend much more on the thickness of the coating rather than the particle size. Increasing the particle size may increase the sensitivity of thickness on flow rate. In other words, the 285µm particles noticeably change with changing thickness where the 4µm particles negligibly change with any change in thickness.

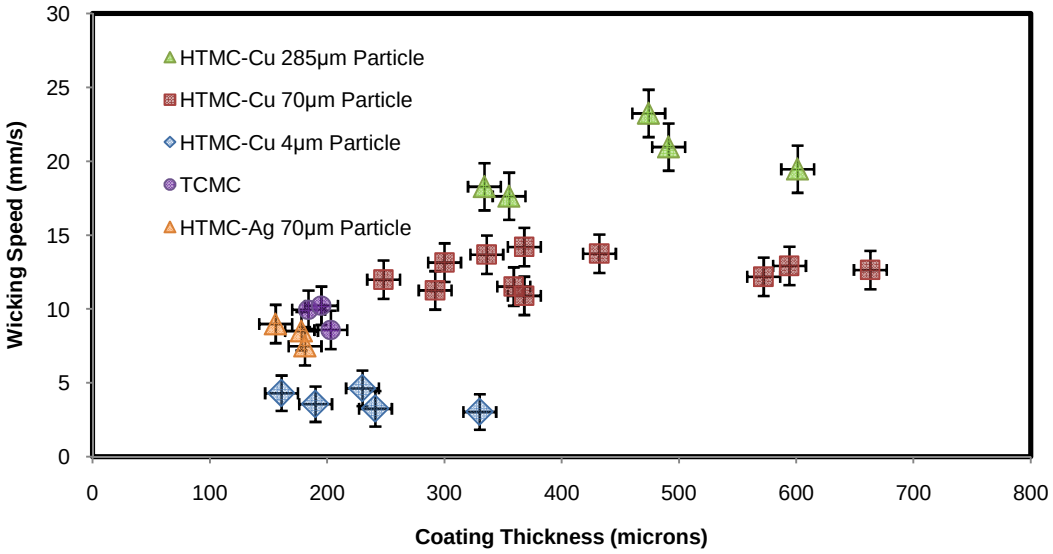

Figure 3.7 – Vertical wicking speed of each particle size, measured in Hexane.

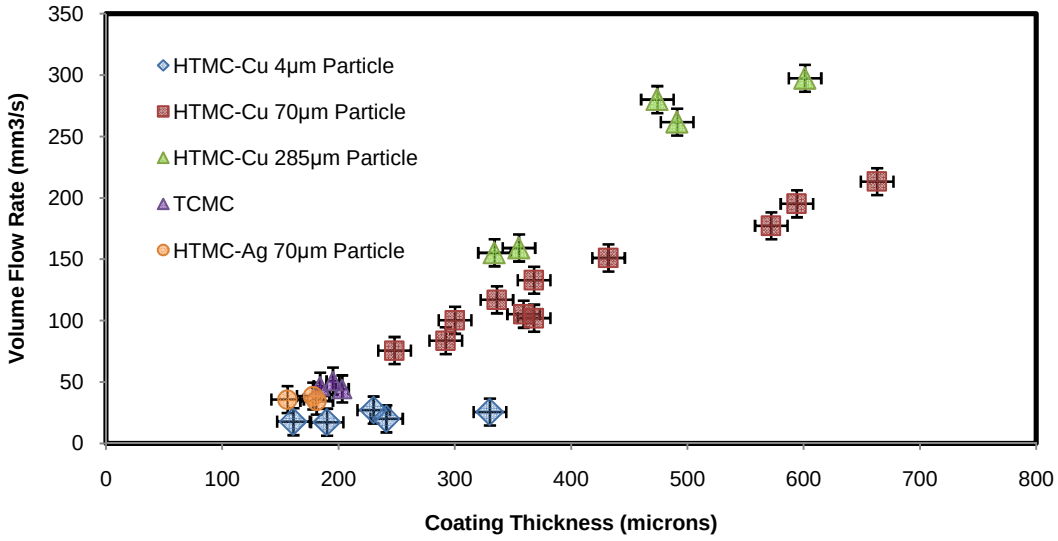

Figure 3.8 - Volumetric flow rate of each particle size, measured in Hexane.

CHAPTER 4

EFFECTS OF PARTICLE SIZE

The HTMC-Cu coatings were created with three different particle sizes, 4μm, 70μm, and 285μm. Kim et al. [7] had already determined the 70μm particle to be the optimal size in water. Large particle size differences were used in this thesis in order to fully observe the effects of wetting and wicking throughout boiling. Each particle exhibited its own unique characteristics. The 4μm particle consistently had a secondary enhancement. The 1st Run, initial boiling test, of the 4μm particles resulted in an erratic boiling curve doubling back on itself. If the test was immediately run again, Run 2, the coating suddenly performed several degrees cooler and was no longer erratic in behavior. This phenomenon was not observed for the 70μm and 285μm particles sizes. The 285μm particles displayed an ultra high CHF when compared to the 4μm and 70μm. This was found to be explainable through the wicking rates of each coating.

4.1 Effects of Particle Size on Nucleate Boiling

4.1.1 Rewetting Phenomenon

Testing of the 4μm particles sizes revealed a shifting phenomenon. The 1st Run of all tests resulted in a somewhat erratic curve where boiling efficiency continuously improved. If the boiling test was immediately rerun, the curve was improved by an approximant 4℃. This shifting is depicted in Figure 4.1.

Time tests were performed in order to characterize this phenomenon. The coatings were held at T-sat: 80℃ for a specified amount of time and then retested. In Figure 4.2, we see that the performance of the coating approaches that of a plain surface if left in the fluid over a long period of time. Every follow-up run always shifted the curve back to that of “Run 2.” The

70µm particle size, Figure 4.3, exhibited a much less pronounced version of the shifting phenomenon. The 285µm particle size, Figure 4.4, exhibited almost no changes with time.

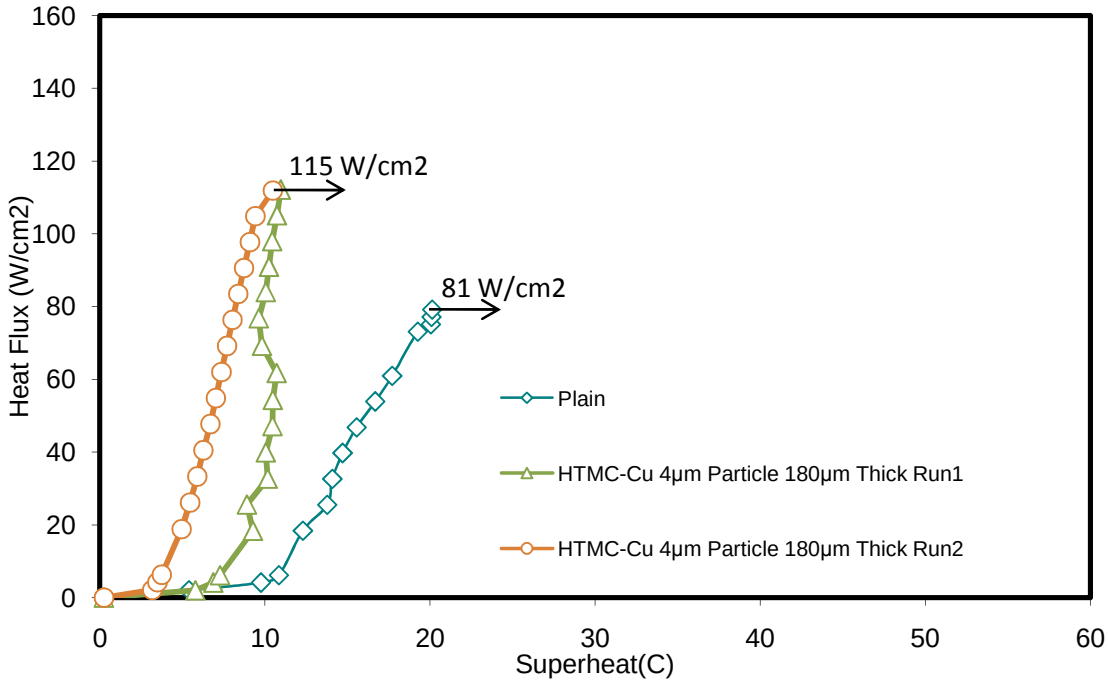

Figure 4.1 – 4µm boiling tests displaying the shifting effect. T-sat: 80℃

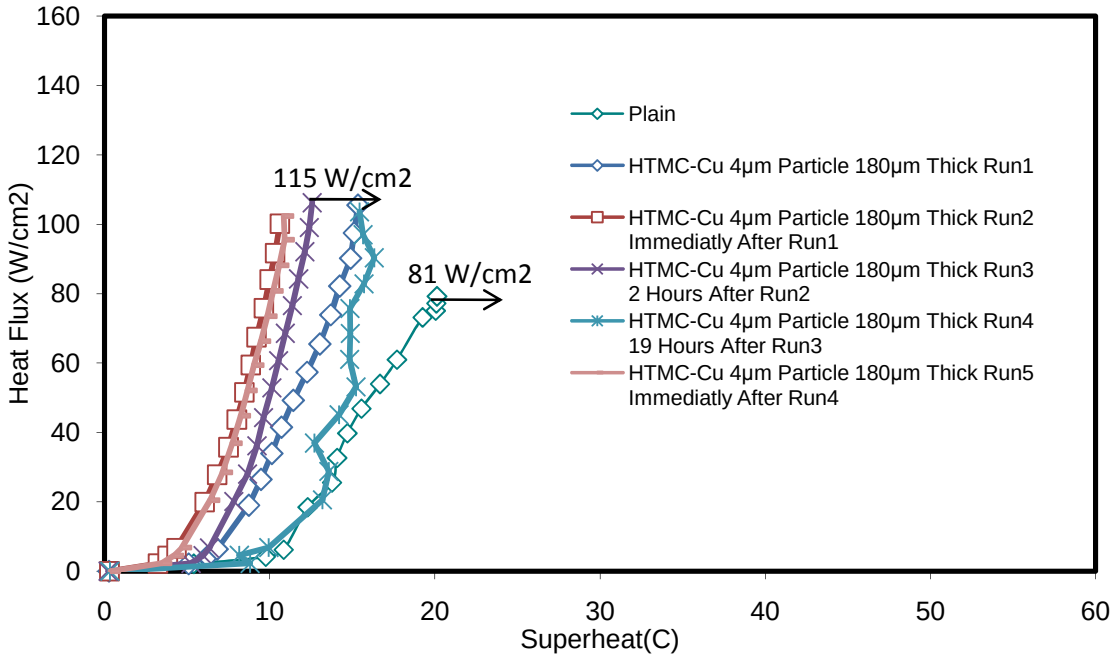

Figure 4.2 – Time tests of the 4µm particle rewetting phenomenon. T-sat: 80℃

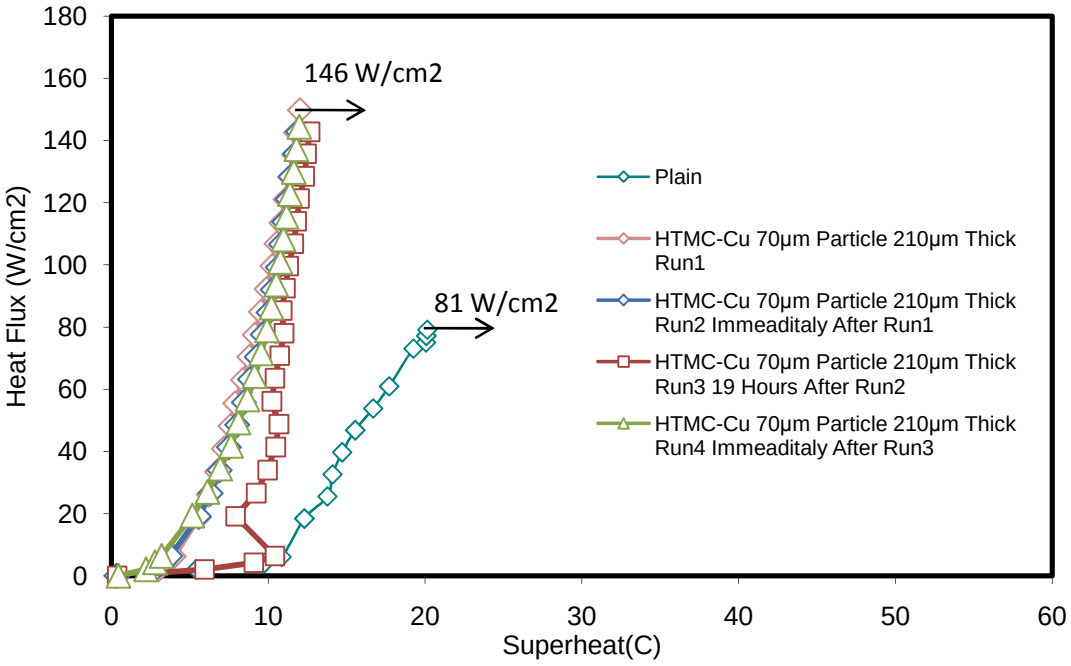

Figure 4.3 - 70µm particle boiling tests displaying the shifting effect. T-sat: 80℃

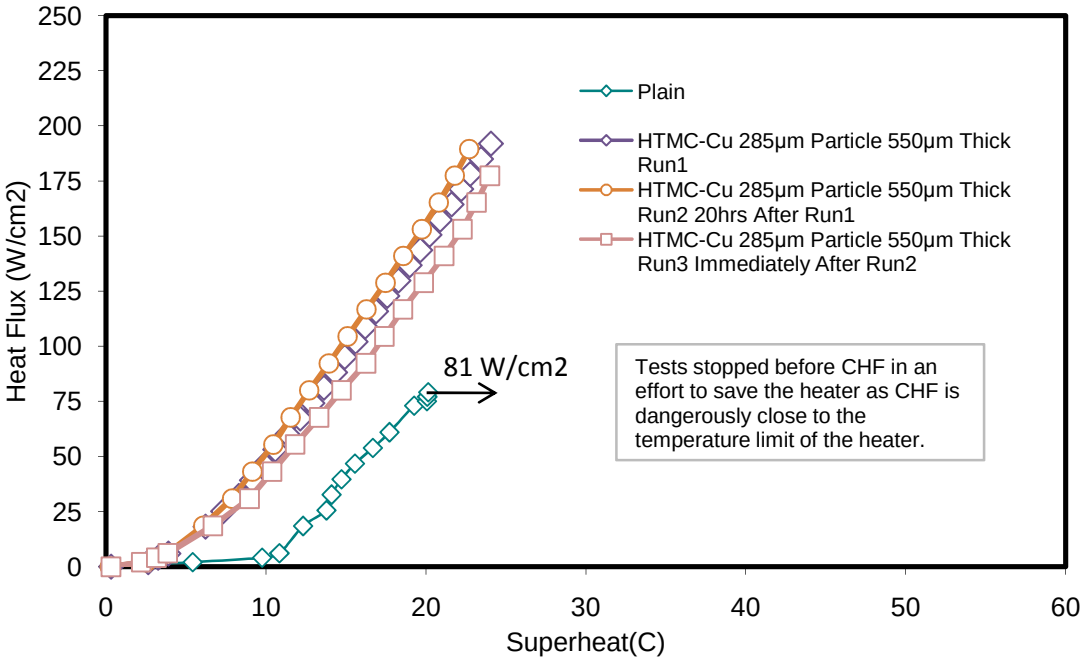

Figure 4.4 - 285µm boiling tests displaying the shifting effect. T-sat: 80℃

The cause of this effect can be explained in two parts. First, we investigate why the incipience is different for each particle size. Second, we observe the effects of condensation on each coating. In the following, we compare only the first runs of each particle size. As was determined by Kim et al. [7], there exists an optimum particle size depending on the working fluid. Solving a simple force balance on a bubble shows:

$$\Sigma F = 0 = P_l A_c - P_v A_c + \gamma P_p$$

$$P_v - P_l = \frac{\gamma P_p}{A_c}$$

$$P_v - P_l = \frac{\gamma \pi d}{\pi d^2}$$

$$P_v - P_l = \frac{\gamma}{d} \qquad \textbf{Eqn. (4.1)}$$

As the particle size decreases the pressure required for departure increases. Using Equation 4.2, derived in [24] and plotted in Figure 4.5, we find that the embryonic bubbles at 80℃ saturation temperature and assuming superheats around 10ºC require a cavity diameter of ~6.5μm.

$$r^* = \frac{2\gamma T_{sat-P-l} v_{lv}}{h_{lv}[T_l - T_{sat-P-l}]} \qquad \textbf{Eqn. (4.2)}$$

The 4μm coating requires a greater superheat to initiate boiling and incipience is shifted to the right when compared to the 70μm coatings. The time tests for the 70μm coatings, Figure 4.3, also exhibit erratic incipience behavior, albeit only after a 19 hour waiting period. The 285μm particle coatings never exhibited incipience problems since the coatings contained larger cavities. Equation 4.1 states that the embryonic bubbles of the larger cavities will have less required superheat for incipience than the 70μm and 4μm coatings.

The 285μm coatings were observed to perform worse than the 70μm coatings due to the poor vapor removal rate. Increasing the thickness of porous coatings is observed to increase the hydraulic resistance, see chapter 3 and You et al. [3] for more examples.

Consequently, it is more difficult for the vapor to escape the coating which reduces the overall boiling efficiency since less fluid is available for latent energy transformation.

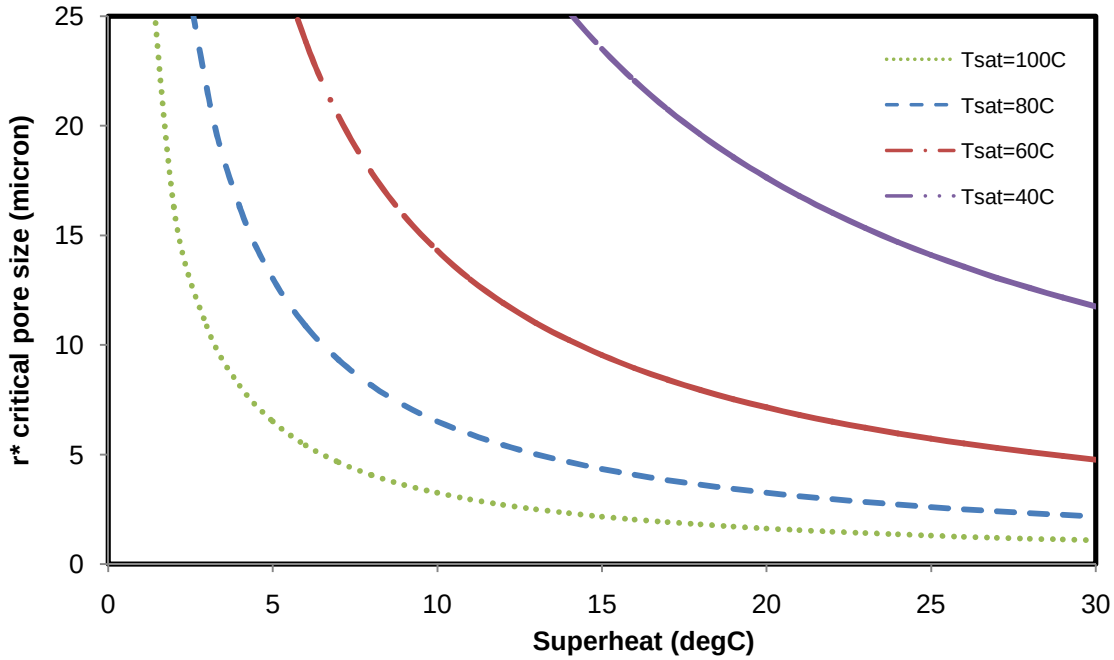

Figure 4.5 – Critical pore radius needed for nucleation.

Explanation of why 4μm coatings initially performed worse than the 70μm coatings was caused by test procedure. Degassing and achieving equilibrium temperatures of the test section takes more than an hour to complete. In this time, the vapor pockets of 4μm coatings were greatly decreased. As the vapor pocket within a cavity condenses it will decrease in size. Equation 4.1 states that this process will be faster with decreasing particle size since the pressure in a bubble will increase creating increasingly subcooled conditions.

After CHF or high heat flux, vapor still existed within the cavities of the 4μm coating and an immediate rerun of the test shifted the curve to the left due to increased nucleation site density. The shift caused by the cavity condensation took much longer for the larger cavities of the 70μm coating in which the effects were only observable after 19 hours. The comparatively ultra large particles of the 285μm coatings were never observed to have nucleation sites "shut-off" from condensation.

4.1.2 Extended Surfaces

Rainey and You [21] explored boiling with extended surfaces. They effectively showed that extended surfaces will shift the natural convection curve upward due to the use of the base area instead of the actual exposed area. The same method was used here to determine whether or not the 285μm coatings (thickest coatings used in this thesis) acted like an extended surface. The results are shown in Figure 4.6 where no evidence of an extended surface is found.

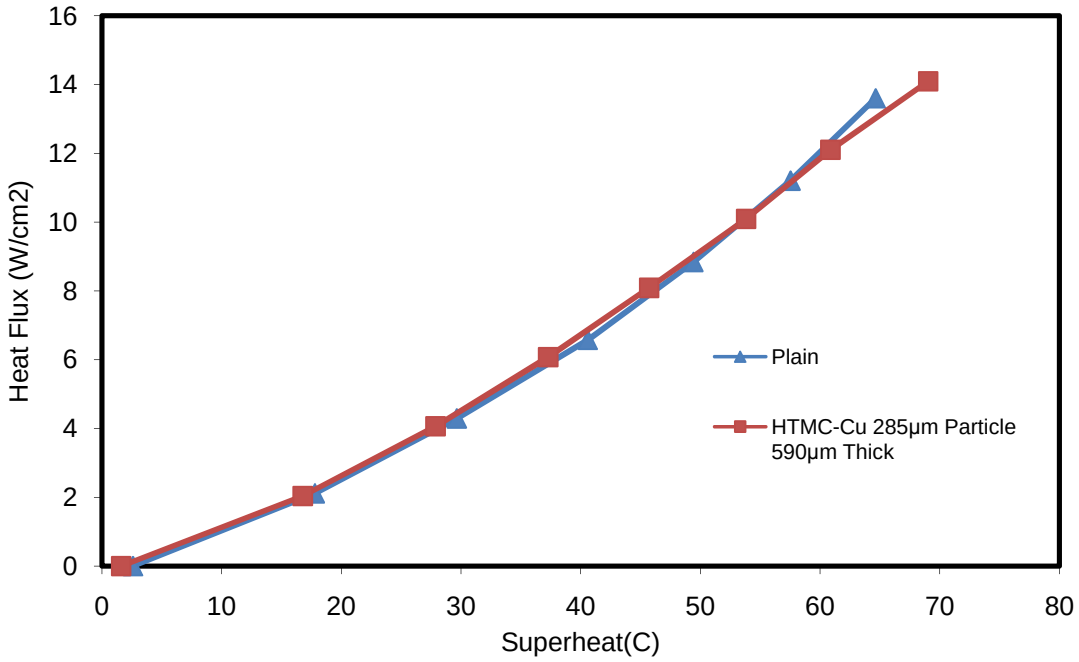

Figure 4.6 – Natural convection curve, open to atmosphere, T-bulk is 30℃.

4.1.3 Comparison of Particle Sizes

Figure 4.7 displays the boiling comparison of all particle sizes. Only the 2nd Run of the 4μm coatings are shown since the 1st Runs are erratic. The 2nd Run of the 4μm coatings performed almost identically to the 70μm coatings. The nucleation site density available during the 2nd Run, 4μm coatings must be similar to the 70μm coatings. From an application perspective, despite the fact that the 4μm, 2nd Runs perform well, the shifting of the 4μm coatings will create unreliable performance.

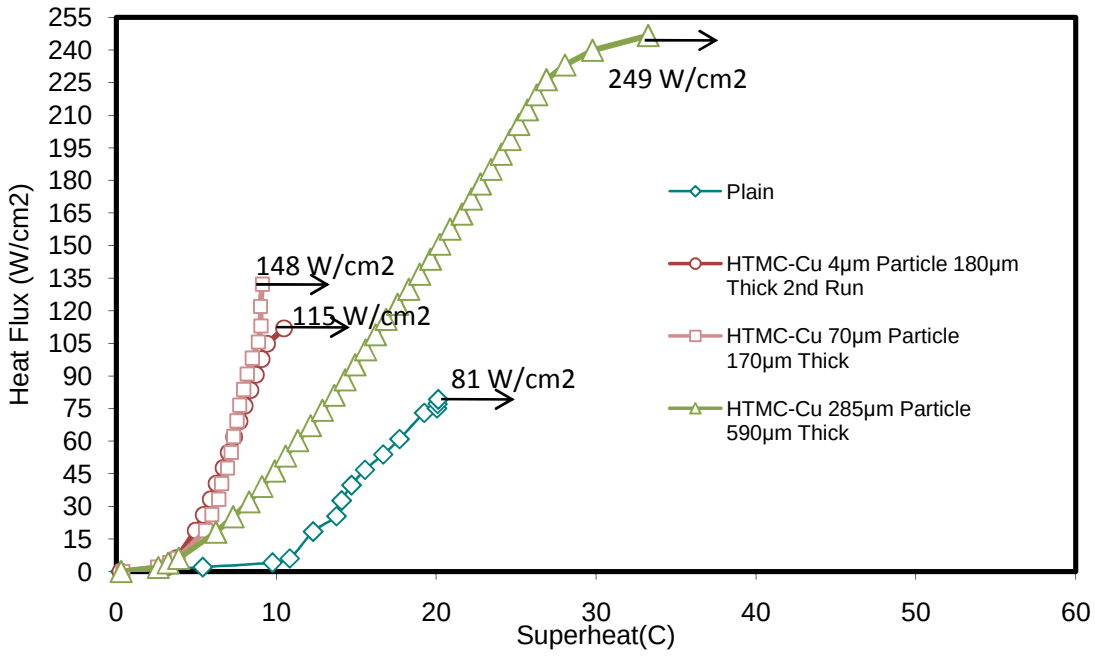

Figure 4.7 – Boiling curve comparison between HTMC-Cu particle sizes. T-sat=80℃, water.

The heat transfer coefficient of each particle size is plotted in Figure 4.8. The 2nd Run, 4µm coatings more closely resembled the profile of the 70µm particle sizes. Both the 4µm and 70µm demonstrate exceptional performance providing at peak heat transfer ~183% and ~295% nucleate boiling enhancement, respectively. The 285µm coating does not quite perform as well providing at peak heat transfer ~114% nucleate boiling enhancement.

By reviewing the apparent contact angle data it was observed that the 4µm and 70µm wetting profiles were quite similar. The 2nd Run of the 4µm and the 70µm coatings did indeed have similar boiling curves and the 285µm coating performed worse. It appears that the apparent contact angle may reflect the nucleate boiling performance. As section 3.1 describes in detail, better wetting is caused by the fluid contacting a greater surface area. Additional surface area indicates there are additional structures for vapor to become impeded on its way out of the coating. The large thickness of the 285µm coatings is unavoidable due to the large particle size, thus vapor impediment is unavoidable. This phenomenon is illustrated in Figure

4.9. This idea and the decreased nucleation site density of large particles caused the boiling performance of the 285μm coatings to be inferior to the 4μm and 70μm coatings.

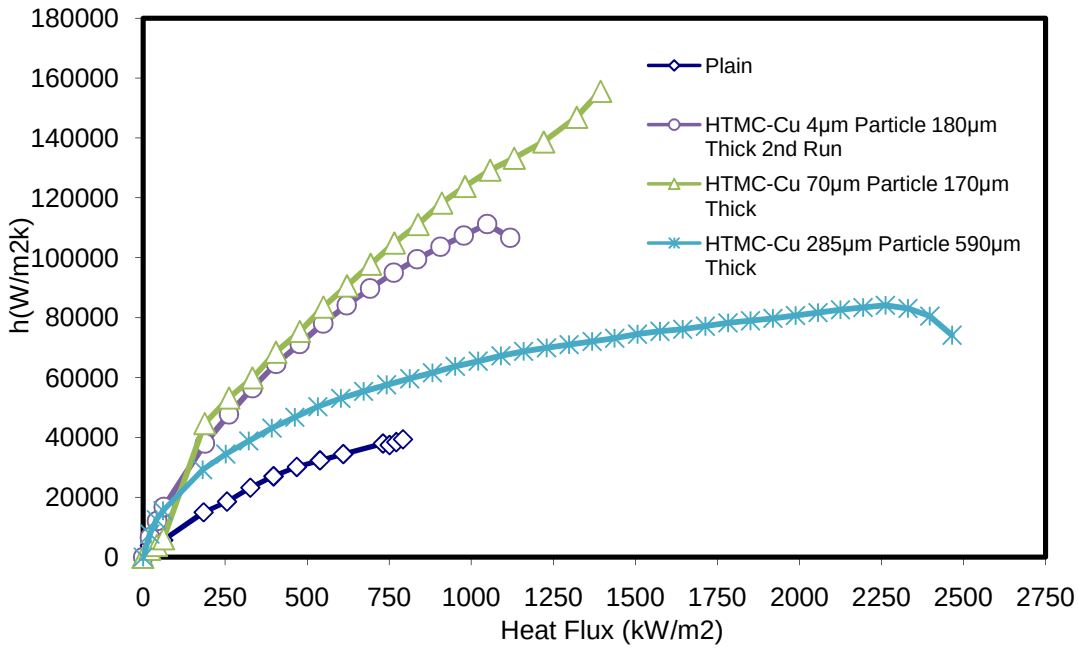

Figure 4.8 – Heat transfer coefficient of HTMC-Cu particle sizes. T-sat=80℃, water.

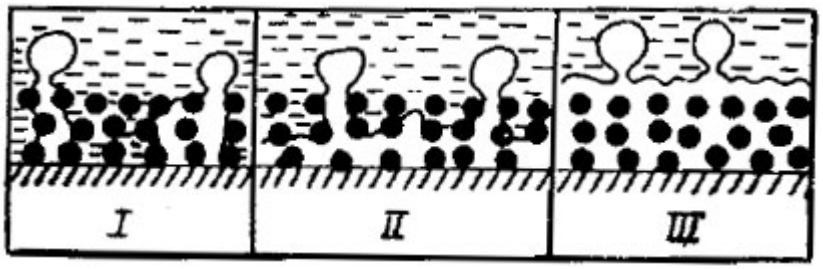

Figure 4.9 - Regimes present in very thick porous coatings 1. Low heat flux regime, normal nucleate boiling in a porous coating. 2. Higher heat fluxes lead to a vapor film within the coating. 3. The familiar CHF symptoms occur once the interior vapor film grows beyond the thickness of the coating. Taken from Malyshenko **[1]**.

4.2 Effects of Particle Size on CHF

The effect of the wicking is very obvious in Figure 4.7. The wicking speed and volumetric flow rates, in Figure 3.7 and 3.8 respectively, were least for the 4μm coatings and greatest for the 285μm coatings. The same trend is observed in the CHF. Increased flow rate means that there is more mass that needs to be converted into vapor. The limiting factor of the 4μm coatings is the rate at which liquid can be transferred back to the dry spots. The limiting factor for the 70μm and 285μm coatings is a little more complicated and is discussed in chapter 5. Another name for the 4μm limiting factor is the well known “wicking limit” previously discussed in chapter 1. At a certain heat flux, fluid mass is removed (transformed to vapor) much quicker than can be supplied. A hydrodynamic ensures since vapor speed is increased with heat flux yet the wick speed is basically constant. If the wicking speed or volume is increased then the CHF should increase as seen in the 70μm and 285μm coatings.

CHAPTER 5

EFFECTS OF COATINGS THICKNESS

Chapter 4 told us how the particle size affected the boiling heat transfer, but due to the physical limitations of the 285μm particles, a coating thickness below 300μm was unachievable. Thus we will now explore how the thickness of the coatings affects the coatings. This type of study has already been done for mesoporous surfaces by Li and Peterson [22]. Unfortunately, they were not concerned with any type of wicking measurements. Similar to Li and Peterson, increases in our coating thicknesses resulted in an increase in CHF. They attributed this to various parameters including wicking and fin effects. Our coatings are not nearly thick enough to simulate fin effects as discussed in section 4.1.2. Through wicking and wetting measurements, we can explain this particular boiling phenomenon.

5.1 Wetting and Wicking Measurements

5.1.1 Apparent Contact Angle Measurements

Increasing the coating thickness resulted in a different regime of apparent contact angle behavior. The two types of regimes are described in section 3.1. Figures 5.1 through Figure 5.4 display the measured apparent contact angles. Take note of the different x-scales used in the plots. The difference between the coating in Figure 5.1 and Figure 5.2 is about 570μm thickness. The sessile drop no longer spreads over the top of the coating, but is absorbed in and wicked away in several orders of magnitude faster compared to the thin coatings. The regime change is marked by the base area no longer increasing with time (not spreading on top of coating); it stays relatively constant until the last remnants of fluid are wicked away. A gradual regime change is shown in Figure 5.3. As stated in chapter 3, the increased wetting should indicate an increased hydraulic resistance. For porous media, increasing the wetting

should lead to boiling degradation. Figure 5.3 leads us to predict that the increased thickness will lead to nucleate boiling degradation.

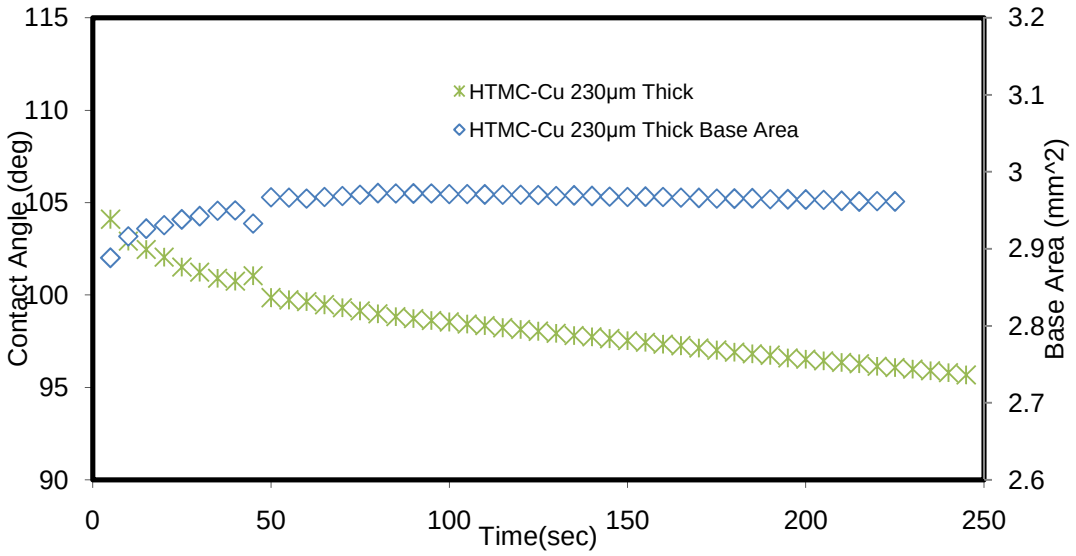

Figure 5.1 – Goniometer measurement of HTMC-Cu 70µm particle 230µm thick, in distilled water.

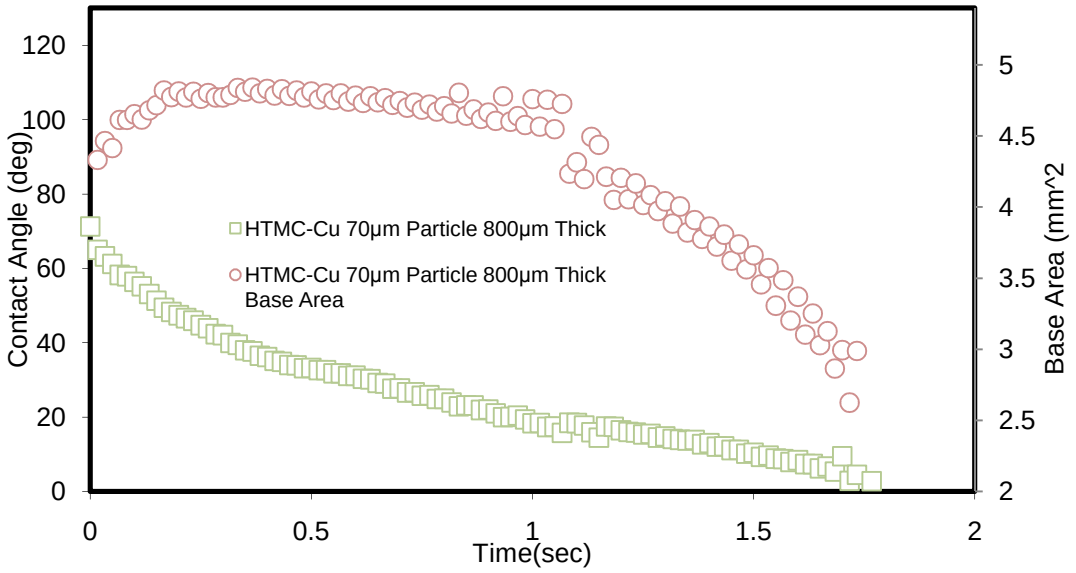

Figure 5.2 – Goniometer measurement of HTMC-Cu 70µm particle 800µm thick, in distilled water. Take note that the x and y scale (contact angle) is several orders of magnitude smaller than Figure 5.1.

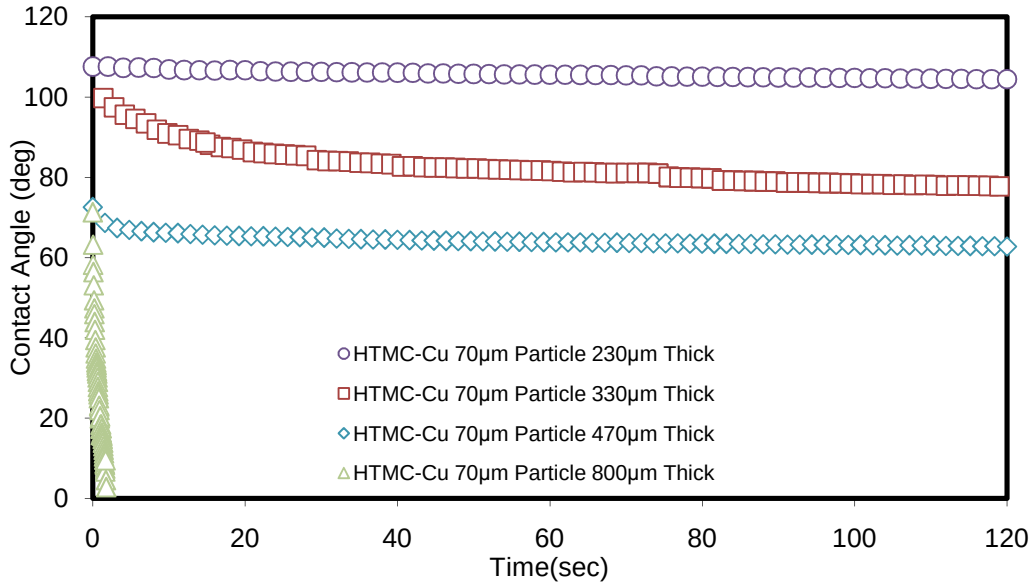

Figure 5.3 - Goniometer measurement of HTMC-Cu 70µm varying thickness, in distilled water. Note the change in the x-scale.

Figure 5.4 displays changes in thickness for the 4µm and 285µm coatings. The 4µm coatings were not observed to exhibit a change in the wetting profile after a 150µm increase in

thickness. The sessile drop is not meeting any change in surface area (poor fluid penetration) and thus the wetting characteristics have not changed. The 285μm coatings were measured to increase the apparent contact angle with increases in thickness. This would mean the sessile drop, assuming hydrophilic intrinsic contact angles, is meeting less surface area than when the test was done on thinner coatings. The measurements were taken immediately after cleaning and therefore adsorption is thought not to be a problem. The increased thickness of the 285μm coating most likely prevented the sessile drop from touching the substrate. Appendix C presents SEM photos of the 285μm coating, Figure C.9. The 285μm particles are not smooth, but contain features on the order 20μm. It is difficult to say, but the knurled surface of the 285μm particles may actually provide even less surface than a smooth surface. If the roughness on the surface of the particle is small enough to prevent liquid penetration, the sessile drop will become balanced with a high contact angle; this does not mean that the increased thickness has less hydraulic resistance.

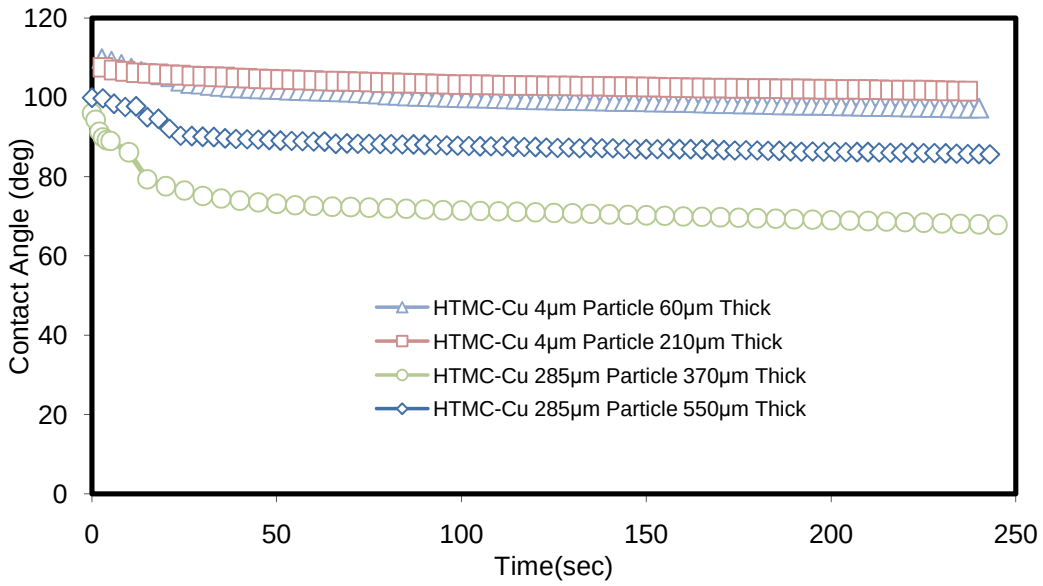

Figure 5.4 - Goniometer measurement of HTMC-Cu 4μm and 285μm varying thickness, in distilled water.

5.1.2 Wicking Measurements

Relevant wicking measurements were shown in section 3.2. To remind the reader, increases in thickness of the 70μm and 285μm coatings increased the volumetric flow rate. The 4μm coatings did not increase flow rate with thickness.

5.2 Effects of Thickness on Nucleate Boiling

Increases in thickness are often observed to decrease the boiling performance, see You et al. [3] for many examples. It is believed this boiling degradation with increased thickness is caused by two mechanisms. The first is the increased hydraulic resistance which impedes the fluid from quickly rewetting the inner most parts of the coating. More information on hydraulic resistance is given in section 3.1. The second is the increased thermal resistance due to the low thermal conductivity of the coating. Hence researchers often created coatings with materials of high thermal conductivity, [3,7,53], in attempt to reduce the thermal resistance.

Figure 5.5 displays the boiling results of several different thicknesses for the 4μm particle coatings. The 4μm coatings tested do not exhibit the effects of an insulating surface just described. An increase in thickness of 120μm still did not produce boiling degradation. This indicates the thermal conductivity may not play as large a role as previously thought. It is proposed that these coatings are simply too thin to restrict the vapor removal rate. The 4μm wetting profile did not change with increased thickness and thus it is believed the hydraulic resistance is not significantly altered.

Figure 5.6 displays the effects of thickness on the 70μm coatings. Here we see a very significant degradation in nucleate boiling. The change in the wetting suggests that there should be a significant increase in the wicking paths. The result is a large resistance to the vapor removal rate which leads to boiling degradation.

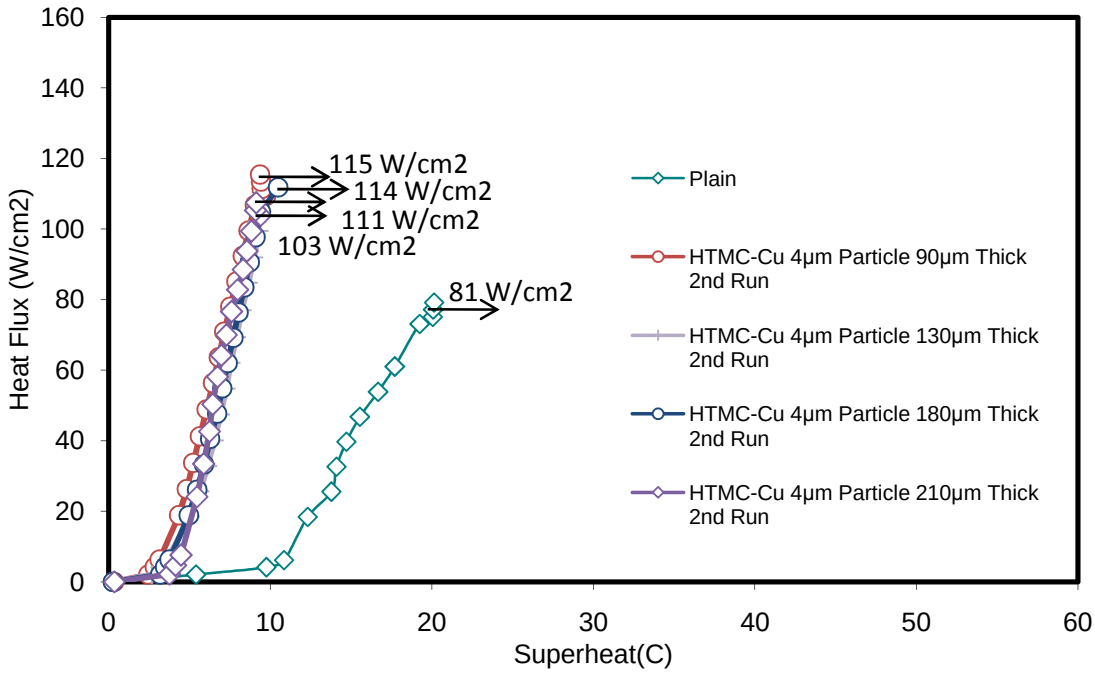

Figure 5.5 – Boiling curve comparison of different 4µm particles, varying thicknesses. Only displaying 2nd runs. T-sat: 80C

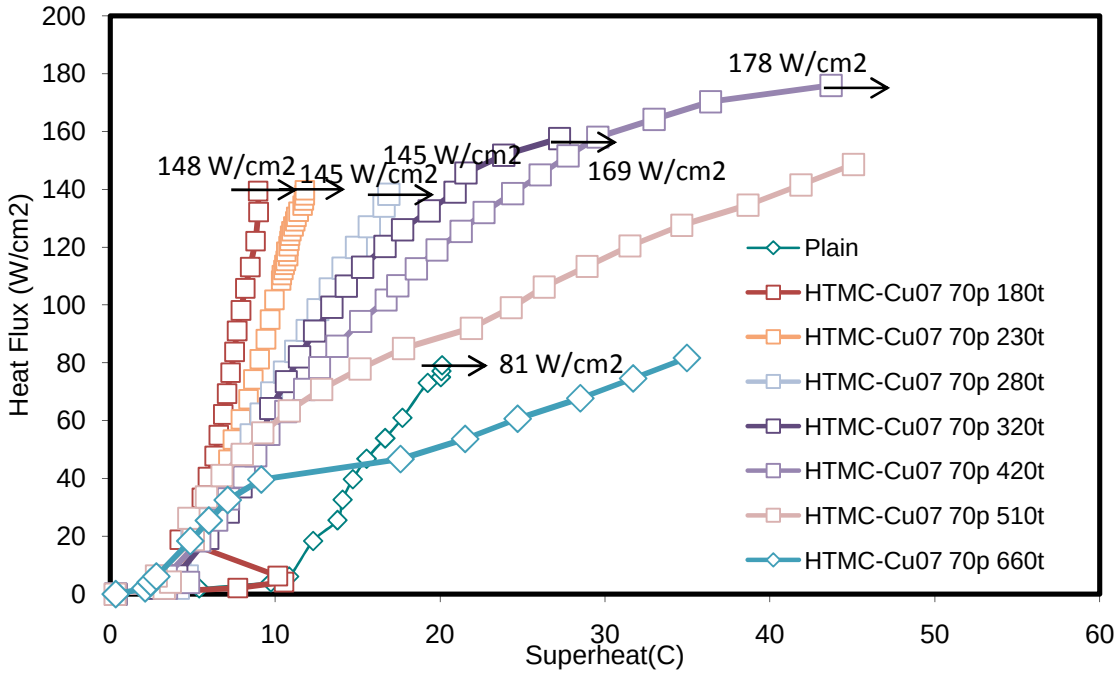

Figure 5.6 - Boiling curve comparison of 70p thicknesses. No CHF achieved for coatings above 500t. T-sat: 80C The letter “p” denotes the particles size and “t” is the coating thickness.

Figure 5.8 displays the effects of thickness on the 285μm particle coatings. Increases in the thickness cause an increase in the boiling efficiency for heat fluxes less than 100W/cm^2. There are two possible explanations: a) The increased amount of cool fluid wicked inward caused heat transfer enhancement b) increases in thickness provided additional nucleation sites leading to additional heat transfer. This is seen too a much lesser extent in the 70μm coatings. Heat fluxes on the 285μm coating above 100W/cm^2 once again result in boiling degradation as thickness is increased. The apparent contact angle measurements were found to increase with thickness. This result is not observed in the boiling curves of Figure 5.8. Increases in thickness only slightly degrade the performance of the 285μm coatings when compared to the 70μm coatings. This type of result is logical since the larger pores should allow an easier escape route for the vapor.

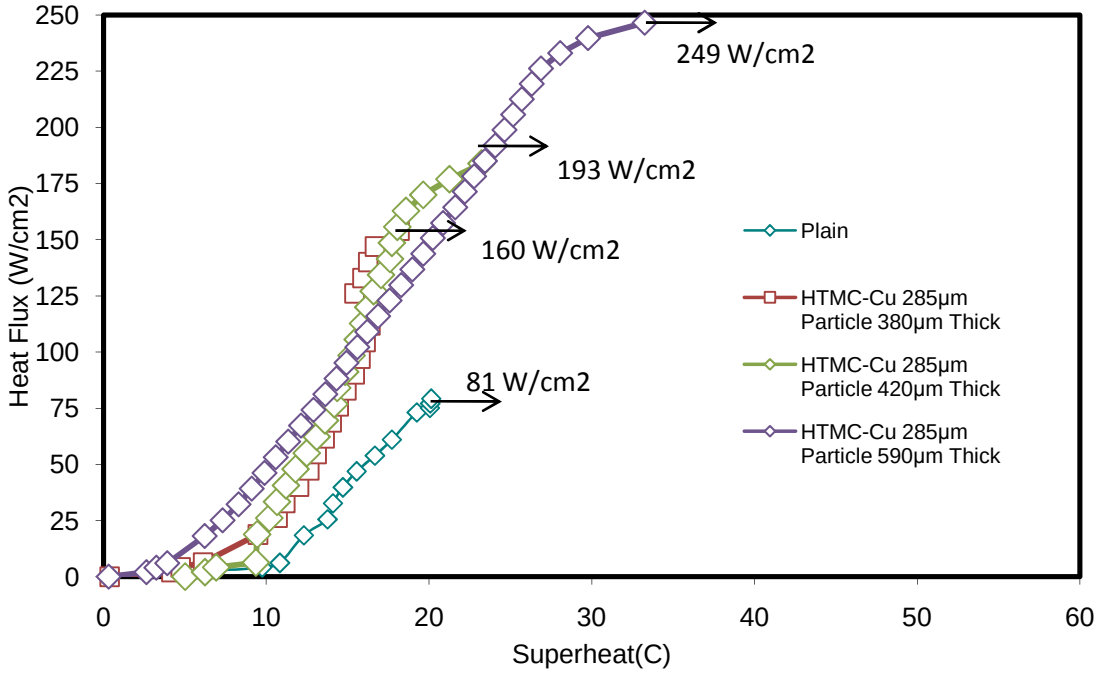

Figure 5.7 - Boiling curve comparison of different 285μm particles, varying thicknesses. T-sat: 80C

Plotted in Figure 5.9 is the heat transfer coefficient for the 70μm coatings. After approximately a 500μm thickness, the heat transfer coefficient drastically reduces. This

behavior has been recorded by other researches such as Malyshenko [1] who used a thick microporous coating and Li and Peterson [22] who used a mesoporous sintered mesh. Malyshenko as well as Li and Peterson conclude that this behavior is a function of the coating thickness, thermal conductivity, and coating vapor permeability. The high flow resistance for the vapor may be the leading cause of the interior vapor layer. Malyshenko also found that in thicker coatings, thermocapillary flows impede the removal of vapor. It was concluded that the critical thickness for an interior vapor layer depended on the ratio of the heater characteristic length to coating thickness which in turn was determined by the ratio of the two-phase to single-phase friction factors.

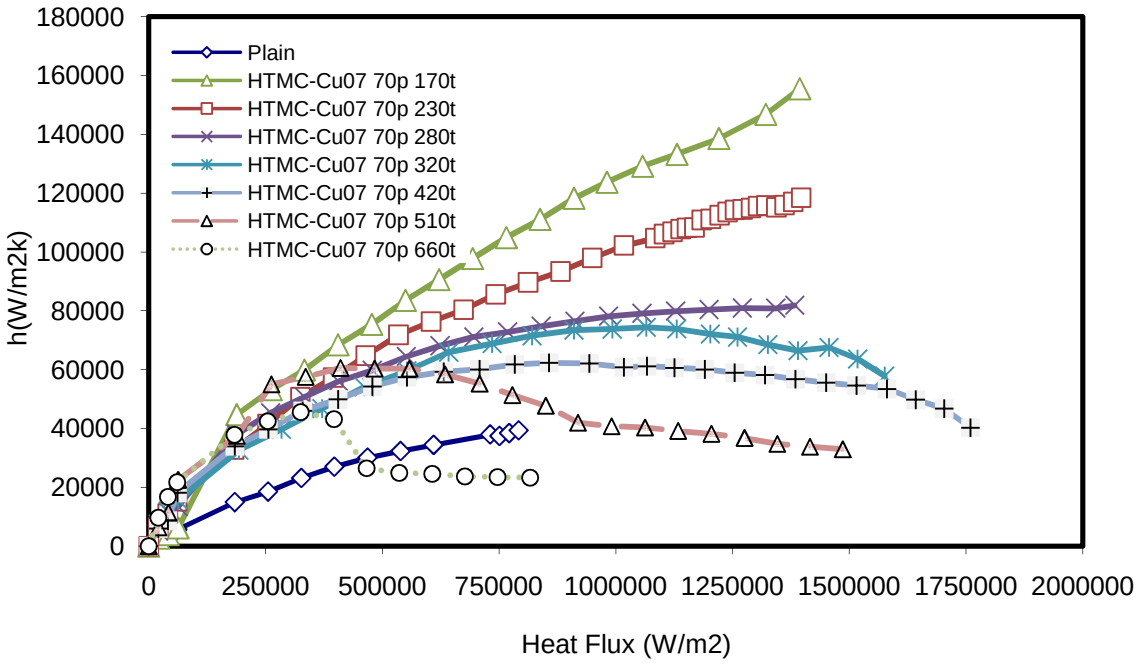

Figure 5.8 – Heat transfer coefficient of 70p coatings. 1x1cm surface at T-sat: 80C. The letter "p" denotes the particles size and "t" is the coating thickness.

It should be noted that for our tests, no CHF was obtained for 70μm coatings larger than a 500μm thickness. The heater arrived at the temperature limit before the formation of a vapor layer that engulfed the entire coating. According to the analytic work done by Li and Peterson [20] our 285μm coatings should be able to continuously increase CHF for much

thicker coatings. The 285μm coatings exhibit over 210% CHF enhancement at 80°C saturation; much thicker coatings (~1mm) at 100℃ should provide massive CHF enhancement. Our heater temperature limits prevented us from performing such tests.

5.3 Effects of Thickness on CHF

The CHF of all coatings depended greatly on the thickness. The 70μm and 285μm particle sizes increased CHF with increased coating thickness. Referring back to the wicking flow rates shown in Figure 3.7, any increase in thickness increased the flow rate. Increases in thickness both provide additional fluid "fuel" to the latent energy and increased the momentum thereby disrupting the formation of vapor clots described in section 1.2.

The initial CHF enhancement over that of Zuber [10] and plain surfaces is attributed to the vapor clot disruption of the numerous vapor columns and the fluid replenishment of the macrolayer by the wicking structure. This mechanism is described in detail by Chang and You [5]. Polezhaev and Kovalev [59] modeled this CHF mechanism shown in Eqn. 5.1. They assume the cause was a hydrodynamic instability.

$$q_{CHF} = .52\varepsilon^{2.28} h_{fg} \sqrt{\sigma \rho_l \rho_v / (\rho_l + \rho_v) R_{br}} \qquad \textbf{Eqn. (5.1)}$$

While Eqn. 5.1 is shown to be very accurate by Polezhaev and Kovalev [59] and Liter and Kaviany [11], Li and Peterson [20] show that the equation deviates wildly from their work. Unfortunately, none of these researchers performed any type of wetting or wicking tests. Li and Peterson used a sintered mesh instead of porous coatings like Polezhaev and Kovalev, and Liter and Kaviany. The missing piece between Li and Peterson and the model of Polezhaev and Kovalev may be the wetting and wicking behavior of their respective structures.

Similar to the plain surface mechanisms described by Dhir [15] and discussed in section 1.2, depending on the coating configuration, it is believed that either the wicking limit is reached or the macrolayer dryout is causing CHF. These limits are described in section 1.2. To remind the reader, the wicking limit is defined as the point in which fluid is transformed to vapor quicker than can be pulled to the surface. The result is vapor coalescence and thus CHF. The

macrolayer dryout is defined as the point in which vapor is generated at a rate that cannot quickly escape the surface. The vapor subsequently blocks or chokes the influx of fluid causing CHF.

No change in the thickness of the 4μm coatings seemed to enhance or reduce CHF. The wicking flow rates in Figure 3.7 showed that the 4μm flow rate is relatively constant with thickness and therefore we do not expect any changes in CHF. Each 4μm coating is believed to hit CHF due to the wicking limit. If we observe the boiling curves near the CHF for each particle size and thickness, we notice a bending for the 70μm coatings greater than 300μm thicknesses and all 285μm particle coatings. No bending is observed for the 4μm coatings. This bending is most likely caused by the macrolayer dryout. The coatings have reached a heat flux that hinders the removal of vapor and boiling efficiency diminishes. The efficiency continues to diminish till the coating reaches the point in which fluid is no longer able to penetrate the coating and CHF occurs. As described in section 3.1, as coating thickness increases the hydraulic resistance will increase, impeding the escape of vapor.

A transition region marking the change between CHF mechanisms was observed for the 70μm coatings. Increases in thickness did not further delay CHF till approximately 320μm. Below 320μm thicknesses no bending is observed and the dominant mechanism of CHF is believed to be the wicking limit. The capacities of the coatings are not great enough to transfer the critical fluid mass needed for CHF enhancement. Above 320μm the wicking flow rate reaches a value that allows for substantial enhancement. A transition region was not observed for the 4μm and 285μm coatings. A uniform thickness for the 4μm particle coatings could not be created at large thicknesses (~300μm) and it is physically impossible to have a 285μm particle coating less than 300μm thick.

Other researchers have observed transition regions in coating thickness. Li and Peterson [20] saw a max limit to CHF enhancement where increases in thickness no longer provided additional enhancement. They conclude that their thin coatings hit CHF due to a

hydrodynamic limit and the thick coatings are governed by vapor removal inefficiencies (macrolayer dryout). Borzenko and Malyshenko [60] experiment with two different configurations. One configuration exhibits a peak thickness in which any decrease or increase in thickness decreases the CHF. The other configuration exhibits a range of thicknesses in which no major changes in CHF are observed. Outside of this range the CHF decreases with changes in thickness. Borzenko and Malyshenko agree that this behavior cannot be simply explained via a hydrodynamic instability. They conclude that the CHF of their coatings cannot be caused by a hydrodynamic limit since the climb to film boiling rose slowly and did not jump in temperature like plain surfaces. We did not have the ability to measure the rate of temperature increase once CHF occurred. They believe the CHF must be caused by a much slower vapor removal inefficiency.

CHAPTER 6

EFFECTS OF RATIO CHANGES

Previous chapters discussed physical changes to the coatings. The chemical makeup of the surface of varying particle sizes and thickness is comparatively the same. The intrinsic contact angle between these different parameters will be minimally affected. This chapter discusses an indirect change in the surface energy. A change in the mixture ratio is defined as altering the copper to binder ratio. These ratios are measured by weight and not volume. As seen by previous researches in our lab, this ratio can have a large effect on the performance the coating. The ratio can affect the porosity and even the surface energy. Decreasing the ratio will mean there is more binder material available to cover the copper surface. Hence, the intrinsic contact angle will approach that of the binder material. The opposite is also true; increasing the ratio results in the intrinsic contact angle of the coating approaching the copper intrinsic contact angle. In this work the change is measured via apparent contact angle which at least gives us some idea of how the intrinsic contact angle is affecting the boiling curve.

During the development of TCMC and ABM, changes in the particle ratios resulted in significant changes in performance. It was found that TCMC had an optimized ratio of 2.0:1 copper powder to binder [7]. This mixing ratio was the initial ratio for HTMC. Based on the mixing ratio investigation by You et al. [3] we see that increases in the ratio will eventually stop enhancing performance. In You's work, both heat transfer coefficient and CHF stopped increasing at some specified ratio where all further ratio increases provided no further enhancement.

The same idea was applied to the mixing ratio of HTMC. An increase in the ratio should have two physical effects. The first is that the increase in copper to binder will increase

the porosity which will hopefully enhance nucleate boiling further than the current ratio. The second effect is that the bonding strength may or may not decrease.

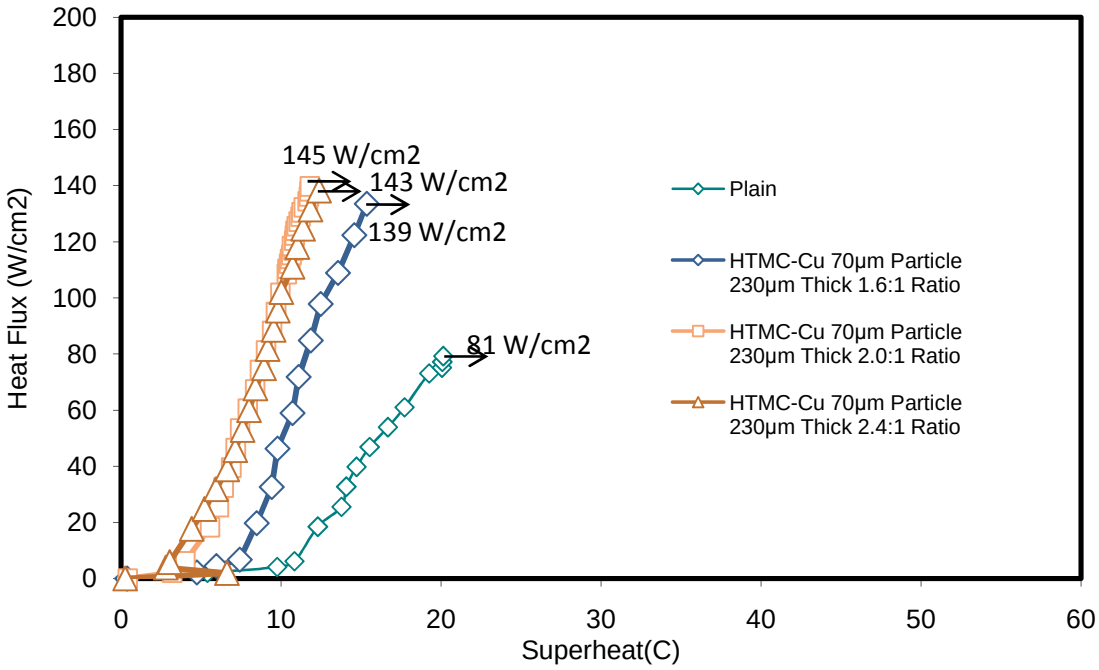

Figure 6.1 – Comparison of 2.0:1 copper ratio, 2.4:1 copper ratio, and 1.6:1 copper ratio same thickness. T-sat:80C.

Figure 6.1 illustrates the boiling result of changes in the mixture ratio. The figure illustrates the 2.0:1 ratio shown throughout this thesis as well as 2.4:1 and 1.6:1 ratios. Increasing the ratio from 2.0:1 to 2.4:1 results in negligible change to the nucleate boiling and CHF is almost exactly the same. This leads to the conclusion that the 2.0:1 ratio has maxed out the performance enhancement. The bonding of the 2.4:1 mixture is found to exhibit questionable bonding; around 5-15% (visual approximation) of the particles detached during an ultrasound stress test[4]. These results solidified the reasoning to stop further increases in the ratio of copper particles. If the ratio was decreased from 2.0:1 to 1.6:1, the nucleate boiling

[4] A stress test is described in chapter 2. The coating is placed in distilled water, ultra sound bath for 40 minutes. If no particles or less than 5% of coated area detach from the surface, the bonding is considered satisfactory.

performance degraded. Chang and You [5] attribute this result to a decrease in porosity, which decreased the nucleation site density. CHF was still observed to be the same as the 2.0:1 and 2.4:1 ratios.

Figure 6.2 shows the apparent contact angle of each ratio. Note that while the exact same thickness of the boiling samples is difficult to obtain, the small difference shown in Figure 6.2 is assumed to be negligible. The 1.6:1 ratio appeared to result in no major changes in porosity, but the wetting was found to be far better. The binder has a very low intrinsic contact angle compared to copper and it is quite logical to see that an increased amount of binder would result in better wetting due to decreased intrinsic contact angle of the coating. Increased wetting should lead to slightly smaller cavity sizes and thus poorer boiling performance.

Unexplainably, the 2.4:1 ratio resulted in ultra fast wetting. Assuming no major change in the intrinsic contact angle, the author speculates that the increased porosity increased the wetting surface area required to be balance in Young's equation, Eqn. 1.1. This answer is somewhat questionable due to the drastic change in the apparent contact angle. Evidence of this contact angle change did not appear in the boiling curve. To fully explain the drastic change, micro-fluidic experimentation is needed which is beyond the scope of this thesis.

Figure 6.3 displays the wicking speed of each ratio. No measurable change in wicking is found between the coatings. Since there is no change in the speed of wicking the Washburn equation, Eqn. 1.8, states that any change in the intrinsic contact angle must be balance by a geometric change. Thus, the 1.6:1 ratio results in a lower intrinsic contact angle, but the porosity decreases leading to no significant change in the wicking. The 2.4:1 ratio increases the porosity, but increases the intrinsic contact angle resulting in no wicking change. It is logical that there exists a ratio that will no longer result in the same amount of wicking; no such test was performed here. The CHF for each ratio was observed to be approximately the same. This further supports the hypothesis that wicking is a good CHF indicator and wetting is a bad measure of CHF.

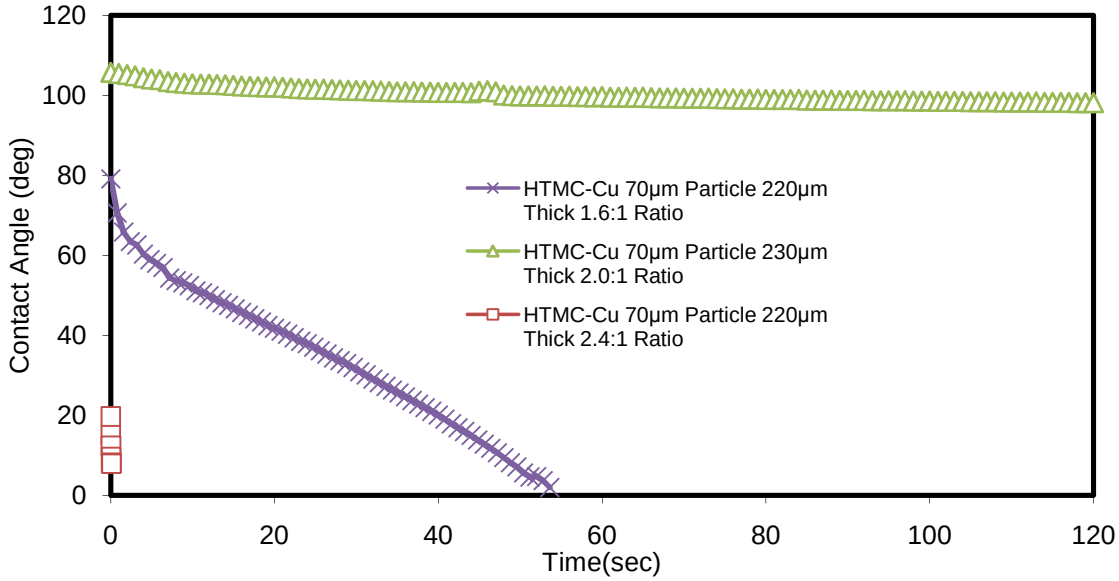

Figure 6.2 – Apparent Contact angle measurements of different coating mixture ratios. Note x-scale is different (zoomed in) compared to other contact angle plots.

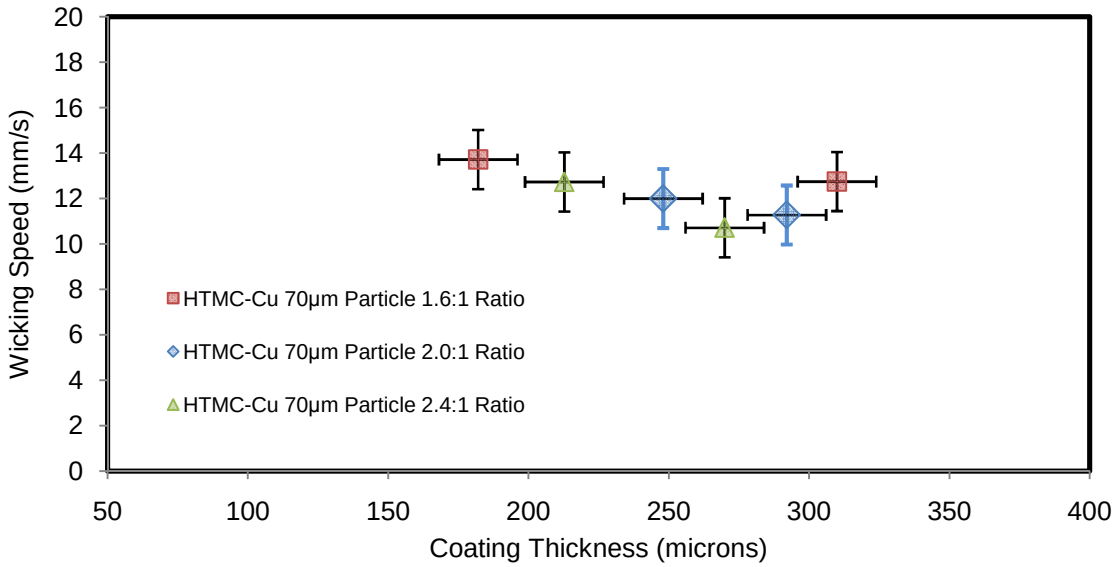

Figure 6.3 – Virtually no change is observed in wicking speeds with changes in mixture ratio.

CHAPTER 7

PRESSURE OBSERVATIONS

Many engineering applications deal with system pressures below atmospheric pressure. It is of engineering importance to understand how a surface will boil at decreased pressures. No physical or chemical changes were made to the coatings during the following tests and only the pressure was altered between tests.

It is well known that plain surface boiling degrades with decreases in pressure. Kim et al. [7] found that porous coatings exhibit the same behavior. Figure 7.1 displays the change in the boiling curve of the 70μm coatings. As expected, changes in pressure alter the performance of the HTMC nucleate boiling. The changes in the nucleate boiling are easily explained through the changes in bubble departure size and fluid properties. The required cavity size for embryonic bubble nucleation, (previously plotted in Figure 4.5) increases with decreases in pressure. If the pressure is decreased a cavity will require a greater superheat to activate. Hence the HTMC incipience is shifted the right. Nucleate boiling is degraded since the bubble departure diameter is much larger which decreases the efficiency of each cavity. Larger bubbles and slower departure frequency use less latent energy and the result is the shift to the right seen in Figure 7.1.

Plain surface CHF decreases by a power law; the most notable correlation is Zuber's equation [10]. Zuber states that the CHF will continuously decrease with decreases in pressure. Unexpectedly, the CHF of the 70μm coatings is observed to stop decreasing or slow to a negligible change.

The change in the viscosity and surface tension of water with decreasing pressure, Figure 7.2 and 7.3, hold the answer to the CHF behavior. As the saturation temperature decreases from 100℃ to 30℃, the surface tension increases by ~17%. Quite

disproportionately, the viscosity increases by ~300%. This property change mismatch will greatly affect the wicking as seen from the Washburn equation, Eqn. 1.8. In order to solidify this idea, we need to know how the intrinsic contact angle changes with pressure. Boyes and Ponter [61] have performed this study, shown in Figure 7.4. The intrinsic contact angle greatly decreases with pressure till it reaches approximately T-sat: 55℃. There appears to be almost no further change in the intrinsic contact angle below T-sat: 55℃. Thus, looking back on the Washburn equation and the relative changes in fluid properties, the wicking speed will have no significant changes after T-sat: 55℃. Since the s tudy done by Boyes and Ponter was done on a plain copper surface, we cannot directly plug numbers into the Washburn equation. Our surface is "roughened" and the intrinsic contact angle is different; Figure 7.4 only gives us an idea of what is happening at lower pressures. According to our hypothesis, if the wicking speed or flow rate is kept constant, then the CHF should exhibit no significant change.

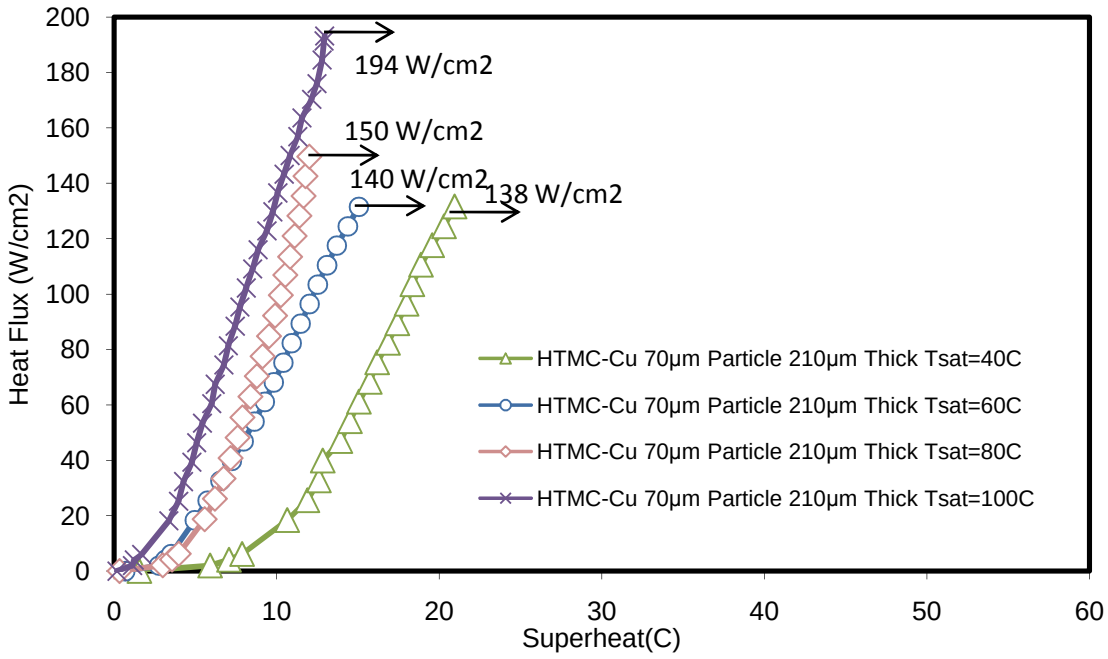

Figure 7.1 – Changes in the boiling curve due to changes in pressure. 70µm particle sizes.

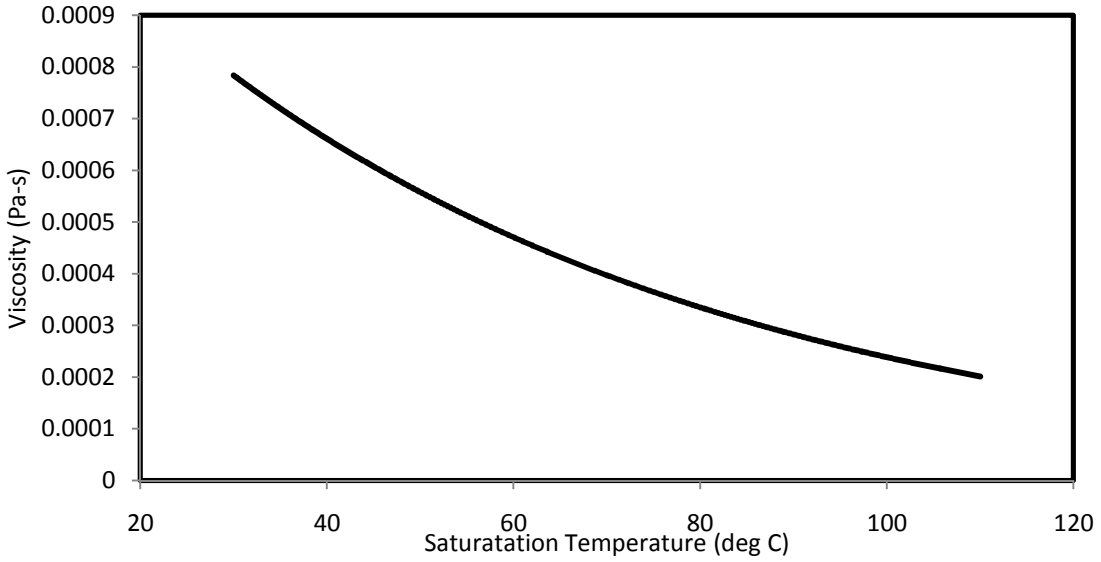

Figure 7.2 – Changes in viscosity of water with changes in pressure.

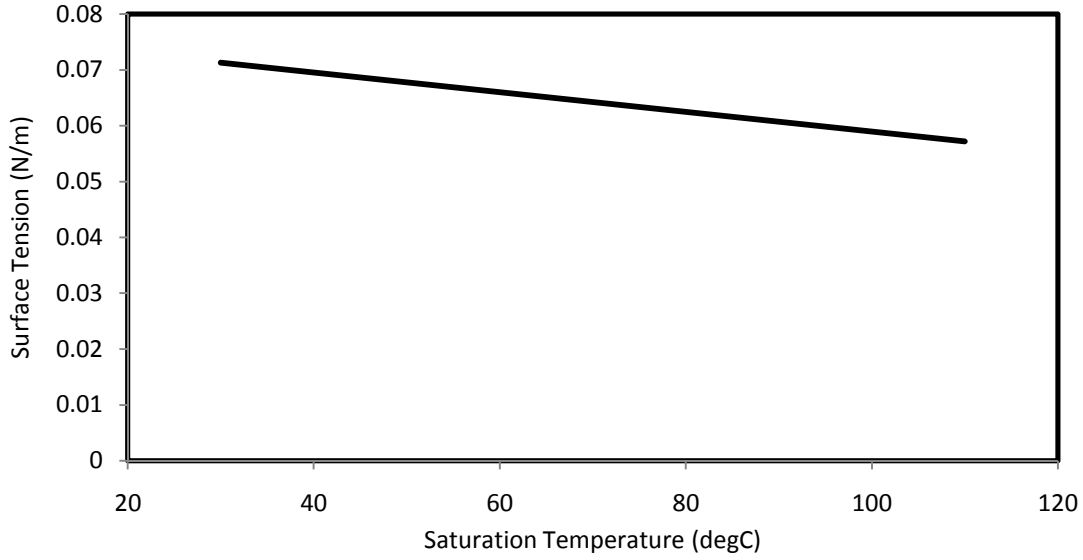

Figure 7.3 - Changes in surface tension of water with changes in pressure.

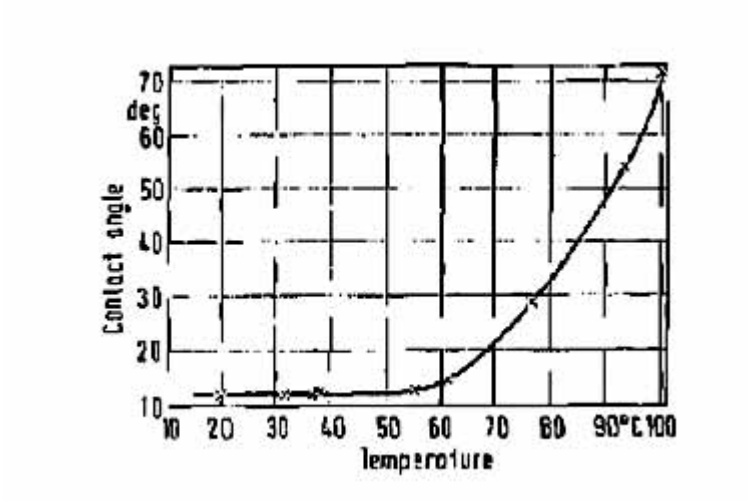

Figure 7.4 – Contact angle of water at the boiling point on a copper surface. Plot taken from Boyes and Ponter **[61]**.

The reader should note that the data shown in Figure 7.4 is at the saturation temperature and pressure of the liquid. The sessile drop is surrounded by saturated vapor. When a goniometer contact angle measurement is made at room temperature, air surrounds the sessile drop and not the fluid vapor. Since the surrounding media is air the solid-vapor surface energy is different than that of Figure 7.4. Also, the goniometer sessile drop must contend with air molecules which interact with the three-phase interface disturbing the measurement. In general, at a specific pressure goniometer sessile drop measurements do not drastically change with temperature [48,62].

CHAPTER 8

SURFACE ENERGY MANIPULATION

8.1 Corrosion

This section discusses how corrosion is used to change the chemical makeup of the coating surface. Unlike chapter 6, this is a deliberate molecular change of the surface chemistry. It is well known that corrosion will degrade boiling performance. Within the industry, corrosion and particle contamination are often lumped together in a blanket term: fouling. There are several orders of magnitude difference between the contaminating particulates and corrosion. Corrosion is a molecular change and is on the nanometer scale where as particulates range from micron to millimeters in size. If corrosion takes place over several years, it will build a layer that is on the order of a millimeter. The common phenomenon deemed surface ageing is also the result of corrosion [42]. Thus it is of interest to observe the effects of corrosion on the wettability and its relation to the boiling curve.

8.1.1 Changes in apparent contact angle and wicking speeds

Boiling tests were done with the use of Ag50-5 brazing paste. The Ag50-5 brazing paste was actually the first paste tested in the switch from solder to brazing. The Ag50-5 was abandoned due to an extreme tendency to corrode. The composition of the Ag50-5 contains a high amount of zinc, which is extremely anodic. The Cu-07 paste is almost entirely copper and therefore should be highly corrosion resistant as far as galvanic corrosion is concerned.

The Ag50-5 samples were corroded by simply leaving them in an electrolyte (de-ionized distilled water) for 72 hours. Since the composition of the Ag50-5 is not a binary alloy, the exact corrosion product was unknown. The corrosion products could be oxides, hydroxides, other salts, or free ions. The fluid itself has chemically changed as well. Fortunately, since the volume ratio of the water in the test section to the surface area of the sample is huge, the fluid

property change is negligible. If the coating was used in a much smaller environment, the change in fluid properties could greatly affect the boiling curve.

Hydroxide was suspected to be the main product in the surface energy change. According to Chavez and Hess [50], if a copper sample is immersed in acetic acid for a period of time and then washed with de-ionized distilled water, the entire surface will be coated in hydroxide. In order to prove that hydroxide was the main corrosion product on HTMC-Ag coatings, we used HTMC-Cu samples because the system is almost entirely copper. The wicking/wetting samples were immersed in 30% acetic acid 70% distilled water for 24 hours. Afterward the samples were immediately given an ultra sound bath in de-ionized distilled water for 10 minutes. Wetting measurements were performed before and after and are shown in Figures 8.1. Drastic changes in the apparent contact angle were observed after corrosion. While the HTMC-Cu 70µm coatings did not fully wet at thicknesses around 230µm, once the chemistry is transformed into hydroxide, the coatings completely wet in less than 15 seconds. Thus we can conclude that hydroxides increase the surface energy of copper. This is a typical result in the chemical industry [23].

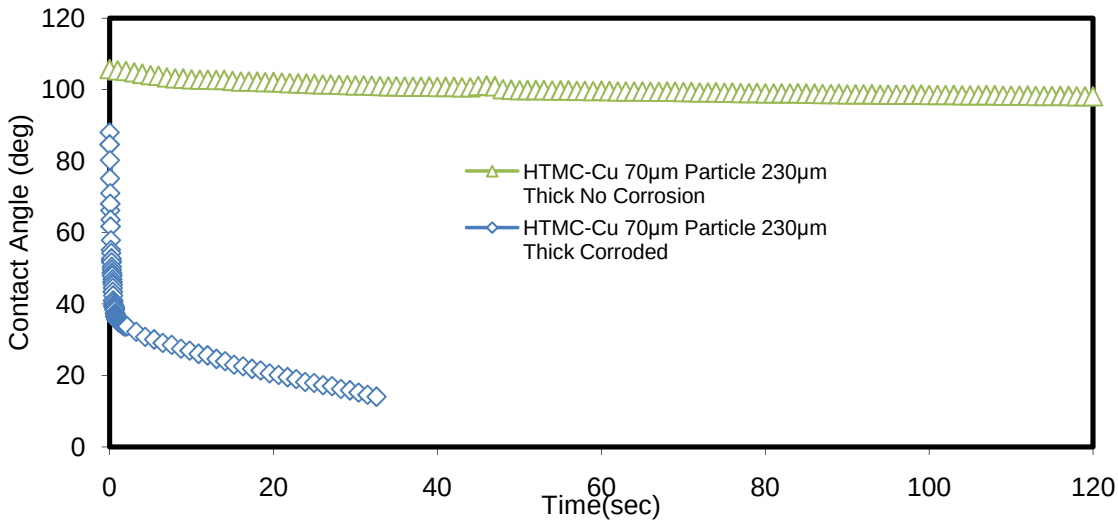

Figure 8.1 – Apparent contact angle of HTMC-Cu 70µm particles before and after the special process described by Chavez and Hess **[50]** and described in section 8.1.1. This data is used to confirm the existence of hydroxide as a corrosion product.

As stated earlier, only water was needed to corrode the HTMC-Ag samples. After the samples were immersed for 72 hours in distilled water, the wicking and wetting measurements were taken. The results are shown in Figure 8.2 and 8.3. Once again, there is a large change in the apparent contact angle post corrosion. The Washburn equation dictates that a lower intrinsic contact angle will produce better wicking provided there is no major change in geometry. As expected, the lower apparent contact angle leads to better wicking, as seen in Figure 8.3. The speed of wicking consistently increases after the process described in section 8.1.1 is performed on the sample. Hence, if the coating thickness is kept constant and the speed of wicking is increased via corrosion, then the mass flow rate should also increase. The increased wetting leads to the prediction that the nucleate boiling performance should be degraded due to a change in nucleation site density. The enhancement of wicking should indicate an increase in CHF.

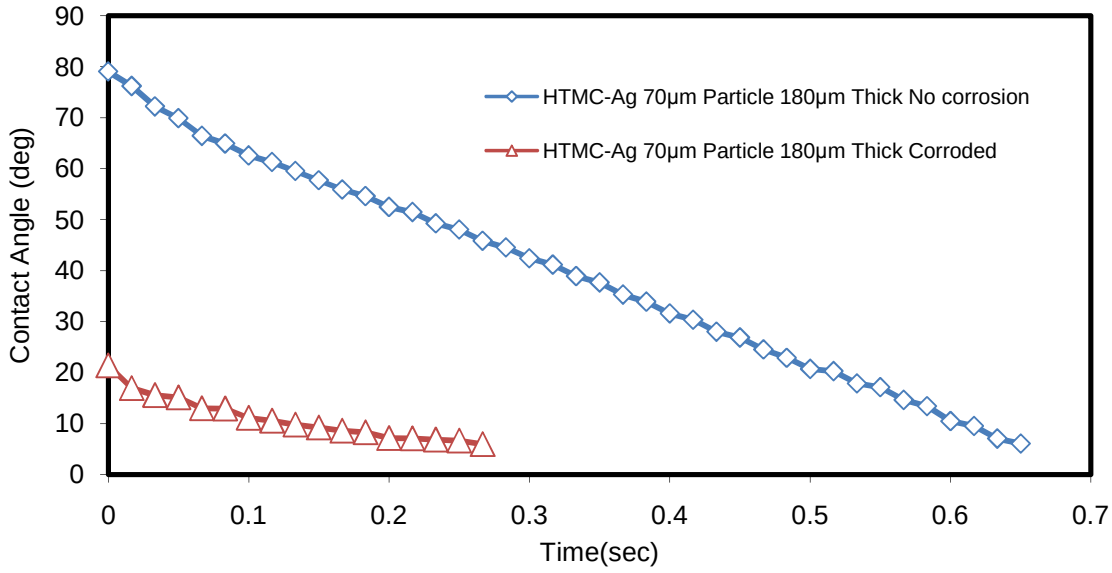

Figure 8.2 – Apparent contact angle of HTMC-Ag 70µm particles before and after corrosion. Corrosion process consisted of de-ionized distilled water immersion for 72 hours. Note large change in x-scale.

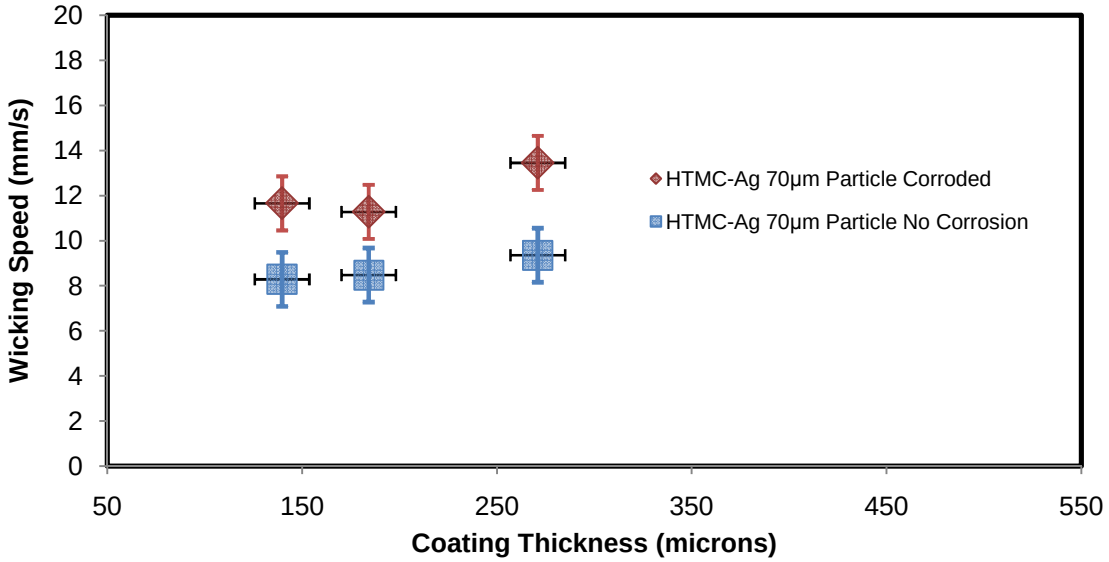

Figure 8.3 – The change in wicking of a hydroxide covered HTMC 70µm particles.

8.1.2 Effects of corrosion on nucleate boiling and CHF

Figure 8.4 shows the nucleate boiling results for the corroded and un-corroded coatings. The corroded sample's performance is severely degraded. At low heat fluxes the corroded microporous coating performs similar to a plain surface. At higher heat fluxes the coating once again shows some enhancement over plain surface. Decreasing the apparent contact angle should decrease the effective radius of the nucleation cavities. Thus the smaller cavities require a greater superheat to activate. The CHF is also found to be enhanced over the un-corroded sample just as the increase in wicking predicts. This result adds a little more evidence to the hypothesis that wicking is the controlling mechanism of CHF in porous coatings.

The CHF enhancement caused by corrosion is not always observed on plain surfaces. Joudi and James [42] repeatedly tested surfaces resulting in nucleate boiling degradation. They take extreme precautions to ensure no particulates contaminate the surface. In the end, they safely conclude that corrosion is the reason for nucleate boiling degradation. Yet, they did not observe CHF enhancement. They did not perform any type of capillary force measurements and so the effect of corrosion on a stainless steel sample is unclear. Hydroxides and oxides

most likely formed on their surface, but did not produce a significant microstructure leading to no capillary enhancement. According to numerous researchers in section 1.7, increasing the wettability will increase CHF which was not observed in Joudi and James' [42] tests. In the next section we present data that also contradicts the general consensus that decreasing contact angle leads to enhanced CHF.

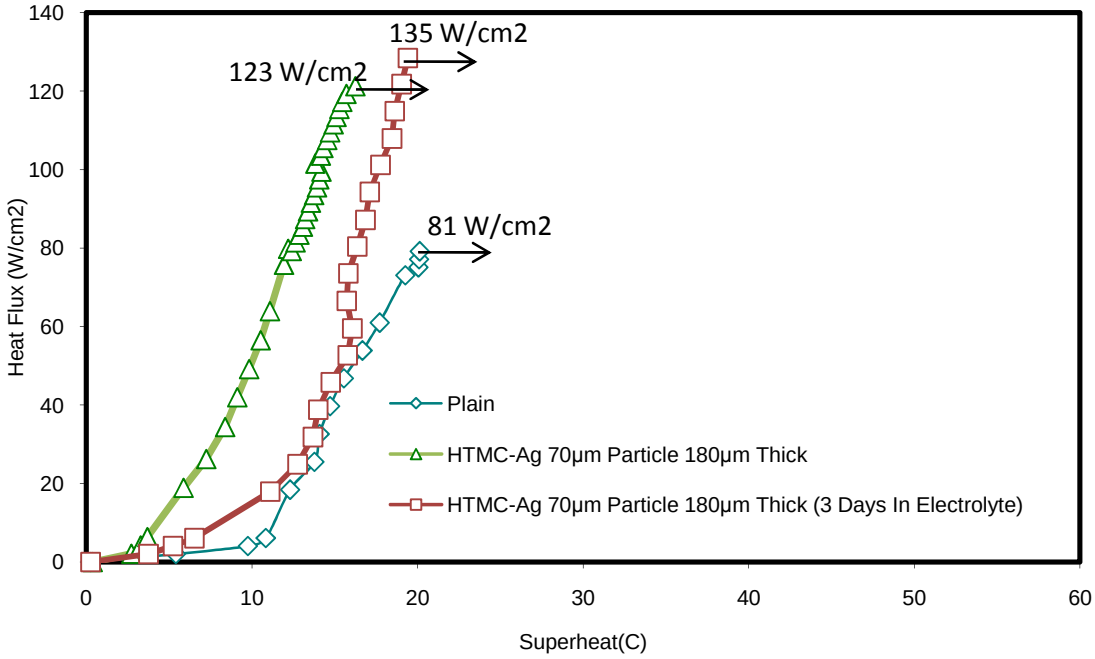

Figure 8.4 –Boiling curve of HTMC-Ag 70µm particles before and after corrosion. T-sat: 80℃

8.2 Oxidation

In this section we will alter the surface chemistry via oxidation. Oxidation is the most common form of surface energy manipulation found in literature. It seems fitting for us to perform our own tests on oxidized surfaces. Researchers who performed oxidation tests fortunately measured the static contact angles, see [15,36]. Even though these tests were for plain surfaces, we at least have some idea of the outcome of oxidized porous surfaces. They all found that oxidation enhances CHF. Oxides, like the hydroxides of section 8.1, are well known hydrophilic surfaces [23]. Once again, the Ag50-5 paste was used for these tests as a more extensive oxidation could be achieved in contrast to the Cu-07 paste.

8.2.1 Process of oxidizing samples

An oxidized sample was achieved by brazing the coatings without the use of nitrogen gas. With respect to the Ag50-5 paste, bonding was still found to be good, but the surface turned completely black, see Appendix C. The Cu-07 paste actually peeled off the surface when this method was used as an attempt to oxidize the surface.

Lee et al. [31] collected data on the structure and thickness of the oxidation of copper. They tabulated the change in oxide thickness with time at 400℃ in an oxygenated environment. For example, 10 minutes produced an oxide coating of ~20nm and 40 minutes produced a ~150nm oxide coating. Since we oxidized our coatings by using an oxygenated environment during the brazing process (150 minute process ranging from 250℃ to 720℃), we cannot directly extrapolate the oxide thickness. Using the data from their tables we estimate our thickness to be on the order of a few microns. Even though the thermal conductivity of an oxide is far lower than pure copper (20W/mK for CuO), the oxide layer thickness is thought to be too thin to significantly increase the thermal resistance of the surface.

Copper oxides have been found to create a whisker structure [31,63] as shown in Figure 8.5. A whisker microstructure could either impede or enhance wetting and wicking depending on the surface energy. It is well known that oxides in general exhibit great wettability. Berg [23] explains that the degree of mutual bonding compensation of the material involved is the dominant determinant of wetting. Systems wet better when both the solid and liquid both have the same or similar bonding (i.e. ionic, covalent, metallic, etc). So, water and oxides have a similar type of molecular bonding which affects the surface energies.

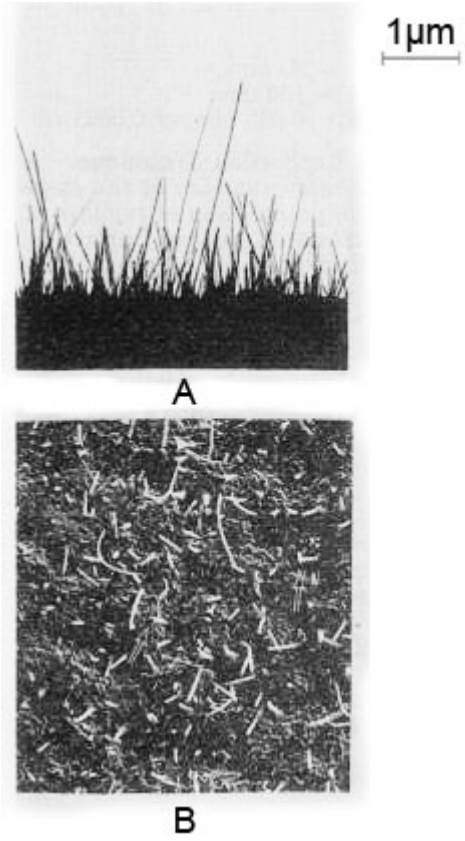

Figure 8.5 - Oxide whiskers formed on copper in air at 400℃, for 30 minutes. Photo taken from Lasko and Tice **[63]**.

Corrosion is assumed to not be a problem for any of the oxidation tests since an oxide layer will effectively pacify the surface. To reiterate, the difference between the stated galvanic corrosion and scaling oxides is that galvanic corrosion occurs when the electrons are exchanged through the metals. Scaling oxidation is when the electrons are exchanged with air to form a new molecule that contains oxygen. The passivation layer is a layer of oxides that will not chemically react with most materials.

8.2.2 Changes in apparent contact angle and wicking speeds

Confirming the well known fact that oxides wet well, Figure 8.6 illustrates the extreme difference in apparent contact angle after oxidation. Comparing the oxidized apparent contact angle in Figure 8.6 to the corroded apparent contact angle in Figure 8.2 reveals a similarity. Oxidizing the HTMC-Ag coating resulted in almost the same wetting profile as the corroded

surface. This data leads us to believe that the nucleate boiling of an oxidized coating will perform similar to the corroded samples.

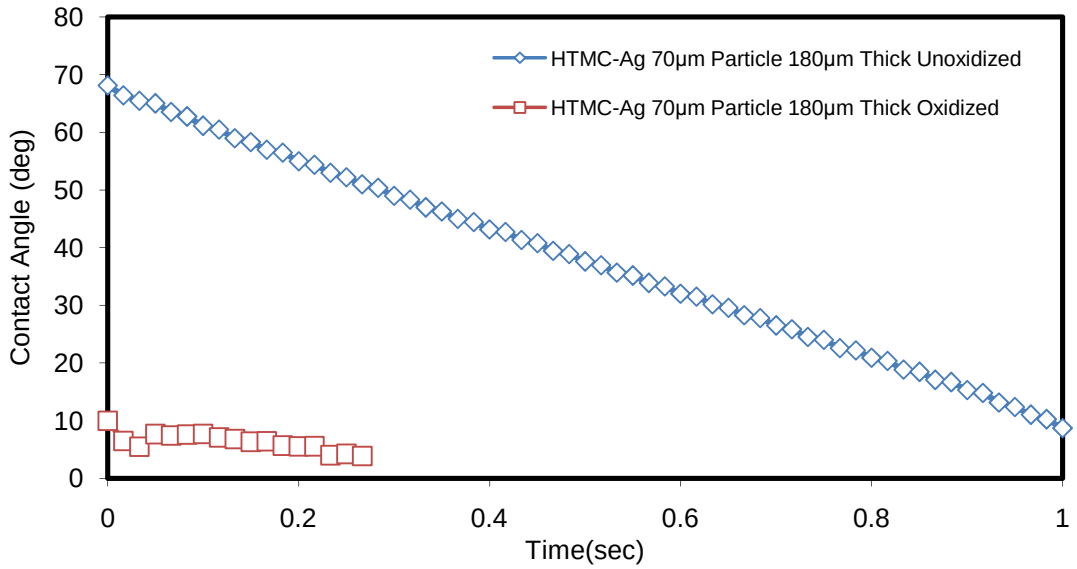

Figure 8.6 - Change in apparent contact angle before and after oxidation of the HTMC-Ag variant.

The wicking of the oxidized surfaces is shown in Figure 8.7. To ensure hexane did not perform differently with oxides, a plain surface copper sample was oxidized via 20 minutes at 350℃. Hexane was still found to have a static con tact angle of zero on the oxidized plain surface. In Figure 8.7, the wicking speeds have decreased post-oxidation. A possible explanation is the growth of whiskers within the pores. The Washburn equation, Eqn. 1.8, states that even though the intrinsic contact angle has drastically reduced, the whiskers would effectively decrease the pore size and impede flow. With a decrease in the wicking speed it would make sense for the CHF to decrease with this amount of oxidation. In Appendix C, we can visually see the pore difference between oxidized and un-oxidized coatings. No SEM pictures are available of our oxidized coatings; to the authors understanding, it is very difficult to view whiskers directly. Our SEM currently cannot provide the magnification needed to capture

the whiskers. Special viewing techniques and powerful electron microscopes are needed which we currently do not have access.

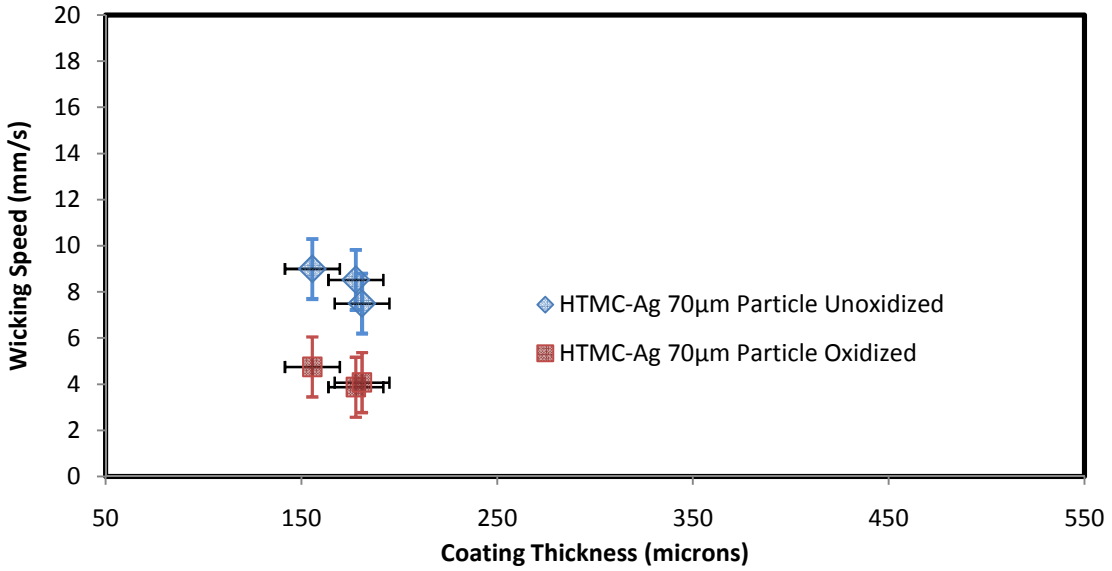

Figure 8.7 - Change in wicking of HTMC-Ag before and after oxidation.

8.2.3 Oxidation effects on nucleate boiling and CHF

Figure 8.8 presents the oxidized boiling curves. Comparable to the corrosion data, the nucleate boiling performance is severely degraded. The oxidized surface offers some enhancement at low heat flux, but at high heat flux the coating performs worse than a plain surface. The enhanced wettability again leads to a decrease in the boiling performance. Unlike the corrosion data, no enhancement ever appears at higher heat fluxes. This is most likely due to a change in the hydraulic resistance. It is likely that whiskers have grown in the pores; the vapor now has a more difficult time escaping the structure.

From an application point of view, it is important to note that the resulting boiling curve of the oxidized surfaces is quite similar to the alumina tests done by Malyshenko [1]. Even if the particles used have a high thermal conductivity, the change in surface energy and additional hydraulic resistance of oxides will result in performance similar to extremely low thermal conductivity materials. Again, the oxide layer is thought to be quite thin and offer no significant

thermal resistance. This is yet another indication that the thermal conductivity of the porous material may not be nearly as important as the surface energy in boiling applications.

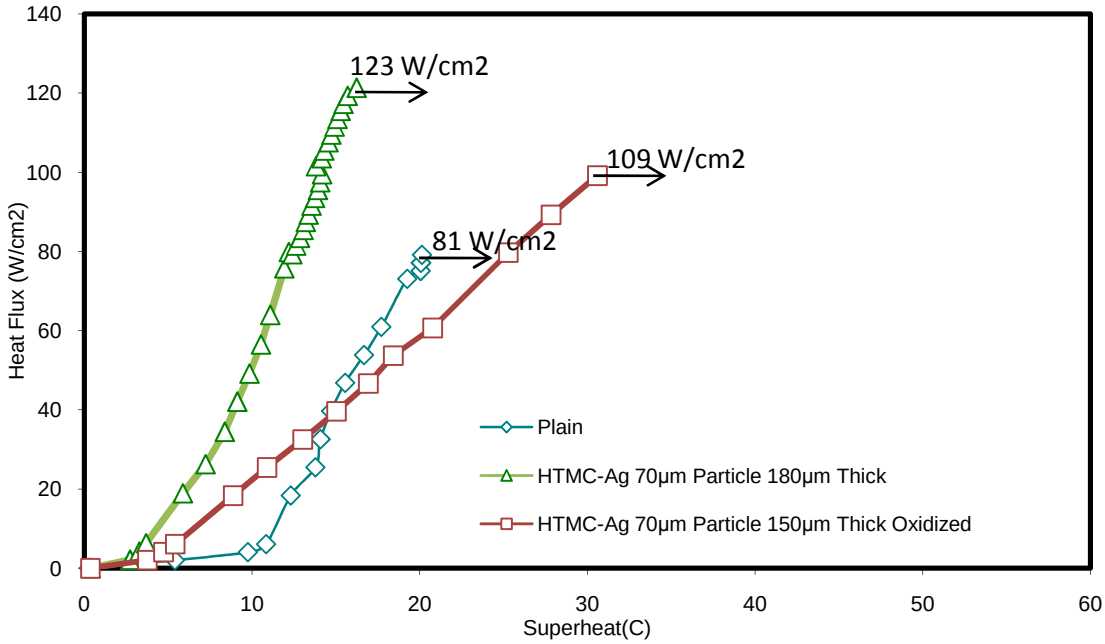

Figure 8.8 - Nucleate boiling curves of HTMC-Ag and oxidized HTMC-Ag. T-sat:80C.

In section 8.2.2 we observed the decrease in wicking speeds with oxidation. Here in Figure 8.8, a decrease in CHF is observed. This yet again corresponds with the changes in the wicking and supports the idea that capillary flow reflects the CHF. This result contrasts with that of Dhir [15] in that an increase in wetting did not drastically increase CHF. As mentioned in section 8.2.1, even low amounts of oxidation alter the microstructure. Oxidized plain surfaces may indeed create a capillary force to aid in the rewetting of the surface.

CHAPTER 9

COMPARISON TO PREVIOUS LAB COATINGS AND HTMC VARIANTS

At this point, the reader should have a firm understanding of the porous coatings tested in this thesis. In chapter 1 we briefly discussed coatings developed by other researchers in our lab. It is of great interest to the previous researchers as well as the author on how HTMC compares with these coatings.

The previous lab coatings were not extensively tested in this thesis work. On the other hand, the data is readily available and thus some comparison is given here. TCMC was retested and some wicking and apparent contact measurements were made. To obtain an understanding of TCMC, a thickness study was done and is shown in Appendix D. HTMC-Ag was the first variant of HTMC and thus is also useful in comparison.

9.1 Wetting and Cleaning Procedures

In Table 9.1 the static equilibrium contact angles are given for the base materials used in each coating. These values can only hint at how an apparent contact angle will result. The Cu-07 brazing alloy has the lowest contact angle of all the materials, yet the Ag50-5 brazing alloy creates the best wetting microporous coating.

Table 9.1 – Static equilibrium contact angles of materials considered in this thesis. Fluid used is distilled water.

Equilibrium Contact Angle	Plain surface material (800 grit sandpaper)
85	Copper
82	Aluminum 6061
81	96/4 Solder
52	60/40 Solder
61	Ag50-5 Brazing Alloy
40	Cu-07 Brazing Alloy

Figure 9.1 illustrates the differences in wetting between the different types of coatings tested. It is unknown why the HTMC-Ag coating wets so much better than all other coatings. The contact angles in Table 9.1 do not explain why the HTMC-Ag coatings exhibit a zero

apparent contact angle. Many different chemicals were used to clean the HTMC-Ag coating in an attempt to determine if the coating wet well due to contaminants. This included distilled water, ethanol, acetic acid, isopropanol, and 2% HCl in which none of these seemed to significantly alter the apparent contact angle except 2% HCl and ethanol. Ethanol caused white particulates to grow on the surface. The 2% HCl solution caused a visible reaction which was guessed to be of silver chloride since it has the greatest potential out of the materials involved. The copper surface became very pale and black spots speckled the surface. The contact angle was drastically increased after the 2% HCl cleaning. An additional 10 minutes in a distilled water ultrasound bath drastically reduced the contact angle. The coating was considered contaminated and no further 2% HCl or ethanol solutions were used on HTMC.

It may be possible that the zinc content in the HTMC-Ag caused a slight amount of corrosion during distilled water cleanings. If this is true then future researchers will need to use fancier cleaning techniques that do not use water.

It is known that acetic acid will not corrode copper [51], but the effects on solder are unknown to us. Colleagues surmised that tin acetate would form and thus 2% HCl was used on a separate sample. The initial apparent contact angle was unaffected by these cleaning processes, the transient portion was greatly decreased possibly caused by contaminants. Only samples cleaned with acetic acid are shown here.

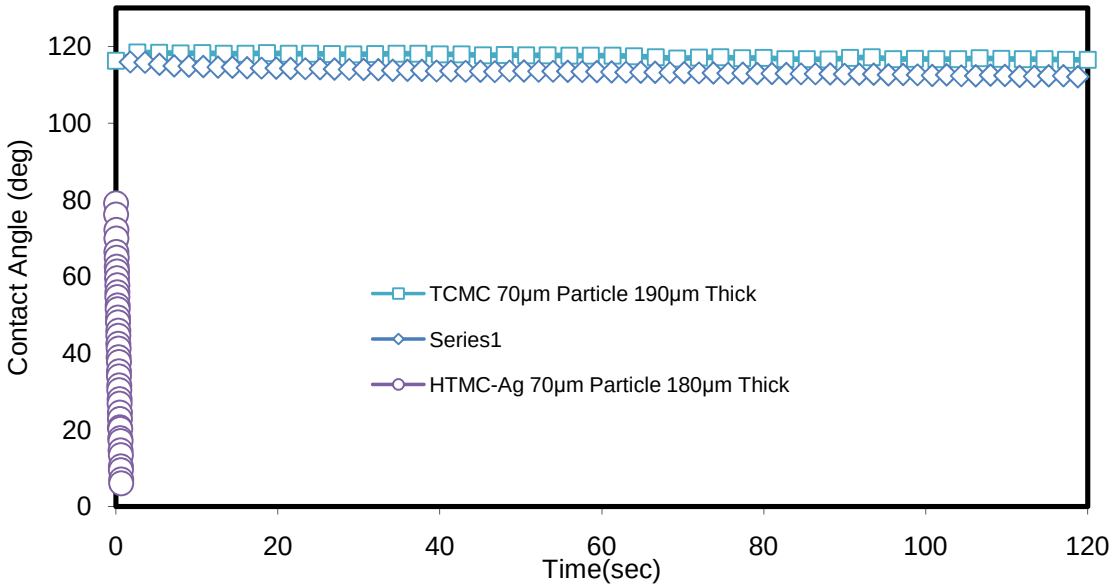

Figure 9.1 – Apparent contact angle measurements of several different microporous coatings.

9.2 Comparison of Boiling Performance

It was hypothesized in the previous chapters that changes in the apparent contact angle may indicate the level of hydraulic resistance. Decreased apparent contact angle led to increased resistance which impeded the escape of vapor followed by boiling degradation. Based on this idea, the apparent contact angles in Figure 9.1, would lead us to believe that TCMC and HTMC-Cu would offer similar boiling performance and HTMC-Ag would perform the worst.

Figure 9.2 displays the boiling performance of each configuration. TCMC definitely performs better than all the other coatings. HTMC-Ag resoundingly performs worse than all other coatings. This does coincide with the apparent contact angle measurements.

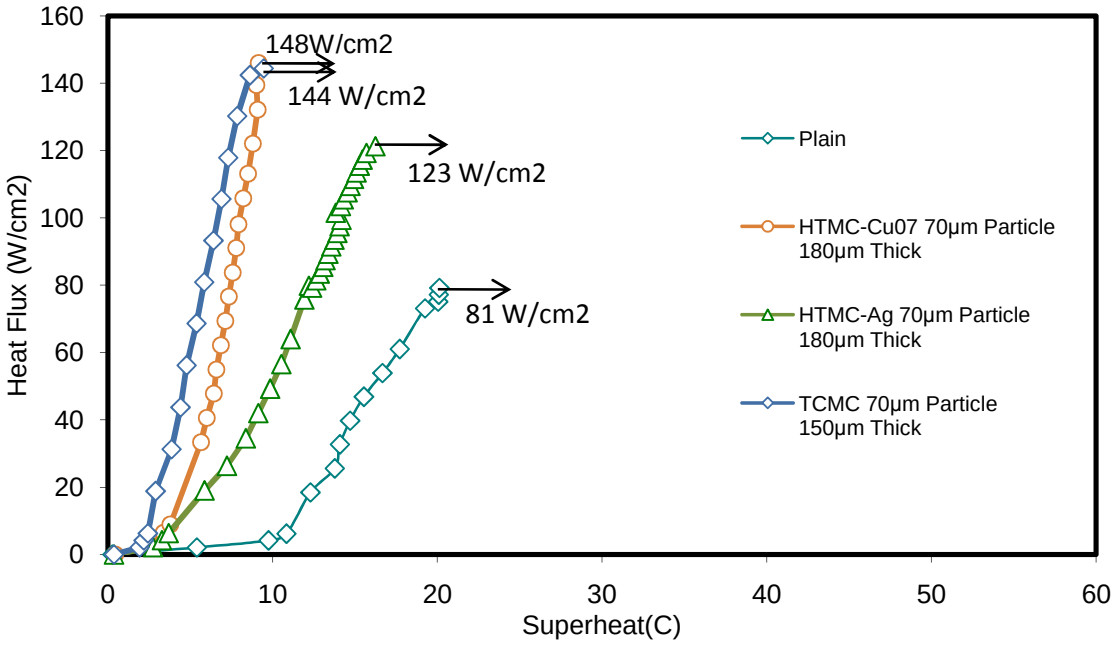

Figure 9.2 – Boiling performance of various types of microporous coatings. T-sat: 80C

Wicking measurements have been taken for TCMC and is included in Figure 3.7 with all the other wicking data. The flow rate of TCMC is just under that of HTMC-Cu 70µm. At T-sat: 80℃, Figure 9.2, the CHF difference between TCMC and HTMC-Cu is negligible. HTMC-Ag, despite the low apparent contact angle, has a lower wicking speed than HTMC-Cu. Yet another piece of evidence that contact angle should not be used to predict values of CHF. The wicking speeds of TCMC and HTMC-Ag are extremely close in Figure 3.7. Yet, the CHF is quite different between the two coatings. Even though the wicking trend is still obeyed, the flow rate does not correspond with the difference in CHF. Wicking must not be the sole factor in the determination of the crisis point.

It is postulated that the increased active nucleation sites of TCMC are aiding in the CHF delay. This is the same mechanism described by Rainey and You [6]. Kim et al. [12] showed that the heat transfer in midrange heat fluxes relies more on micro-convection than latent energy whereas heat transfer just before CHF relies mostly on latent energy. If TCMC is utilizing the heat transfer of micro-convection much more effectively than HTMC-Ag, the boiling

efficiency should be higher; this is indeed observed in Figure 9.2. When micro-convection is the dominant mode of heat transfer, more areas will be flooded and exhibit a cooler temperature. HTMC-Ag is hotter and therefore using more latent energy than micro-convection when compared to TCMC. It follows that an increase in latent energy use will bring about an earlier CHF value since the wicking limit will be met sooner. This would explain why TCMC exhibits a higher CHF than HTMC-Ag.

9.3 Comparison of Thermal Conductivity

Another comparison between the coatings is the thermal conductivity. Comparisons of the respective base material thermal conductivities are given in Table 9.2. Even though TCMC uses solder, by far the least thermally conductive binder, the coating still performs well at high heat flux. As a reminder, the only difference between HTMC and TCMC is the binder composition. This lends support to the idea that in boiling, the thermal conductivity is not as important as surface energy and coating geometry. The author speculates that HTMC-Ag must exhibit a much higher porosity than TCMC with HTMC-Cu lying somewhere in the middle. Currently this lab does not have the ability to test porosity and this observation is left for future researchers.

Table 9.2 – Thermal conductivity of materials used in this thesis. Brazing properties taken from **[64]**. The exact composition of the Ag50-5 brazing paste is not listed in the reference. Compositions quite similar to the Ag50-5 are listed and therefore we can state the order of magnitude of the Ag50-5.

Material	**Conductivity (W/mK)**	**Material**	**Conductivity (W/mK)**
Copper	400	96/4 Solder	33
Nickel	91	Ag50-5 Brazing Alloy	O(98)
Aluminum	237	Cu-07 Brazing Alloy	64

CHAPTER 10

SUMMARY AND CONCLUSIONS OF EACH CHAPTER

10.1 Conclusions of Chapter 3

1) Use of smaller particle sizes resulted in increases in apparent contact angles. 70μm and 4μm particle size coatings had very similar apparent contact angle profiles. It is believed the large pores of the 285μm particles allowed the fluid to interface with the substrate. The smaller the particle, the less the fluid can sufficiently penetrate the pore.
2) Each particle size resulted in a band of wicking velocities. The thickness of the coating was observed to have no affect on the bulk wicking velocity. This depended mostly on the particle size.
3) Changes in the intrinsic contact angle altered the bulk wicking velocity as seen in the TCMC coating. The change in velocity did not cause a large deviation from the wicking band. The geometry of a wicking surface appeared to play a bigger role than the wetting of the surface.
4) If velocity is constant with thickness, then the flow rate is increasing. All HTMC-Cu coatings are observed to linearly increase the flow rate with increases in coating thickness. Increasing the particle size resulted in a greater sensitivity of thickness change. In other words, the rate of change in flow rate increased with particle size.

10.2 Conclusions of Chapter 4

1) The 4μm coatings exhibit a shifting of the boiling curve depending on the time in the working fluid. The small pores created by the 4μm particles more quickly condense than the other particle sizes. The 70μm coatings did show slight shifting after 19 hours. The 285μm coatings were never observed to shift.

2) The coating thicknesses tested did not exhibit the symptoms of an extended surface. Thus, CHF enhancement and/or boiling degradation was not caused by fin effects for our tests.
3) The 285μm coatings had the worst nucleate boiling efficiency, but the highest CHF (~212% enhancement). The 70μm coatings had the best boiling efficiency. The "2nd Runs" of the 4μm coatings resulted in efficiency almost equivalent with the 70μm coatings.
4) Comparison of the apparent contact angle measurements with the boiling curves showed a correspondence with each other. The apparent contact angle correctly predicted which coating tested would perform better. The largest measured angle performed the best in boiling.
5) The measured wicking flow rates correctly predicted which coating would have the highest CHF.
6) The wicking flow rate of the 4μm coatings did not change with thickness. Multiple 4μm coating thicknesses were boiled. The CHF was not observed to change with any thickness. It was concluded the same mechanism described for partially wetted surfaces dictated the 4μm CHF mechanism (hydrodynamic limit of the wick). The CHF occurred at a heat flux that vaporized liquid quicker than was wicked inward.

10.3 Conclusions of Chapter 5

1) Increasing the thickness of the 4μm coatings did not result in increasingly poor boiling efficiency. This led to the proposition that the coating thermal conductivity may not be as important as previous researches thought.
2) Increasing the thickness of the 70μm and 285μm coatings resulted in increasingly poor boiling performance. It is thought this was caused by increased hydraulic resistance affecting the vapor removal rate. If the vapor has a more difficult time leaving the coating, the boiling efficiency will decline. Apparent contact angles of the 70μm coatings did

correspond with the resulting boiling curves. The contact angles of the 285μm coatings did not correspond with boiling tests.

3) At thicknesses higher than 500μm, the 70μm coatings resulted in massive efficiency loss. This result has been seen by other researches and is described as internal film boiling. As the heat flux is increased the film increases in size until the entire coating is covered in the vapor layer resulting in the standard CHF symptoms.
4) Increasing the thickness of the 70μm coatings passed 300μm resulted in increasingly enhanced CHF. This is explained as a CHF mechanism change. Under 300μm the coatings hit CHF due to the wicking limit (faster fluid vaporization than is wicked in). After a 300μm thickness, the CHF occurs due to the macrolayer dryout limit. The vapor is unable to properly escape the coating, blocking fluid influx, and resulting in complete vapor coalescence.
5) Only the CHF wicking limit is observed for the 4μm coatings as flow rate did not change with increases in coating thickness. Fabrication limitations could not produce an even, greater than 300μm thickness, coating.
6) Only the macrolayer dryout limit was observed for the 285μm coatings since a slow flow rate was not obtainable. It is physically impossible to make a 285μm coating thinner than what was fabricated.

10.4 Conclusions of Chapter 6

1) Increasing the coating mixture ratio did not result in increased boiling enhancement. The bonding of the increased mixture ratio resulted in poor particle bonding.
2) Decreasing the mixture ratio resulted in decreased boiling performance.
3) No change in CHF was observed for all tests, which was correctly predicted by the wicking measurements.

10.5 Conclusions of Chapter 7

1) Reducing the pressure resulted in decreased CHF. Pressures below T-sat: 60℃ resulted in no change in CHF. This was due to the contact angles on copper no longer changing at pressures below T-sat: 55℃. Thus, the wicking speeds between T-sat: 60℃ and T-sat:40℃ will be quite similar to each other.

10.6 Conclusions of Chapter 8

1) Corroding the HTMC-Ag surfaces was found to drastically reduce the boiling enhancement.
2) Corroded surfaces were measured to have enhanced wetting characteristics. The apparent contact angle was found to be drastically reduced. This measurement correctly predicts the nucleate boiling degradation.
3) Hydroxide was found to be the most probable cause of the apparent contact angle change.
4) The wicking speeds were also found to be enhanced post corrosion.
5) The CHF was observed to be enhanced post corrosion. The wicking speeds predicted this behavior. No conclusion is made on how much change in wicking speed is needed to increase CHF.
6) Oxidation of HTMC-Ag resulted in wetting enhancements similar to that of the corrosion wetting enhancement.
7) It is believed that oxidation whiskers grew within the pores of the coatings. This would explain why the wicking speed decreased with oxidation. Unfortunately, our current electron microscopes cannot capture these whiskers.
8) The nucleate boiling of an oxidized surface is found to greatly degrade compared to un-oxidized coatings. Based on other researcher's results, the poor thermal conductivity of oxides is thought to have a small affect on the poor boiling performance. Instead, the

increased wetting and increased hydraulic resistance is thought to have a greater effect on the poor boiling performance by impeding the vapor removal rate.

9) Wicking was found to decrease and the resulting boiling curves resulted in decreased CHF. Hence, wicking measurements again were able to predict the change in CHF.

10.7 Conclusions of Chapter 9

1) Apparent contact angle measurements were made for the previously developed TCMC. When compared to HTMC-Cu and HTMC-Ag, TCMC exhibited the highest angle and HTMC-Ag exhibiting the lowest angle.
2) The apparent contact angle correctly predicted the nucleate boiling performance relationship. TCMC performed better than all coatings tested and HTMC-Ag performed worst.
3) Comparison of all available wicking data did predict the correct trend in CHF, but the difference between the CHF of TCMC and HTMC-Ag was much farther apart than expected. The difference between TCMC and HTMC-Ag is concluded to be caused by an increased use of micro-convection by TCMC.

10.8 Final Comments

In chapter 1, we argued that wicking speeds were a better CHF index than contact angle measurements. The measured apparent contact angle measurements were found to incorrectly predict CHF enhancement for several different coating configurations. Throughout this thesis, wicking measurements consistently predicted the CHF trends. Although, wicking measurements were not perfect as seen when comparing TCMC to HTMC-Ag, chapter 9. The author believes that an equation including both the wicking speed and a characterization of the active nucleation site density could provide a formidable way of predicting CHF. Contact angle measurements were observed to still provide some useful information. They provided a quick estimate of a coating's relative hydraulic resistance. The apparent contact angle of the largest

particles or ratio changes did not correctly predict boiling degradation. Therefore, in the author's opinion, wicking measurements offer a useful CHF index, but contact angle measurements must be used with care.

CHAPTER 11

RECOMMENDATIONS

The following are recommendations for future study based on the interest of the author as well as possible future enhancements of the coatings.

11.1 Capillary Measurements of Plain Surfaces

A series of plain surface roughness tests characterized by either a tensiometer or Wilhelmy angles will provide great insight into the validity of the Kandilikar equation, Eqn. 1.9. In other words, repeat the parameters that Berenson [38] tested with the added capillary force measurements.

Repeating the roughness tests would be quite simple, but repeating the material tests would pose a problem. Current setup requires the ability to easily solder the heater to different materials. Soldering to aluminum, stainless steel, et cetera, would require very aggressive fluxes and/or high temperature brazing. Gold solder paste (80%Au 20%Sn) may be able to wet the material surface easily (liquidus 280℃ requires N-environment). Some low alloy copper-tin and/or indium solders may also be able to wet non-copper metals.

11.2 Parametric Changes to HTMC

Unmistakably, the next step in the high temperature microporous coating evolution is to match the performance of HTMC with that of TCMC without losing any of the CHF enhancements.

11.2.1 Material Change

A change in the binder material will greatly affect the performance of the coatings. There is a plethora of brazing choices available. Instead of randomly guessing, based on the information given in this thesis, there is a starting point that must be met when choosing new

material. The new material should exhibit an intrinsic contact angle higher than its predecessor while still maintaining a low galvanic potential.

Copper exhibits one of the highest intrinsic contact angles out of the base elements. Other standard choices such as aluminum, gold, nickel, and silver all exhibit intrinsic contact angles at least 18° lower than copper. Zinc (ZnO passivation layer) has shown to have an intrinsic contact angle comparable to copper. Unfortunately, zinc will create a galvanic potential of .9V with copper. This combination will corrode quite badly within a very short amount of time. Therefore, only copper and copper-phosphorus brazing pastes can be considered for HTMC improvement[5].

Since this greatly narrows down the brazing paste choices, an alternative to surface energy manipulation is presented. The addition of a very thin layer of low thermally conductive material should have little effect on the effective conductivity. Thus, electroless, electroplating, nano-particle deposition, et cetera, could create a hydrophobic intrinsic contact angle. Shrestha et al. [65] showed that SiO_2 would easily create a super-hydrophobic surface via electrodepostion. This may be an easier approach than the techniques used for Teflon deposition, which is the typical technique for creating a hydrophobic surface.

This type of modification may enhance nucleate boiling, but the wicking speed may decrease resulting in a lower CHF. A third alternative is the creation of a nano-structure on top of the particles that will increase the intrinsic contact angle.

11.3 Wetting and CHF Applications

11.3.1 Wetting via Material Change

In our tests, silver brazing pastes were found to exhibit excellent wettability. The corrosive effects of the zinc within this particular composition may be undesirable. Brazing pastes containing much higher amounts of silver and less zinc are available and would be an

[5] It is very possible that an alloy of nickel, aluminum, gold, etc, will create a high intrinsic contact angle. With this taken into consideration, the amount of choices explodes and would take years to measure all compositions.

excellent starting place for coatings in which wettability maximization is desired. The reader is reminded that any type of system that relies on wettability must minimize the effects of adsorption. This is usually done by environment control.

Swapping the particle material can also increase wetting and CHF, particularly SiC. This material has a midrange thermal conductivity (120W/mK). Just like oxides, carbides are known for their excellent wettability. The challenge here is that high temperature (above 1000℃) brazing pastes containing titanium are required to wet carbides. The brazing environment needs to be a vacuum as nitrides are easily formed.

Depending on the system temperature surfactants and salts will greatly enhance wetting. The downside is that these materials are often thermally unstable and dissolve at elevated temperatures.

11.3.2 Wicking via Particle Size

Our tests state resoundingly that the larger the particle size the faster the wicking. Increasing the particle size further should increase the wicking speed, but there is a limit. This limit exists at the point in which the pore is too large to create a sufficient capillary force.

11.3.3 CHF via Particle Size and Material

Increasing the CHF further with particle size or material change has exactly the same drawbacks mentioned in section 13.3.1 and 13.3.2. The nuclear industry often considers CHF enhancement more pertinent than nucleate boiling enhancement. An increase in CHF allows the designer more leeway when choosing system parameters. Delaying CHF would allow power plants to operate at lower pressures which are safer and more cost effective.

As our data shows, corrosion is not always an undesirable result as long as the corroded material is not a system critical component. The introduction of large galvanic potentials may result in even higher CHF enhancement. The use of aluminum brazing pastes may actually create an ultra high CHF.

11.4 High Temperature Corrosion

Temperature has the nasty habit of exacerbating corrosion. Temperature limitations of our current heater setup prevented us from exceeding 150ºC. If HTMC is immersed in water the amount of oxides formed should be minimized, but hydroxides may readily form at elevated temperatures. Tin is well known to form tin acetate in water and at elevated temperatures (~200ºC) this should happen much quicker. Thus, TCMC may have a very big problem with corrosion if held at higher temperatures for long periods of time. HTMC should be relatively immune to corrosion in degassed water, but we cannot say with absolute certainty that the performance will not degrade if a high temperature (~400-600ºC) is held for extended periods of time.

Nuclear reactors often use pressurized water (~15MPa or ~150atm) to cool the system. This means the boiling point of water is ~350ºC. Hence, the coatings would be exposed to elevated temperatures for a long period of time.

A new heater setup is needed to properly test the coatings without endangering the members of the lab. Consultation with a corrosion expert should lead to insight on how to test high temperature corrosion at low pressures or low temperatures. The reader is directed to Berenson [38] or Ramilison and Lienhard [34] where superheated steam was used to provide heat to the sample instead of an electric heater. This allowed them to achieve high temperatures in a variety of fluids.

APPENDIX A

CORROSION INFORMATION

SAMPLE GALVANIC SERIES:

Working fluid stagnant (low oxygen content) seawater.

- Graphite
- Palladium
- Platinum
- Gold
- Silver
- Titanium
- Stainless steel (316 passive)
- Stainless Steel (304 passive)
- Silicon bronze
- Stainless Steel (316 active)
- Monel 400
- Phosphor bronze
- Admiralty brass
- Cupronickel
- Molybdenum
- Red brass
- Brass plating
- Yellow brass
- Naval brass 464
- Uranium 8% Mo
- Niobium 1% Zr
- Tungsten
- Stainless Steel (304 active)
- Tantalum
- Chromium plating
- Nickel (passive)
- Copper
- Nickel (active)
- Cast iron
- Steel
- Lead
- Tin
- Indium
- Aluminum
- Uranium (pure)
- Cadmium
- Beryllium
- Zinc plating (see galvanization)
- Magnesium

The rule of thumb used in industry is that harsh environments should allow a potential difference no more than .15V. For non-high temperature and or storage, a potential of .25V is acceptable. Highly controlled environments can use up to .5V. A Cu-Sn (solder) system has a potential of .3V and may be considered a corrosion risk.

Table A.1 - Anodic Index

Metallurgy	Index (V)
Gold, solid and plated, Gold-platinum alloy	**0**
Rhodium plated on silver-plated copper	**0.05**
Silver, solid or plated; monel metal. High nickel-copper alloys	**0.15**
Nickel, solid or plated, titanium an s alloys, Monel	**0.3**
Copper, solid or plated; low brasses or bronzes; silver solder; German silvery high copper-nickel alloys; nickel-chromium alloys	**0.35**
Brass and bronzes	**0.4**
High brasses and bronzes	**0.45**
18% chromium type corrosion-resistant steels	**0.5**
Chromium plated; tin plated; 12% chromium type corrosion-resistant steels	**0.6**
Tin-plate; tin-lead solder	**0.65**
Lead, solid or plated; high lead alloys	**0.7**
Aluminum, wrought alloys of the 2000 Series	**0.75**
Iron, wrought, gray or malleable, plain carbon and low alloy steels	**0.85**
Aluminum, wrought alloys other than 2000 Series aluminum, cast alloys of the silicon type	**0.9**
Aluminum, cast alloys other than silicon type, cadmium, plated and chromate	**0.95**

Table A.2 – Anodic Index Continued

Hot-dip-zinc plate; galvanized steel	**1.2**
Zinc, wrought; zinc-base die-casting alloys; zinc plated	**1.25**
Magnesium & magnesium-base alloys, cast or wrought	**1.75**
Beryllium	**1.85**

APPENDIX B

MATERIAL PROPERTIES

Table B.1 - Composition of microporous coatings analyzed.

	Particles	Binder	Substrate	Thinner
ABM	Aluminum	Brushable Ceramic Epoxy	Copper	MEK
MTSP	Nickel	96/4 Solder	Copper	Denatured Alcohol
TCMC	Copper	96/4 Solder	Copper	Denatured Alcohol
HTMC-Ag	Copper	Ag 50-5 Brazing Paste	Copper	Isopar M ™ (Isoparaffin)
HTMC-Cu	Copper	Cu 0-7 Brazing Paste	Copper	Isopar M ™ (Isoparaffin)

Table B.2 – Composition of binders used in coatings analyzed.

Industry Name	Element Percentages	Liquidus
96/4 Solder	96% Sn, 4% Ag	220ºC
Ag 50-5	50% Ag, 20% Cu, 28%Zn, 2%Ni	707 ºC
Cu 0-7	86.75% Cu, 6.25%P, 7%Sn	677 ºC

Table B.3 – Properties of Exxon Mobil Isopar M ™

Property	Units	Typical Values
Flash Point	ºC	92
Density	kg/dm^3	.792
Viscosity	mm^2/s	3.8
Surface Tension	mN/m	25

APPENDIX C

SEM AND MICROSCOPE PICTURES OF COATINGS

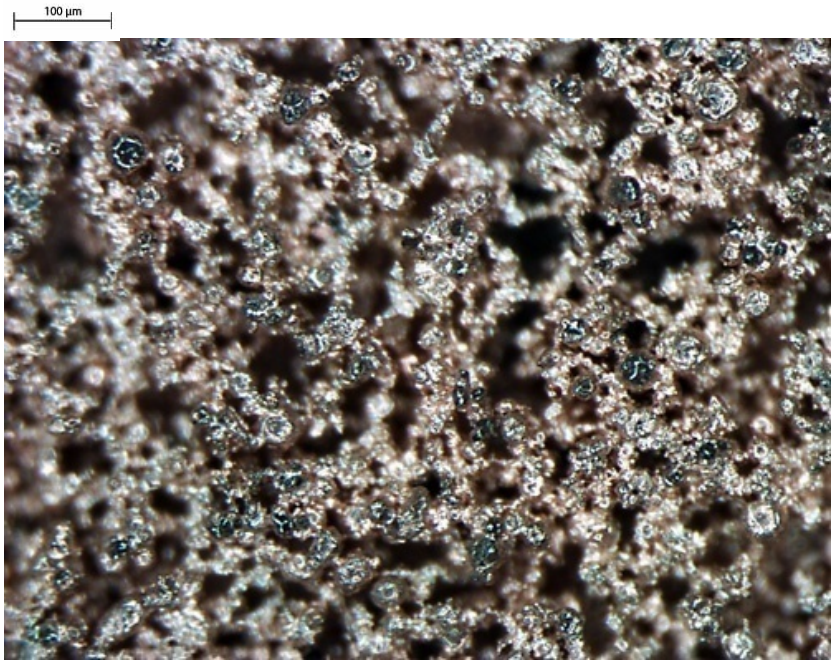

Figure C.1 – HTMC-Ag 70µm

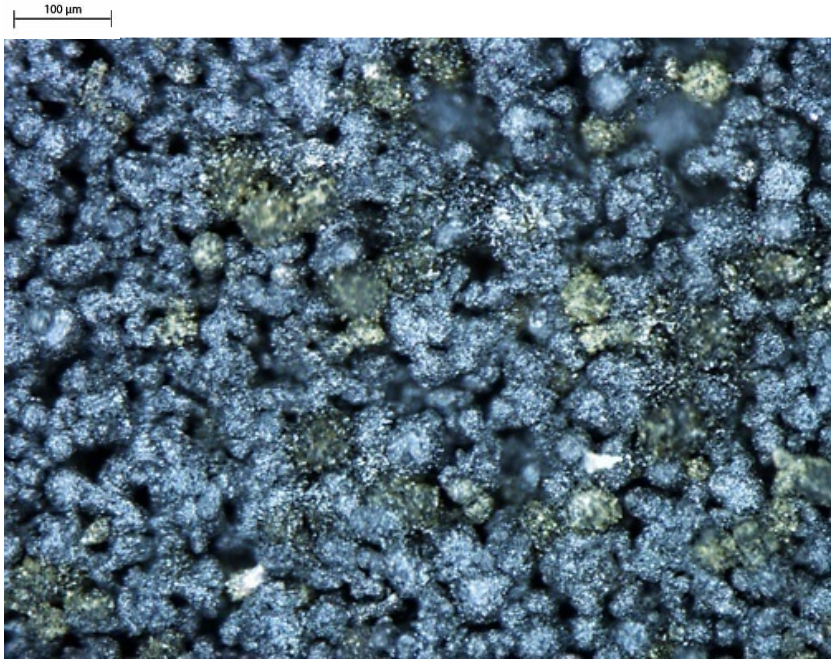

Figure C.2 - Oxidized HTMC-Ag 70µm

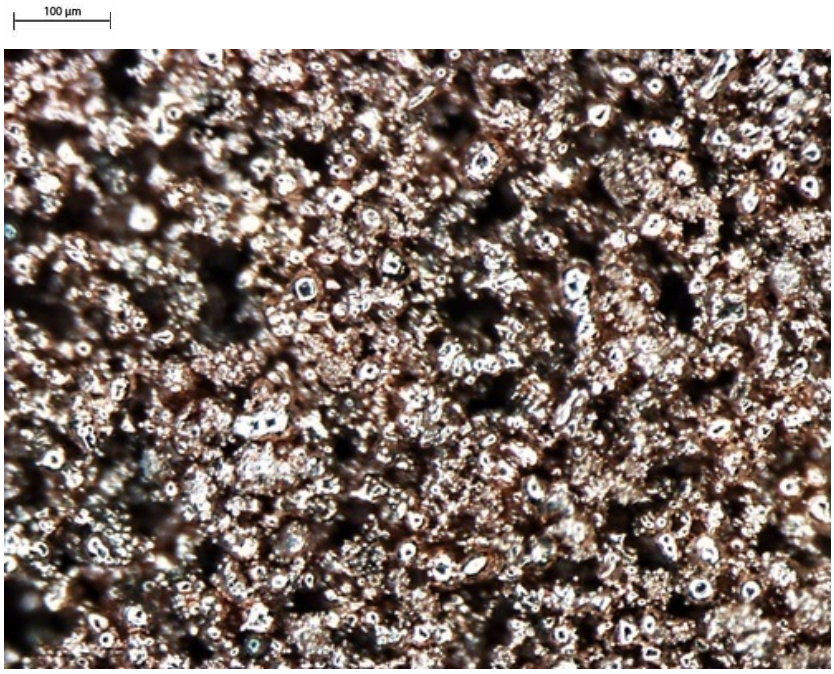

Figure C.3 - HTMC-Cu 70µm

Figure C.4 - HTMC-Cu 4µm

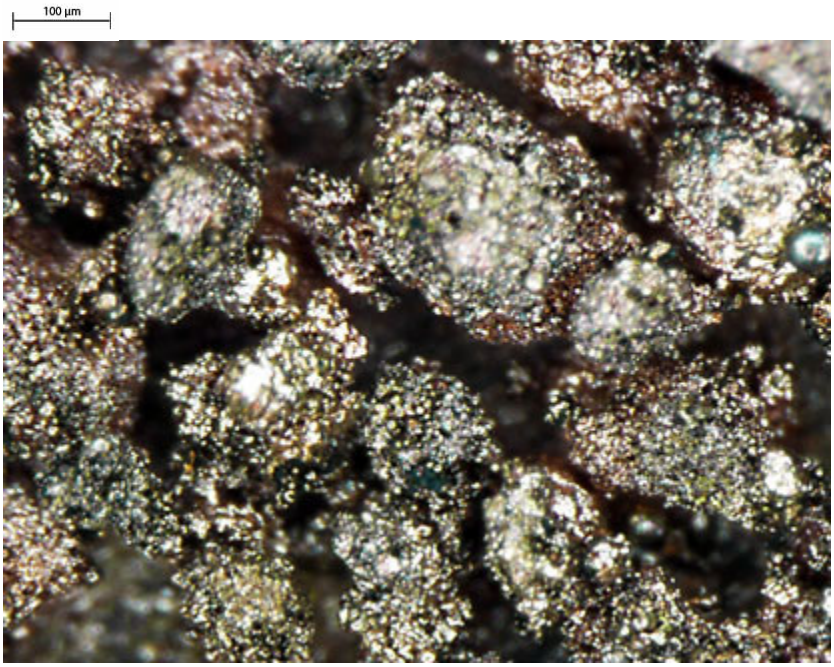

Figure C.5 - HTMC-Cu 285µm

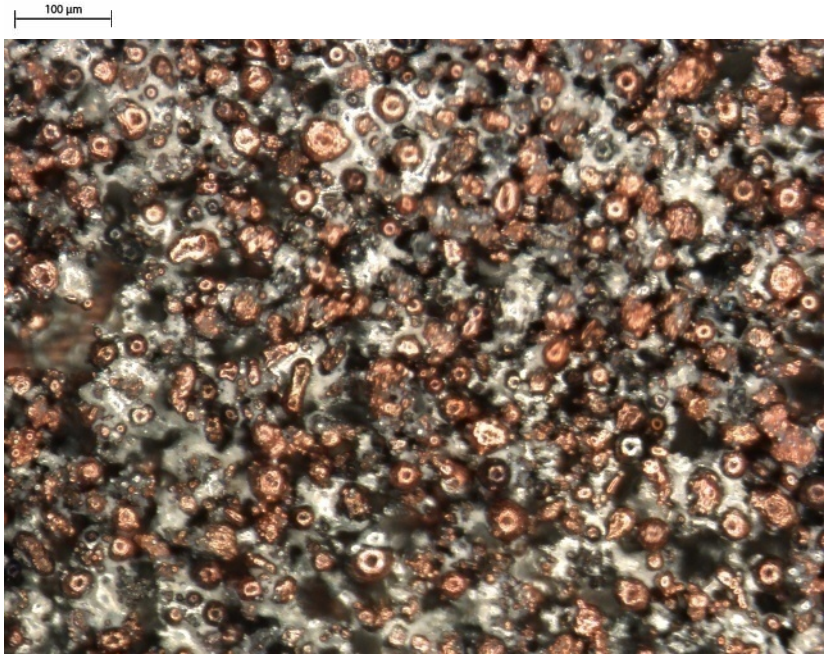

Figure C.6 – TCMC

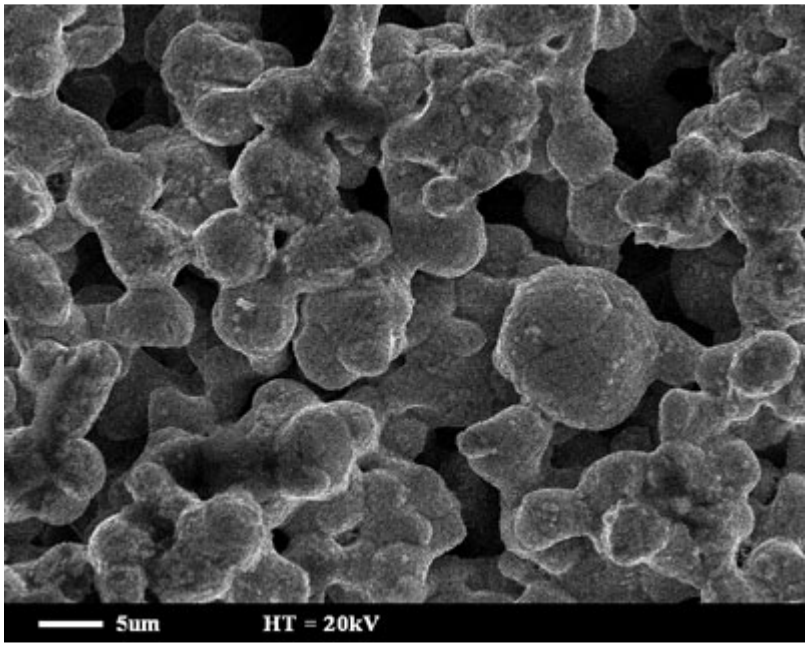

Figure C.7 - HTMC-Cu 4µm SEM photo

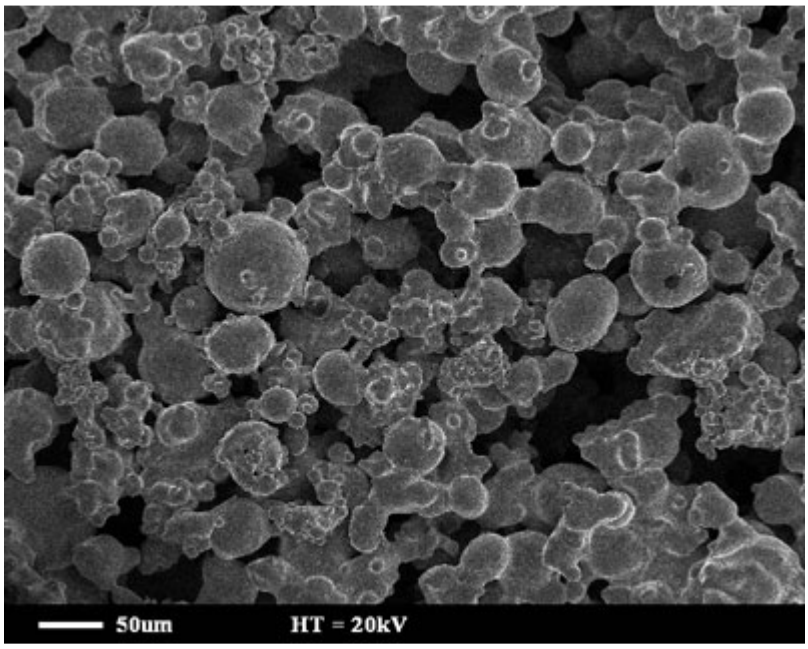

Figure C.8 - HTMC-Cu 70µm SEM photo

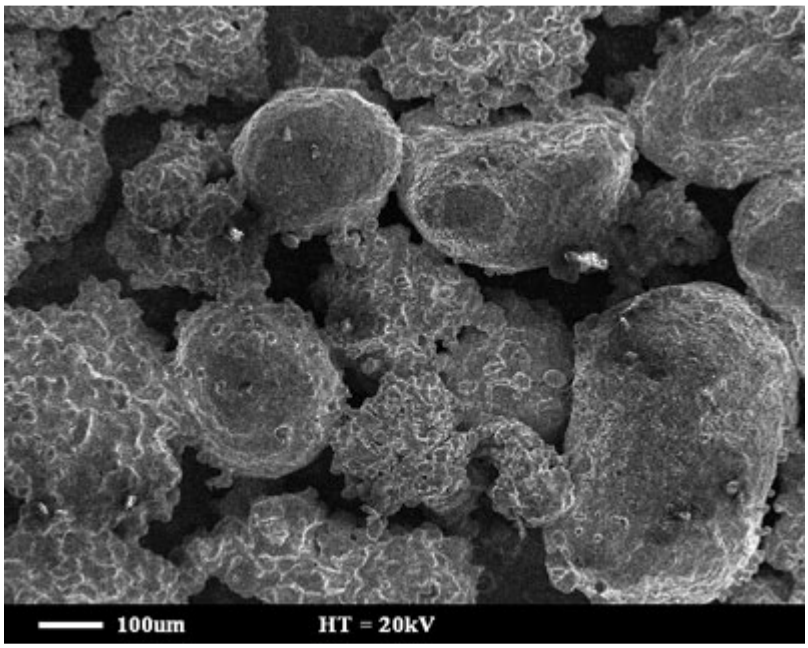

Figure C.9 - HTMC-Cu 285µm SEM photo

APPENDIX D

ADDITIONAL EXPIRMENTAL DATA

Figure D.1 displays the boiling difference in TCMC with increases in thickness. The fact that little difference is seen in the boiling curve with increased thickness when compared to HTMC-Cu indicates there is less hydraulic resistance.

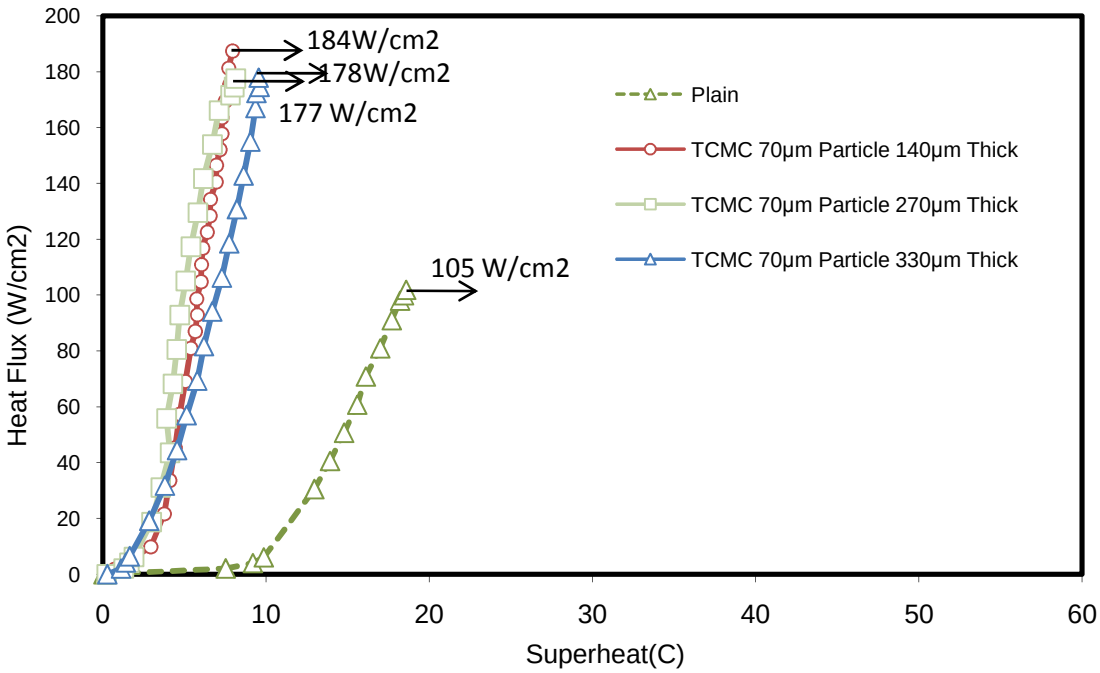

Figure D.1 - Thickness comparison of TCMC coatings. T-sat:100C

REFERENCES

[1] Malyshenko, S P. "Features of heat transfer with boiling on surfaces with porous coatings." Thermal Engineering 38, no. 2 (1991): 81-88.

[2] Bergles, A E, and M C Chyu. "Charactersitics of Nucleate Pool Boiling From Porous Metallic Coatings." J. Heat Transfer 104 (1982): 279-285.

[3] Ammerman, Rainey, and Seung M You. "A New Microporous Surface Coating for Enancment of Pool and Flow Boiling Heat Transfer." Advances in Heat Transfer 38 (2004): 73-142.

[4] Cieslinksi, Janusz T. "Nucleate pool boiling on porous metallic coatings." Experimental Thermal and Fluid Science 25 (2002): 557-564.

[5] Chang, J Y, and S M You. "Enhanced boiling heat transfer from microporous surfaces: effects of a coating composition and method." Int. J Heat Mass Transfer 40 (1997): 4449-4460.

[6] Rainey, K N, and S M You. "Effects of heater orientation on pool boiling heat transfer from microporous coated surfaces." Int. J. Heat Mass Transfer 44, no. 14 (2001): 2589-2599.

[7] Kim, Joo Han. "Enhancement of Pool Boiling Heat Transfer Using Thermally Conductive Microporous Coating Techniques." PhD Thesis, UT Arlington, 2006.

[8] Moss, R A, and A J Kelly. "Neutron Radiographic Study of Limiting Plannar Heat Pipe Performance." Int. J. Heat Mass Transfer 13 (1970): 491-502.

[9] Katto, Y. "Critical Heat Flux Mechanisms." Edited by John C Chen. Int. Conference on Convective Flow Boiling. Washington, DC: Taylor & Francis, 1996. 29-42.

[10] Zuber, N. "Hydrodynamic aspects of boiling heat transfer." Physics and Mathematics (US Atomic Energy Commission), 1959.

[11] Liter, Scott G, and Massoud Kaviany. "Pool-boiling CHF enhancement by modulated porous-layer coating: theory and expirment." Int. J. Heat Mass Transfer 44 (2001): 4287-4311.

[12] Kim, Joo Han, K N Rainey, S M You, and J Y Park. "Mechanism of Nucleate Boiling Heat Transfer Enhancment From Microporous Surfaces in Saturated FC-72." Journal of Heat Transfer 124, no. 3 (2002): 500-506.

[13] Bar-Cohen, Avram, and A McNeil. "Parametric Effects on Pool Boiling Critical Heat Flux in Dielectric Liquids." Pool and External Flow Boiling. ASME, 1992.

[14] Kumada, Toshiaki, and Hiroto Sakashita. "Proposed Model for Kutateladze Correlation and New Correlation of CHF." Pool and External Flow Boiling. ASME, 1992.

[15] Dhir, V K. "Some Observations From Maximum Heat Flux Data Obtained on Surfaces Having Different Degrees of Wettabiltiy." Pool and External Flow Boiling. ASME, 1992.

[16] Unal, Cetin, Pratap Sadasivan, and Ralph A Nelson. "On the Hot-Spot-Controlled Critical Heat Flux Mechanism in Pool Boiling of Saturated Fluids." Pool and External Flow Boiling. ASME, 1992.

[17] Carvalho, Ricardo D. M., and Arthur E Bergles. "The Effects of the Heater Thermal Conductance/Capacitance on the Pool Boiling Critical Heat FLux." Pool and External Flow Boiling. ASME, 1992.

[18] Golobic, Iztok, and Arthur E Bergles. "Effects of Thermal Properties and Thickness of Horizontal Vertically Oriented Ribbon Heaters on the Pool Boiling Critical Heat Flux." Pool and External Flow Boiling. ASME, 1992.

[19] Tehver, J. "Influences of porous coating on the boiling burnout heat flux." Recent advance in heat transfer, 1992: 231-242.

[20] Li, Chen, and G P Peterson. "Experimental Studies on CHF of Pool Boiling on Horizontal Conductive Microporous Coated Surfaces." Space Technology and Applications Int. Forum 969 (2008): 12-20.

[21] Rainey, K N, and S M You. "Pool Boiling Heat Transfer From Plain and Microporous, Square Pin-Finned Surfaces in Saturated FC-72." J. of Heat Transfer 122 (2000): 509-516.

[22] Li, Chen, and G P Peterson. "Parametric Study of Pool Boiling on Horizontal Highly Conductive Microporuos Coated Surfaces." J. of Heat Transfer 129 (2007): 1465-1475.

[23] Berg, John C, ed. Wettability. New York: Marcel Dekker, Inc., 1993.

[24] Carey, Van P. Liquid-Vapor Phase-Change Phenomena. 2nd. New York: Taylor & Francis, 2008.

[25] Washburn, Edward W. "The Dynamics of Capillary Flow." The Physical Review 17 (March 1921): 273-283.

[26] Van Oss, Carel J. Interfacial Forces in Aqueous Media. 2nd. Boca Raton: CRC Press, 2006.

[27] Bar-Cohen, A. "Fundamentals of nucleate pool boiling of highly-wetting dielectric liquids." In Cooling of Electronic Systems, by Sadik Kakac, H Yuncu, K Hijikata and H Hijikata, 415-455. Springer, 1994.

[28] Jansen, F, M Mineur, and J J Schroder. "The Influence of Wetting Behavior on Pool Boiling Heat Transfer." Pool and External Flow Boiling. ASME, 1992. 55-61.

[29] Takata, Y, S Hidaka, M Masuda, and T Ito. "Pool Boiling on a superhydrophilic surface." International Journal of Energy Research, 2003: 111-119.

[30] Takata, Y, S Hidaka, and T Uraguchi. "Boiling Feature on a Super Water-Repellent Surface." Heat Transfer Engineering 27, no. 8 (2006): 25-30.

[31] Lee, S Y, S H Choi, and C O Park. "Oxidation, grain growth and reflow characteristics of copper thin films prepared by chemical vapor deposition." Thin Film Solids 359, no. 2 (2000): 261-267.

[32] Nagai, Niro, and Van P Carey. "Assessment of Surface Wettability and Its Relation to Boiling Phenomena." Thermal Science & Engineering 10, no. 3 (2002): p.1-9.

[33] Kandlikar, Satish G. "A Theoretical Model to Predict Pool Boiling CHF Incorporating the Effects of Contact Angle and Orientation." Journal of Heat Transfer 123 (2001): p. 1071-1079.

[34] Ramilison, J M, and J H Lienhard. "Transition Boiling Heat Transfer and the Film Transition Regime." J. Heat Transfer 109 (1987): p. 746-752.

[35] Hahne, E, and T Diesselhorst. "Hydrodynamic and Surface Effects on the Peak Heat Flux in Pool Boiling." Proceedings, 6th International Heat Transfer Conference. 1978. p.209-214.

[36] Liaw, S P, and V K Dhir. "Effect of Wettability on Transition Boiling Heat Transfer from a Vertical Surface." Proceedings, 8th International Heat Transfer Conference. 1986. p. 2031-2036.

[37] Marcy, M, and R.H.S. Winterton. "Hysteresis and Contact Angle Effects in Transition Pool Boiling of Water." International Journal of Heat and Mass Transfer 31 (1988): p. 1443-1449.

[38] Berenson, P. "Transition Boiling Heat Transfer from a Horizontal Surface." PhD Thesis, Massachusetts Institute of Technology, 1960.

[39] Bonilla, C F, J J Grady, and G W Avery. "Pool Boiling Heat Transfer from Scored Surface." Chem. Eng. Prog. Symp. Ser., 1965.

[40] Haramura, Yoshihiko. "Steady State Pool Transition Boiling Heated With Condensing Steam." ASME/JSME Thermal Engineering Proceedings. ASME, 1991. 59-64.

[41] Hay, K M, and M I Dragila. "Physics of Fluid Spreading on Rough Surfaces." International Journal of Numerical Analysis and Modeling 5 (2008): 85-92.

[42] Joudi, K A, and D D James. "Surface Contamination, Rejuvenation, and the Reproducibilty of Results in Nucleate Pool Boiling." Journal of Heat Transfer 103 (1981): 453-458.

[43] Urquiola, Erwin, and Yasunobu Fujita. "Contact Angle Effects in Boiling Heat Transfer." Memoirs of the Faculty of Engineering, Kyushu University 62, no. 1 (2002): 55-65.

[44] Diesselhorst, T, U Grigull, and E Hahne. "Hydrodynamic and Surface Effects on the Peak Heat Flux in Pool Boiling." In Heat Transfer in Boiling, edited by E Hahne and U Grigull, 99-133. Washington: Hemisphere Publishing Corporation, 1977.

[45] —. Pressure Vessel Design Handbook. New York: Van Nostrand Reinhold Company Inc., 1986.

[46] Harvey, John F. Theory and Design of Pressure Vessels. New York: Van Nostrand Reinhold Company Inc., 1985.

[47] Megyesy, Eugene F. Pressure Vessel Handbook. 6th. Tulsa: Publishing Inc., 1983.

[48] Rajayi, Maryam, and Apostolos Kantzas. "Effect of Temperature and Pressure on Contact Angle of Quartz-Water-Bitumen System." International Symposium of the Society of Core Analysts . Abu Dhabi, 2008.

[49] Wu, Souheng. "Effect of Temperature On Contact Angle." In Polymer interface and adhesion, 139-147. New York: Marcel Dekker, 1982.

[50] Chavez, K L, and D W Hess. "A Novel Method of Etching Copper Oxide Using Acetic Acid." Journal of The Electrochemical Society 148, no. 11 (2001): 640-643.

[51] Xia, Xianping, Changsheng Xie, Shuizhou Cai, Zhihong Yang, and Xiangliang Yang. "Corrosion characteristics of copper microparticles and copper nanoparticles in distilled water." Corrosion Science 48 (2006): 3924-3932.

[52] Kagwade, Sanjay V, Clive R Clayton, Devicharan Chidambaram, and Gary P Halada. "Photochemical breakdown of acetone on copper." Electochimica Acta 46 (2001): 2337-2342.

[53] O'Connor, J P, and S M You. "A painting technique to enhance pool boiling heat transfer in saturated FC-72." J. Heat Transfer 117 (1995): 387-393.

[54] Quere, David. "Wetting and Roughness." Annual Review of Materials Research 38 (2008): 71-99.

[55] Cazabat, A M, and M A Cohen Stuart. "Dynamics of Wetting: Effects of Surface Roughness." Journal of Physical Chemistry 90, no. 22 (1986).

[56] Amaya, Miguel, interview by Ross Pivovar. Regimes of Wetting in Porous Media (November 23, 2008).

[57] Wang, C H, and V K Dhir. "On the prediction of active nucleation sites including the effect of surface wettability." Pool and External Flow Boiling. ASME, 1992. 111-118.

[58] Bear, Jacob. Dynamics of Fluids in Porous Media. New York: American Elsevier Publishing Company, Inc., 1972.

[59] Polezhaev, Yu V, and S A Kovalev. "Modelling heat transfer with boiling on porous structures." Thermal Engineering 37, no. 12 (1990): 617-620.

[60] Borzenko, V I, and S P Malyshenko. "Mechanisms of Phase Exchange under Conditions of Boiling on Surfaces with Pourous Coatings." High Temperature 39, no. 5 (2001): 714-721.

[61] Boyes, A P, and A B Ponter. "Wettability of Copper and Polytetrafluoroethylene Surfaces with Water--the Influence of Environmental Conditions." Chemie-Ingenieur-Technik 45 (1973): 1250-1257.

[62] Murshed, S M Sohel, Say-Hwa Tan, and Nam-Trung Nguyen. "Temperature dependence of interfacial properties and viscosity of nanofluid for droplet-base microfluids." Journal of Physics D: Applied Physics 41 (2008): 1-5.

[63] Lasko, William, and W K Tice. "Determination of the Surface Population of Copper Oxide Whiskers by Electron Microscopy Techniques." Anal. Chem. 34, no. 13 (1962): 1795-1797.

[64] Arenas, M F, V L Acoff, and R G Reddy. "Physical properties of selected brazing filler metals." Science and Technology of Welding and Joining 9, no. 5 (2004): 423-429.

[65] Shrestha, Nabeen K, Genta Kobayashi, and Tetsuo Saji. "Electrodeposition of Hydrophobic Nickel Composite Containing Surface-Modified SiO2 Particles under the Influence of a Surfactant with an Azobenzene Moiety." Chemistry Letters 33, no. 8 (2004): p. 984-985.

[66] Cazabat, A M, and Cohen Stuart. "Dynamics of Wetting: Effects of Surface Roughness." Journal of Physical Chemistry 90, no. 22 (1986).

[67] Schwartz, Mel. Brazing. 2nd. Ohio: ASM International, 2003.

[68] Roberge, Pierre R. "Galvanic Series." Corrosion Doctors. August 1999. http://corrosion-doctors.org/Definitions/galvanic-series.htm (accessed August 20, 2008).

[69] Bejan, Adrian. Convection Heat Transfer. 3rd. Hoboken: John Wiley and Sons, Inc., 2004.

[70] Callister, William Jr. D. Fundamentals of Materials Science and Engineering. Edited by 2nd. New Jersey: John Wiley & Sons, Inc., 2005.

[71] Craig, and David B Anderson, . Handbook of Corrosion Data. 2nd. Ohio: ASM International, 1995.

[72] Kim, Choon Gun, interview by R Pivovar. Corrosion Information (August 28, 2008).

[73] McHale, G. "Cassie and Wenzel: Were They Really So Wrong?" Langmuir 23 (2007): 8200-8205.

[74] Montgomery, Runger, and Hubele. Engineering Statistics. 2nd. New York: John Wiley & Sons, Inc., 2001.

[75] Tong, L S. Boiling Heat Transfer and Two-Phase Flow. 2nd. Washington: Taylor & Francis, 1997.

[76] Bico, J, C Tordeux, and D Quere. "Rough Wetting." Europhysics Letters 55, no. 2 (2001): 214-220.

[77] Bejan, Adrian, and Allan D Kraus. Heat Transfer Handbook. Wiley-IEEE, 2003.

BIOGRAPHICAL INFORMATION

Ross completed his Bachelors of Science in Mechanical Engineering at UT Arlington in Dec. 2007. As an undergrad, he worked in the Micro-Scale Heat Transfer Laboratory where he would go on to do his masters under Dr. Seung-Mun You. A self-taught programmer he has written applications that conveniently optimize heat sinks for the lab. While he has done extensive work in dynamic heat sinks for electronic cooling, he has spent the majority of his time on microporous coatings with applications in nuclear power cooling.

Ross' research interests include all types of thermal applications as well as material science. Currently he is focused on two-phase heat transfer and micro/nano-scale fluidics.

Ross received his M.S. at UT Arlington in May 2009. He plans to take a short academic hiatus in order to work in the defense industry. His company interests include military defense and/or power generation. In the near future he plans to return to academia and obtain his Ph.D.